ORE SORTING USING MICROWAVE IRRADIATION

Mlamli Booi
B.Sc.(Eng) Cape Town.

Thesis submitted to the Faculty of Engineering at the University of Cape Town in partial fulfilment of the Degree of Master of Science in Electrical and Electronic Engineering.

Cape Town, April 1989.

D E C L A R A T I O N

I declare that this dissertation is my own unaided work. It is being submitted in partial fulfilment of the requirements for the degree of Master of Science in Engineering at the University of Cape Town. It has not been submitted before for any degree or examination at this or any other University.

M. BOOI

Signed by candidate

28th day of April, 1989

ABSTRACT

Automatic ore sorting machines are in common use in the mining industry. These machines generally separate valuable mineral-bearing rocks from waste rocks. At the Premier Diamond Mine in South Africa kimberlite, a diamond-bearing rock is separated from gabbro which is a waste rock.

Work had been conducted previously in the Department of Electrical Engineering at the University of Cape Town to find a viable method for discriminating between gabbro and kimberlite. A technique using microwave irradiation attenuation was successful when using parallel-sided smooth-surfaced rocks. This technique used linearly polarized square antennas at 35GHz. Problems were experienced, however, with irregularly shaped rocks. The aim of the present study was therefore to develop a technique which will sort irregularly shaped rocks and eliminate the problems associated with them.

A study of the effects of frequency change was conducted, with emphasis on the variation of attenuation with frequency. It was found that as the frequency increases, so does the attenuation of the microwave signal. It was concluded, therefore, that a frequency of 10.525GHz offers a reasonable operational compromise, because, as the attenuation goes up with frequency, the scattering of microwaves also increases.

An investigation into the use of lower frequency microwaves utilising electrically small antennas was also carried out. This was achieved by dielectrically loading S-band waveguides with teflon. The operating frequency of these antennas was 3GHz. It was found that dielectrically loaded antennas do not reduce the effect of surface reflections.

Equipment operating at 10.525GHz was therefore designed and constructed.

Circularly polarised antennas were investigated but the results showed no improvement over the linearly polarised system.

A technique which proved to be more viable was "space diversity" where three separate microwave channels were used together in a different space orientation. This reduced the effects of surface reflections and provided a 94.5% kimberlite recovery and 59% gabbro rejection in static tests. Dynamic tests at particle speeds of 5m/s gave a 49% gabbro rejection for a 94.5% kimberlite recovery. Improved separation can be achieved by passing the ore particles through the system more than once.

To improve the throughput multiple parallel channels were used. Problems of interchannel interference and multipath reflections from the vertical channel dividing walls were experienced and successfully solved.

The results obtained using the space diversity technique were considered to be acceptable and the objective of this thesis was met.

A pre-production-three- channel full sized plant has been constructed at De Beers Diamond Research Laboratories in Johannesburg and results to date are very promising.

ACKNOWLEDGEMENTS

I wish to thank Professor B J Downing for his guidance and support during this project. Thanks are also due to Sean Mercer for his technical assistance.

I would also like to thank the De Beers Diamond Research Laboratory Personnel for their co-operation, and for making their equipment available for experiments. Thanks are also due to Dr D. Salter for his technical assistance. Thanks are also due to Mrs J Fold for typing this thesis.

I would also like to thank DAAD Scholarship for their financial support.

TABLE OF CONTENTS

LIST OF ILLUSTRATIONS

CHAPTER 1

INTRODUCTION

Diamonds have been discovered in many different parts of the world, but in only a few of these is diamond mining a commercially viable proposition. The usual host rock for diamonds in primary deposits is kimberlite. Diamonds are also found in alluvial deposits, following the weathering of kimberlite, where they accumulate because of their inert chemical nature, their extreme hardness and high specific gravity.

Although the bodies of kimberlite vary in size and shape, many are roughly circular at surface with a pipelike shape and are referred to as "kimberlite pipes'. Many kimberlite pipes are known to occur in South Africa, but only a few contain sufficient diamonds to warrant mining. Kimberlite is an igneous intrusive rock and, because of this, kimberlite pipes contain a variety of inclusions: fragments of rocks from greater depths, and other fragments from above, which must have fallen into the up-welling magma. Generally, the up-welling magma was not hot enough to alter these fragments significantly [2].

1.1 PREMIER DIAMOND MINE

One of the world's largest and most productive diamond mines, the Premier Mine, east of Pretoria, South Africa, has been in operation since 1902 and produces approximately 3 million carats of diamonds per year. It was at the Premier Mine in 1905 that the worlds largest diamond, the Cullinan, weighing 3024 carats, was found [1].

The Premier pipe is a complex multiple intrusion which consists of a variety of diamond bearing kimberlites. This

pipe is intruded by a sill of diamond barren rock known as gabbro. This sill has resulted in problems of access to the kimberlite below the level of the sill.

When mining began at Premier, open cast mining techniques were used. Conventional sub-level or open bench mining techniques were used until the discovery of the gabbro sill, approximately 400m below the surface as shown in Figure 1.1. The gabbro sill is about 75m thick and consists of approximately 52 million tons of rock within the confines of the pipe [3]. The gabbro sill cannot be removed entirely due to its volume and the high cost of removal.

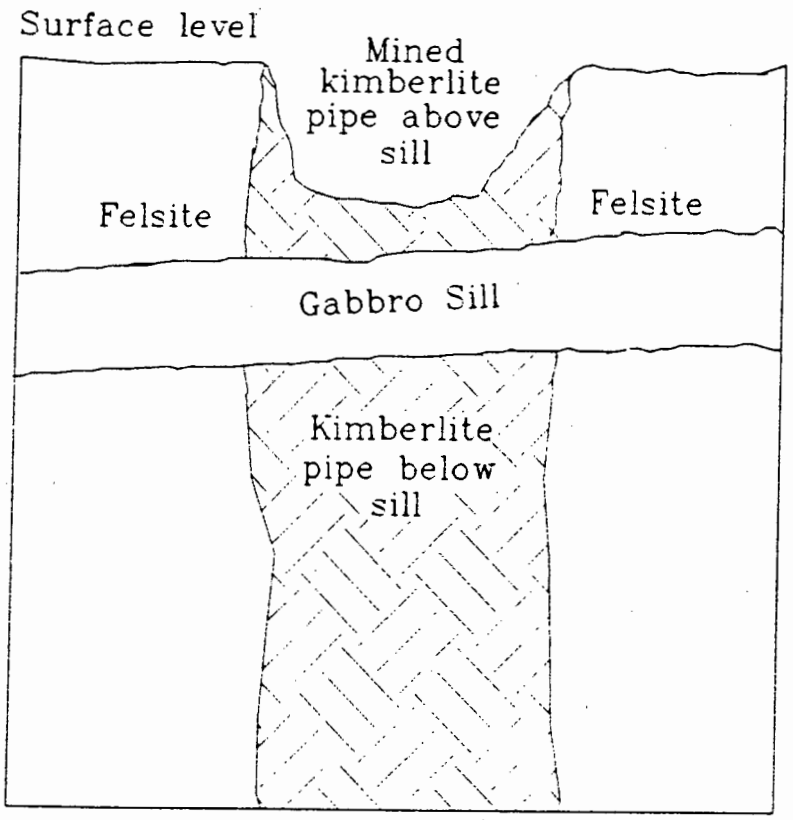

Figure 1.1 Premier Kimberlite pipe in simplified form.

It was therefore decided to mine the kimberlite pipe underneath the gabbro sill. Unfortunately, due to the poor geotechnical properties of the sill, large volumes of gabbro have fallen into the mining area causing large scale dilution of the kimberlite.

The Premier Mine is being mined both above and below the sill but the above-the-sill reserves will be mined-out within a few years. It is anticipated that the below-the-sill mining will be viable for another 25 to 30 years.

The presence of gabbro in the diamond recovery operations creates the following problems:

(a) It reduces the revenue earning capacity of the treatment plant because it displaces the diamondiferous kimberlite.

(b) Gabbro is far more abrasive than kimberlite, produces a high rate of machine wear, and thus increases the plant's operating cost.

(c) Gabbro has a specific gravity causing it to follow the diamond route through the plant. As this process route is designed to condense the diamonds into a low mass, low volume stream, it is, consequently, overloaded when large volumes of gabbro accompany the diamond products [3]. This leads to extensive operating difficulties.

In order to improve the economics of the plant, a means of on-line separation of gabbro from kimberlite was required. There is no existing on-line technique to separate kimberlite from gabbro and the two rock types are very similar in appearance. In this thesis, however, a

successful microwave discrimination technique is described. Before describing the technique, it is important to discuss the properties of minerals in general and the way in which they interact with microwave irradiation.

1.2 PROPERTIES OF MINERALS

Before analysing the properties of minerals, it is essential to define what a mineral is in a generally accepted form. "A mineral is a naturally occurring homogeneous solid with a definite (but generally not fixed) chemical composition and an ordered atomic arrangement"[2]. It is usually formed by inorganic processes.

Gabbro and kimberlite are rock types that have differing properties due to the minerals that constitute them. It is important to know the rock properties of the diamond-bearing kimberlite in order to differentiate it from other type of rock.

1.2.1. KIMBERLITE AND GABBRO

Kimberlite is a diamond bearing rock which is characterized by its black colour due to the presence of dark minerals. The dark minerals are chiefly pyroxene and olivine in varying proportions but hornblende may be present [2]. Since kimberlite is diamond bearing, it may well have properties which, when irradiated by microwaves, cause it to react differently from gabbro. Diamond itself is distinguished from minerals that resemble it by its extreme hardness, adamantine luster and cleavage. Diamond is insoluble in acids and alkalis, and at a high temperature will burn to CO_2 gas leaving no ash. Diamond is a high pressure carbon polymorph with a high specific gravity due to its fairly close atomic packing. The mineral composition of kimberlite differs significantly from the mineral

composition of gabbro and so the rocks may have different electrical properties.

The electrical properties of a rock can be defined by its dielectric constant and loss tangent. These will, in a practical microwave irradiation system, manifest themselves in a reduction in propagation velocity and a degree of absorption within the rock samples. The following tests were conducted to determine if there was a difference between these two rock types.

Firstly, kimberlite and gabbro samples were placed in a domestic microwave oven to try to determine whether kimberlite absorbed more or less microwave energy than gabbro.

After leaving the samples in the microwave oven for the same period, all the kimberlite samples were hotter than the gabbro samples. The experiment was repeated several times and the results were always the same. This shows that kimberlite absorbs more microwave energy than gabbro when irradiated in a closed microwave cavity (microwave oven).

Secondly, kimberlite and gabbro samples were placed in a microwave transmission line test jig, as shown in Figure 1.2. Using a Hewlett Packard 8410 Network analyser at a frequency of 10GHz, the phase shift, or propagation delay, through the samples was measured.

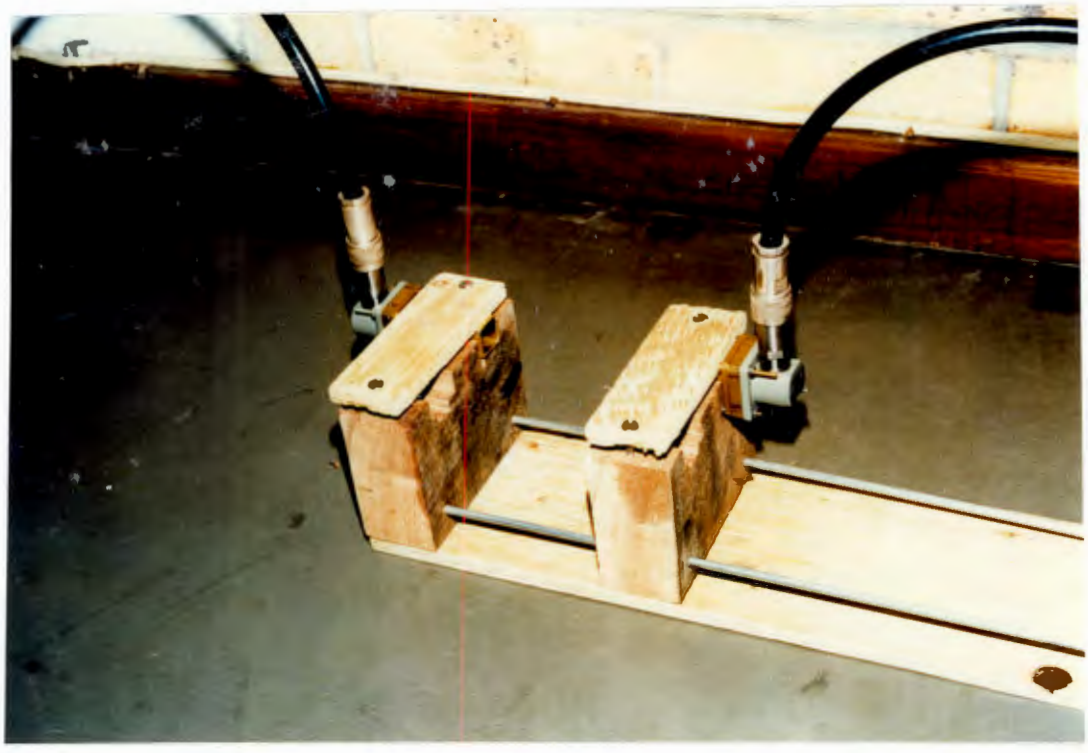

Figure 1.2 Transmitter line test jig.

The kimberlite samples showed a larger phase delay than the gabbro samples. However, the results were variable and inconclusive. The dielectric constant of kimberlite is higher than gabbro, but the difference in absorption between the two rock types was shown to be greater than the difference in propagation velocity. The variation of propagation velocity measured between the kimberlite samples may have been caused by different amounts of moisture within the samples (ϵr of water = 80).

1.3 REVIEW OF THE EXISTING TECHNIQUES

Research in mineral processing has shown that it is possible to differentiate between gabbro and kimberlite rocks using microwave irradiation. Experiments performed by heating gabbro and kimberlite in a domestic microwave oven showed that kimberlite gets hotter than gabbro when heated over the same period of time. This indicates that kimberlite absorbs or attenuates more microwave power than gabbro.

This observation led to a technique of rock differentiation using microwave attentuation measurement. To perform rock differentiation, a microwave transmitter - receiver pair was used. Two methods were investigated in rock differentiation:

(a) phase shift measurement
(b) attenuation measurement

Phase measurement produced good results. However, the technique requires the development of a system with a coherent source and detector. At microwave frequencies this leads to a complex and expensive technique. Attenuation measurements proved to be simpler, cheaper and very reliable.

1.4 THE SCOPE OF THIS THESIS

The objective of this thesis is to re-evaluate the method used previously in differentiating between gabbro and kimberlite and particularly the surface reflection problem so that present problems can be identified and then solved. The investigation of multiple parallel channel operation is reported in order to increase the overall throughput.

The layout of this thesis is as follows:

Chapter 2: the overall system is described with special emphasis on the transmitter and receiver units.

Chapter 3: the effects of frequency and choice of optimum frequency are described. Particular emphasis on rock shape, reflections and antenna size is considered in order to choose the most suitable frequency for the system.

Chapter 4: the effects of polarization are described and the results are presented.

Chapter 5: describes space diversity, what it is, and why it is necessary to employ this method. A method of improving the throughput, multi-channel operations is employed.

Chapter 6: describes the effects of using multi-channel operations.

Finally, Chapter 7 deals with the analysis of results and conclusions.

CHAPTER 2

SYSTEM DESCRIPTION

2.1 INTRODUCTION

A system for separating gabbro from kimberlite was developed by Mercer [3] which recorded the attenuation of microwave signals propagating through individual rock samples travelling along a conveyor belt. The system works well for flat parallel sided rock samples, but problems were encountered with irregularly shaped samples caused by reflections from the surface.

The system was used for the basis of the work reported in this thesis and was extended further to reduce the problem of surface reflections. The system developed by Mercer is shown diagrammatically in Figure 2.1 and consists of a transmitter and receiver pair.

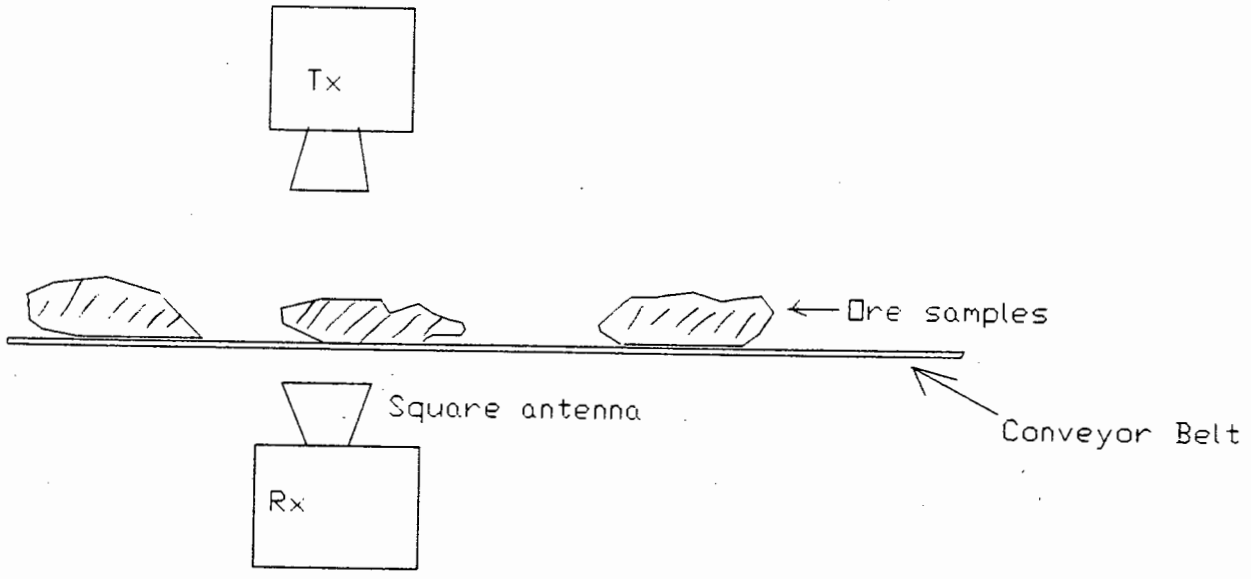

Figure 2.1 Transmitter and receiver pair for rock sorting

The procedure for designing a transmitter and a receiver was determined by the type of microwave components available. A Gunn diode was used as an oscillator to transmit the required microwave signals. At the receiver end, a rectifier or detector diode was used to detect the transmitted signals. Several precautions were taken when designing the transmitter following from the specifications of the Gunn oscillator.

The Gunn diode requires biasing to oscillate at a specified frequency. The specified bias voltage should not be exceeded. Spurious signals from the supply rail can damage the Gunn diode, and this was eliminated by designing a protection circuit which is shown in the transmitter circuit diagram (Figure 2.6). For the Gunn diode to oscillate at its specified frequency, it must be biased above the threshold voltage where negative resistance is greatest.

The transmitter and receiver units were designed so that various microwave sources and detectors could be connected to the same circuits. This design was followed with the aim of investigating effects of frequency by observing the system's performance over a range of microwave frequencies. In order to avoid the problem of drift or DC-offset in the receiver, pulses of microwave power are transmitted. The advantage of this is that the receiver can employ an AC amplifier tuned to the transmitter pulse frequency using chopped DC amplification. Thus the errors introduced by DC amplification are eliminated when a pulsed transmitter is used.

Investigations, using a Hewlett Packard 8410 Network analyser with rock samples placed on a transmission line

test jig as shown in Figure 2.2, led to the design and development of a transmitter and a receiver.

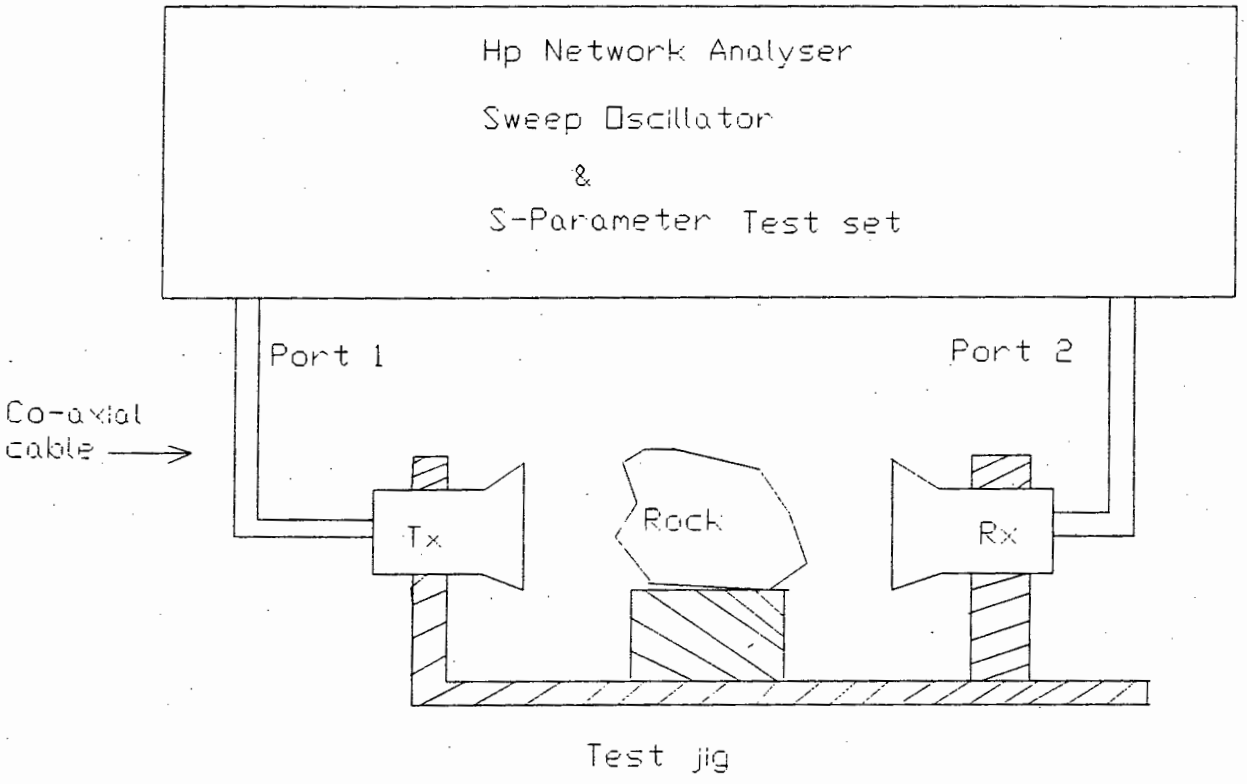

Figure 2.2 S_{21} Measurement for Rock Samples

The transmitter and receiver were developed as separate modules to facilitate the passing of rock samples between them, thus leading to measurement of attentuation as rock samples pass through. The transmitter and receiver are housed in different cabinets as shown in Figure 2.3.

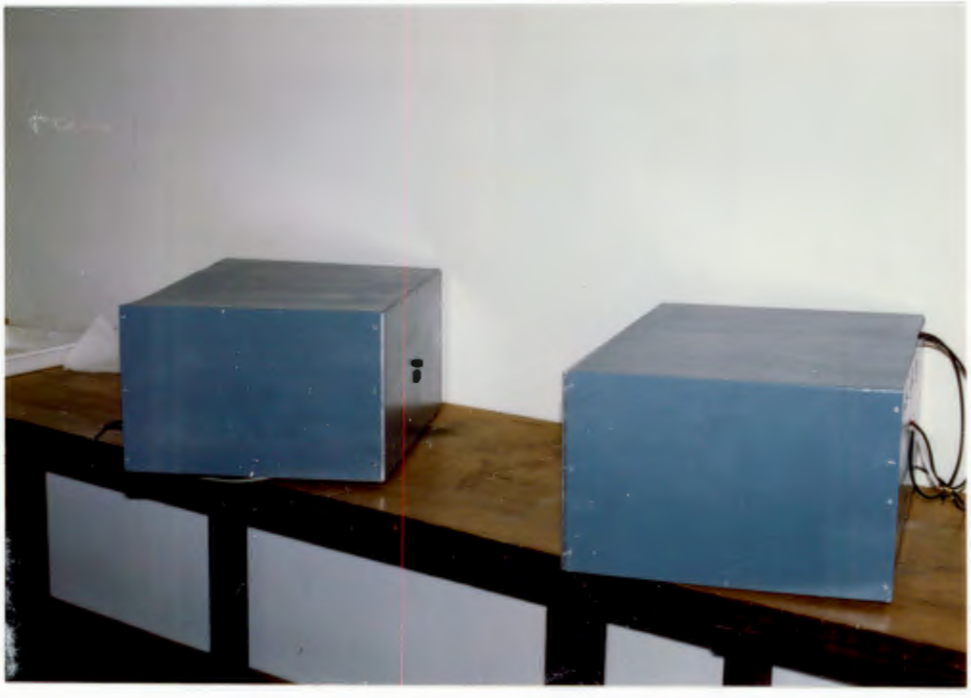

Figure 2.3. Transmitter and receiver modules.

A pulsed transmitter was designed for reasons mentioned above. The transmitter and receiver were powered from the mains. It was decided that separate power supplies be designed for the transmitter and receiver. This eliminates voltage spikes on the supply rail caused by the pulsed transmitter and they affect the operation of the receiver if a common power supply is used. The transmitter and receiver

were housed in separate shielded cabinets to prevent interaction.

The system was designed for operating in a dynamic mode as shown in figure 2.4. This led to the need to take certain precautions. For example, the separation between the transmitter and receiver must be sufficient to allow rocks to pass through and the antennas must be small enough for rocks to completely obscure the microwave beam. The former dictated the minimum power output of the transmitter whereas the latter was dictated by the size of the rocks to be sorted.

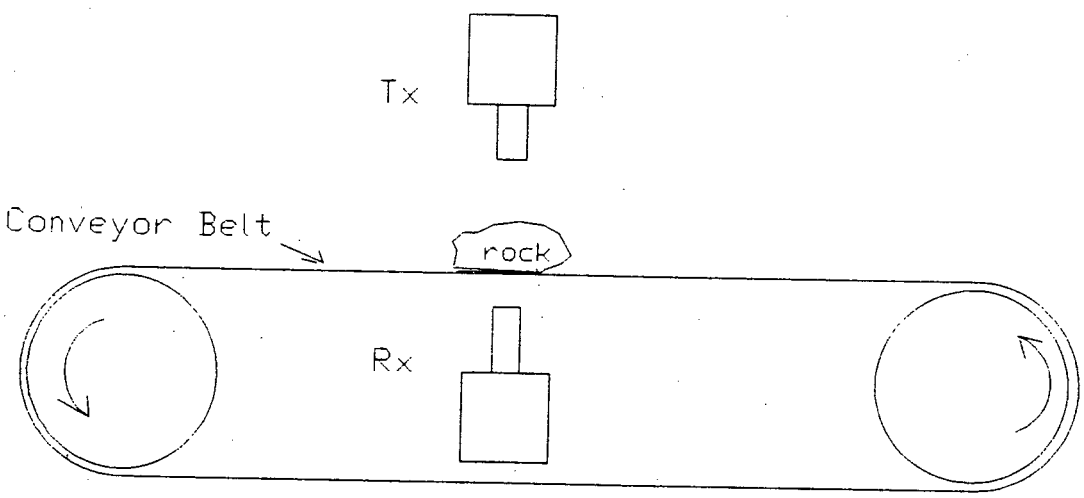

Figure 2.4 Dynamic System Configuration

2.2 TRANSMITTER CIRCUIT DESCRIPTION

In designing any kind of circuitry, it is good practice to follow a top-down design philosophy. This design strategy makes fault-finding and testing easier. The following description is based on this philosophy.

The block diagram which shows the schematic diagram of the transmitter unit is shown in Figure 2.5. As shown in the block diagram the transmitter unit consists of six modules:

(i) an oscillator
(ii) an adjustable attenuator
(iii) a pulse driver
(iv) Gunn source
(v) an Isolator
(vi) an antenna.

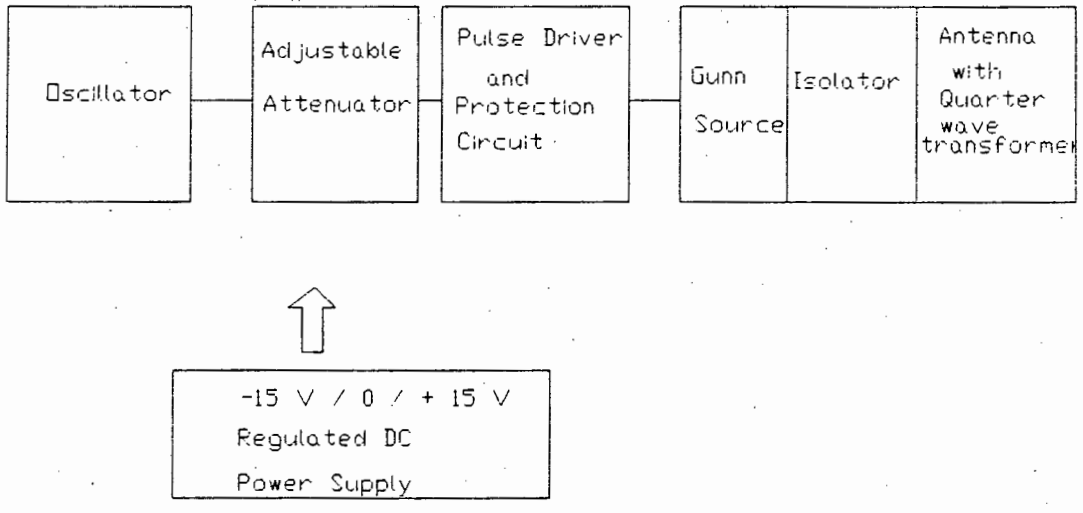

Figure 2.5 Transmitter Module

Three modulation frequencies were chosen to facilitate the use of the three separate channels having three transmitter and receiver pairs. The reason for using three transmitters

and receiver pairs was to reduce errors caused by surface reflections, and reflection from the rocks surface experienced through single Channel operation. This mechanism will be discussed in Chapter 5. The three modulation frequencies chosen were 1KHz, 5KHz and 10KHz.

In describing the transmitter circuitry, a 1KHz oscillator is used as an example and the design procedure is identical for 5KHz and 10KHz oscillators. In designing the oscillator, a 50% duty-cycle square-wave was chosen. This allows for a smooth 1KHz fundamental sine-wave to be obtained at the receiver after band-pass filtering the received signal.

A circuit diagram of the transmitter module, excluding the isolator and an antenna, is shown in Figure 2.6. The oscillator at the initial stage serves to make it a pulsed transmitter unit. The oscillator has a square wave output that drives the Gunn diode and has a fundamental sine wave of 1KHz. Capacitors C_3 and C_4 are power decoupling capacitors. Their function is to eliminate any voltage spike that can appear at the power supply rails. Capacitor C_4 eliminates low-frequency voltage spikes and capacitor C_3 eliminates high-frequency voltage spikes which could not be effectively suppressed by the large capacitance value of C_4.

The oscillator is made up of an LM555 timer chip. The frequency of oscillation is set by the values of resistors R_1 and R_2 as well as capacitor C_2. According to Horowitz and Hill [5], the frequency of oscillation is given by $f_0 = 1.44/(R_1+2R_2)C_2$. In choosing the frequency of oscillation, high-frequency limitations in the stages that follow were taken into account. The output of the oscillator is fed to an adjustable attentuator circuit. This attentuator was chosen to facilitate the adjustment of the voltage amplitude that is required to bias the Gunn Diode thus causing it to

oscillate. The output of the attentuator was limited to ensure that the output voltage peak does not exceed the Gunn diode maximum specified bias voltage.

The LM555 Chip has to deliver only a few milliamperes of current to the attentuator to ensure that temperature stability problems do not occur. The square-wave signal from the attenuator is fed into a non-inverting input of the LF351 operational amplifier which is configured as a follower and is used to drive the base of Tr2, a BC107 small-signal transistor. Transistor Tr_1 and Tr_2, a TIP 31C power transistor pair, are connected in a Darlington configuration to form a high-gain output module capable of delivering output of more than 1 ampere. The switching speed of the circuit is improved by a negative feedback configuration which is achieved by connecting the non-inverting input of the LF351 operational amplifier to the emitter of Tr_2.

The pulse driver consists of TR1 and TR2 connected in Darlington configuration and the LF351 operational amplifier configured as a non-inverting follower. The Gunn Diode requires a maximum threshold current of about 1- Ampere. This warrants the use of Darlington connected TR1 and TR2 to provide the necessary current since the output of an operational amplifier can only supply a few milliamperes of current. The TIP31C (Tr_2) power transistor was well heat-sunk and can deliver up to 3 Amperes of current continuously.

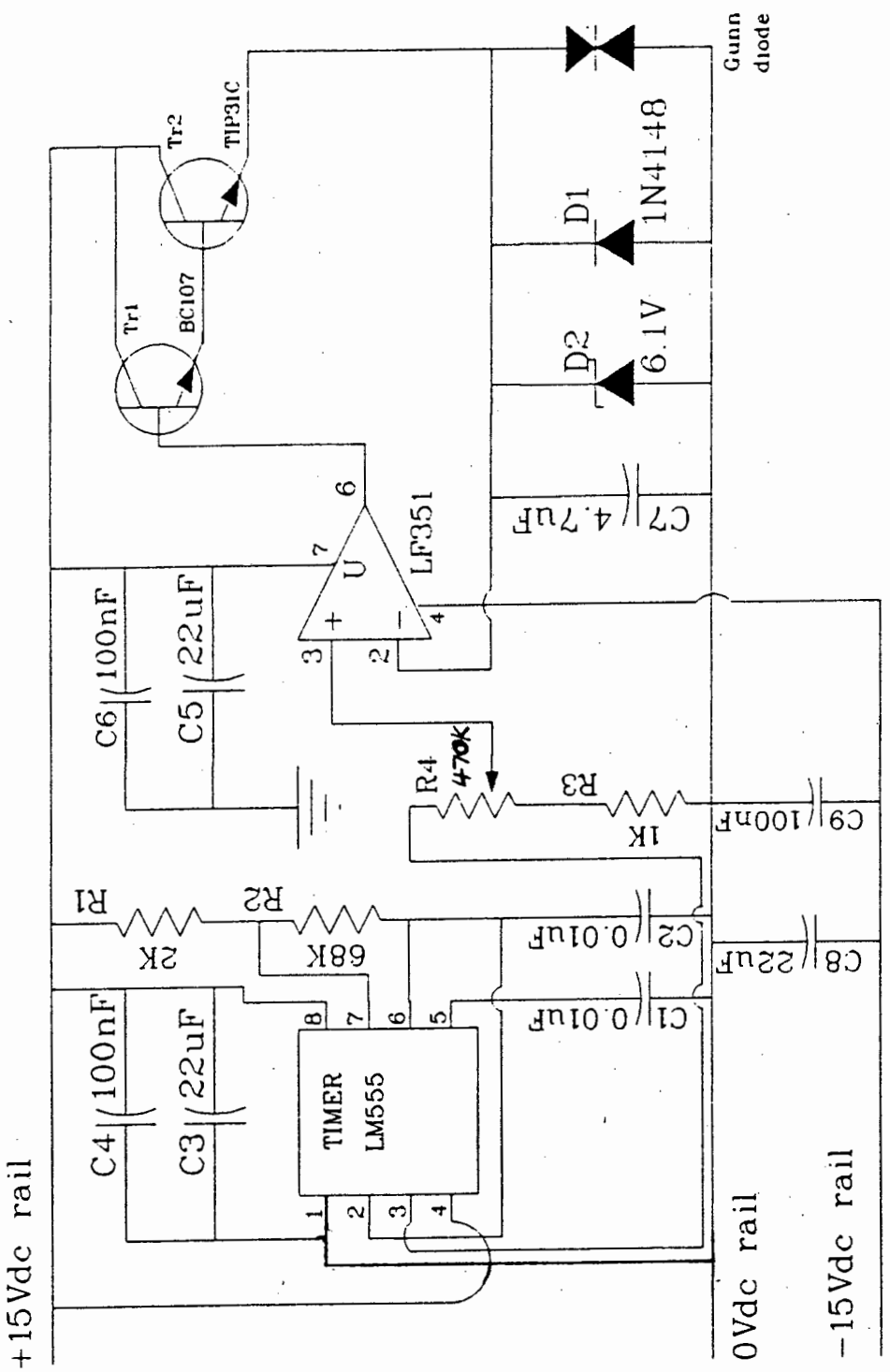

Figure 2.6 Transmitter Circuit diagram

The output voltage droop was tested by using resistive test loads of 1-ampere and no detectable voltage droop was measured.

A protection circuit was designed for the Gunn oscillator and was connected at the output of the pulse driver. This circuit consists of a diode D_1 that prevents damage, which may be caused by reverse biasing the Gunn diode and a zener diode D_2 rated 10V which clamps the square-wave output. The emitter of TIP31C power transistor is fed to the Gunn oscillator.

Capacitor C_7 connected across the Gunn oscillator terminals is used to improve the circuit stability by suppressing bias current oscillations. The rise-time of the pulses applied to the Gunn oscillator is an important factor related to the frequency stability of the oscillator. This rise-time should be as short as possible to reduce the frequency drift of the oscillator. In this application, however, absolute frequency stability is not essential. The amplitude of the received signal is more important than the exact frequency since the technique of attentuation measurement is unaffected by small changes in microwave frequency. The transmitter circuit was mounted on a printed circuit board with the exception of the Gunn oscillator. The printed circuit-board layout is shown in Appendix A.

The Gunn oscillator used in this transmitter is a commercially manufactured unit and needs a bias voltage of 10V to deliver maximum output power. The Gunn oscillator is housed in a metal co-axial cavity which has an X-band rectangular waveguide aperture at its output. The biasing voltage is fed into the Gunn oscillator input via a coaxial cable.

The output of the Gunn oscillator is transmitted by an electrically small antenna which is made up of a square waveguide at X-band frequency. The difference in the impedances between the square waveguide antenna and the rectangular waveguide output of the Gunn source casing required a matching section. An isolator was also used to prevent any small impedance mismatches causing power to be reflected back into the output port of the Gunn source. The arrangement of this microwave front-end is shown in Figure 2.7. The isolator prevents the reflected wave from affecting the operation of the Gunn source.

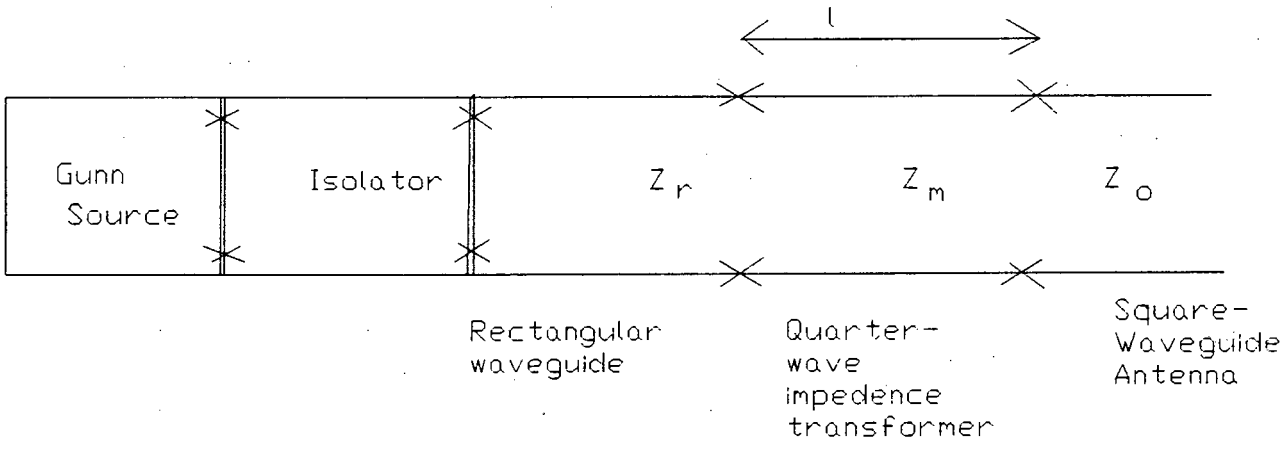

Figure 2.7 Microwave Front End

The matching section is a quarter-wavelength impedance transformer and its length 'l' can be explained as follows:

Consider Z_r as the impedance of the source and Z_0 as the impedance of the load. The difference between the impedances causes the signal transmitted from the rectangular waveguide to be reflected back from the square waveguide and only a certain fraction is absorbed to be propagated through the air.

According to Harvey [6], the impedance Z_r is given by

$$Z_r = Z_m \{(Z_0 + jZ_m \tan\beta l)/(Z_m = Z_0 \tan\beta l)\}$$

where Z_m is the impedance of the matching section
and $\beta = \omega/c$

where ω = frequency in radians
and c = velocity of the wave
down the waveguide.

If $l = \lambda/4$, $\tan\beta l = \infty$ and thus $Z^2_m = Z_r Z_0$. A quarter-wave impedance transformer inverts the terminating impedance which is the impedance of a square waveguide antenna in this case. The design of the quarter-wave transformer is given in Appendix C.

The rectangular to square waveguide transformers were designed for 10.525GHz, 23GHz and 35GHz. The design criteria for square waveguide and rectangular to square waveguide transformer is given in Appendix B.

2.2.1 GUNN DEVICE CONSTRAINTS

Gunn devices are solid state components which are used to generate energy at microwave frequencies from a DC power input. They act as DC converters to microwave energy, using the negative resistance characteristics of bulk gallium arsenide. These devices are commercially manufactured

oscillators that are packed individually in a closed metal casing. They have the following constraints and characteristics:

a) The upper frequency is limited to about 50GHz by the intervalley scattering time known as the domain growth time. For frequencies above 50GHz, Impatt diodes are normally used to generate microwave power.

b) The lower frequency limit of about 4GHz is defined by the heat sinking capability of the thick device, heat is dissipated from one face only. For frequencies below 4GHz transistors are normally used.

c) The maximum power depends on frequency and a C.W. output power of about 500mW is available at X-band.

2.2.2 TRANSMITTER POWER SUPPLY

Nearly all electronic circuits, from simple transistor and op-amp circuits up to elaborate digital and microprocessor systems, require one or more sources of stable DC voltage. Therefore, the description of a transmitter circuit is not complete without its power-supply circuit description.

For the transmitter shown in Figure 2.6 to operate effectively, a +/-15V DC split power supply is required. This power supply was designed to run from 220V AC mains supply. The circuit diagram of the transmitter power supply is shown in Figure 2.8.

The mains supply live and neutral wires are connected across the primary windings of the mains stepdown transformer. A mains switch is used to switch the 220V mains supply. A 1-ampere fuse is connected in series to protect the circuit against current overload.

The secondary winding (centre tapped) of the mains transformer is rated at +18V, and -18V at 1.5A. The output from the transformer is rectified using a full-wave bridge rectifier that can deliver up to 2 amperes of current to the next stages of the circuit. The centre tap on the transformer secondary winding is connected to ground.

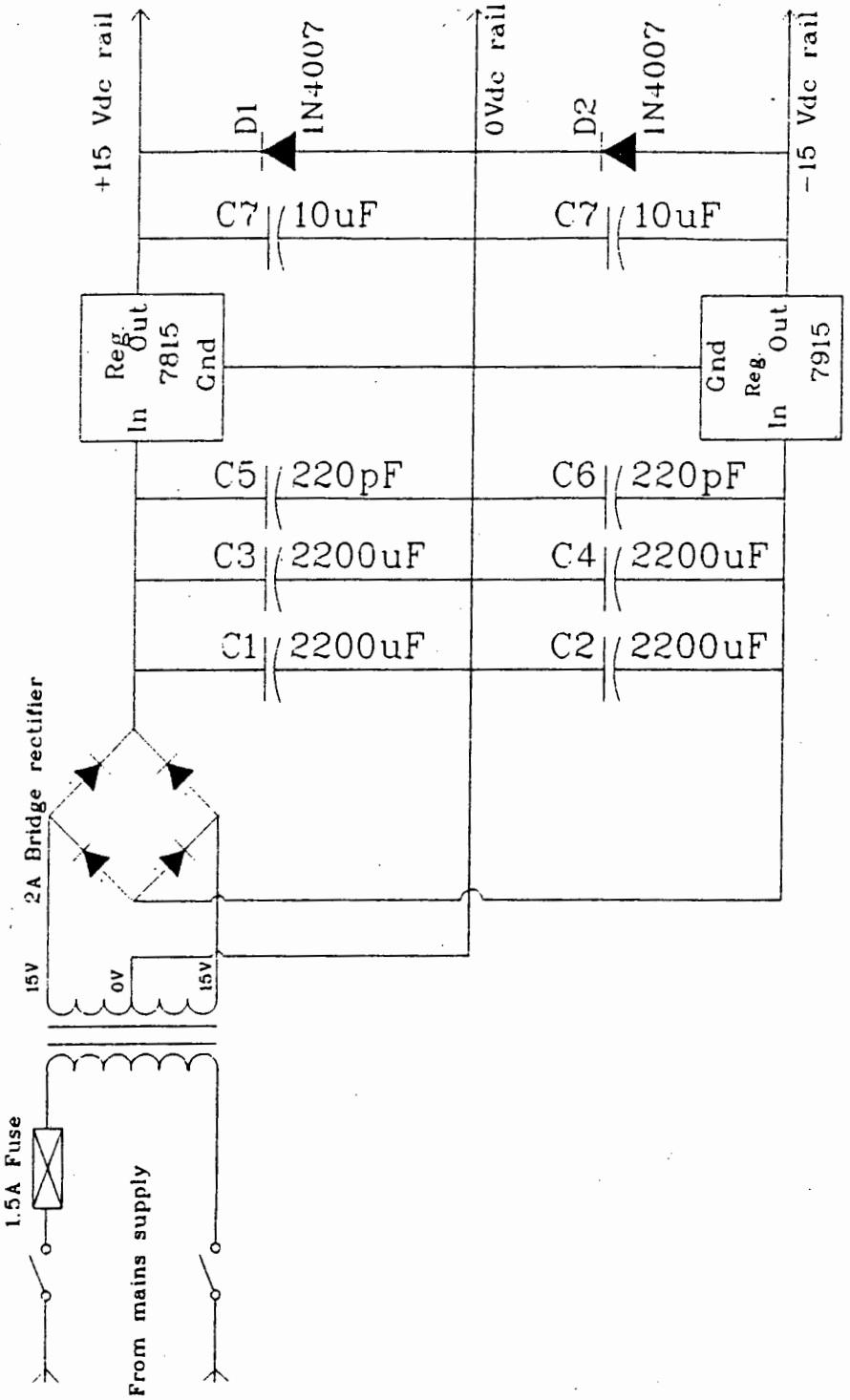

Figure 2.8 Circuit diagram of transmitter power supply.

The positive and negative outputs of the bridge rectifier are both connected to the smoothing circuit. The latter consists of two parallel-connected 2200μF electrolytic capacitors rated at 40V each. High-frequency spikes can occur unexpectedly, but these are suppressed by 220pF capacitor C_5 and C_6, thus eliminating the high-frequency harmonics associated with the spikes. The output of the smoothing circuit is fed into the voltage regulators for both positive and negative DC voltages.

The power supply voltage of the transmitter circuit should not exceed +/-15V, in order to ensure that no damage occurs to components and that the circuit functions properly. Voltage regulators were therefore used. The positive output of the rectifier is connected to a LM7815 voltage regulator to provide a stable +15V power supply rail. The negative output of the rectifier is connected to a LM7915 voltage regulator to provide stability in the negative rail of the split-power supply. According to the specifications, these voltage regulators can provide output currents of up to 1.5A each. To improve thermal stability, the regulators are adequately heat sunk.

In order to ensure proper circuit performance, 10μF tantalum capacitors C_7 and C_8 are connected between the positive and negative outputs of the voltage regulators and the ground rail. These capacitors are used to smooth the +/-15V DC rails if voltage spikes or dip occurs. The output short-circuit protection is provided by diodes D_1 and D_2 connected between each regulator output and ground rail. The +/-15V and 0V power supply is connected to the circuit.

2.3 DESCRIPTION OF RECEIVER CIRCUITRY

The microwave receiver is made up of three main modules, the front-end microwave signal detection module and the signal processing module. The block diagram of the receiver module is shown in Figure 2.9. Three receivers were designed with operating frequencies of 1KHz, 5KHz and 10KHz respectively.

The receiver module provides a continuous 0-5V DC output for interfacing to an A/D card to facilitate data capture by a personal computer. The use of a personal computer enables accurate differentiation betweeen signal attenuation caused by gabbro and kimberlite.

The modulated microwave signal is received via a square waveguide antenna which is similar to the one used in the transmitter module. This antenna is connected to a detector diode through a quarter-wave matching transformer and isolator. The detector diode used is packaged in a metal casing which has a rectangular aperture. These packaged diodes are also suitable for use in coaxial and stripline applications. The configuration of the microwave front-end of the receiver module is shown in Figure 2.10.

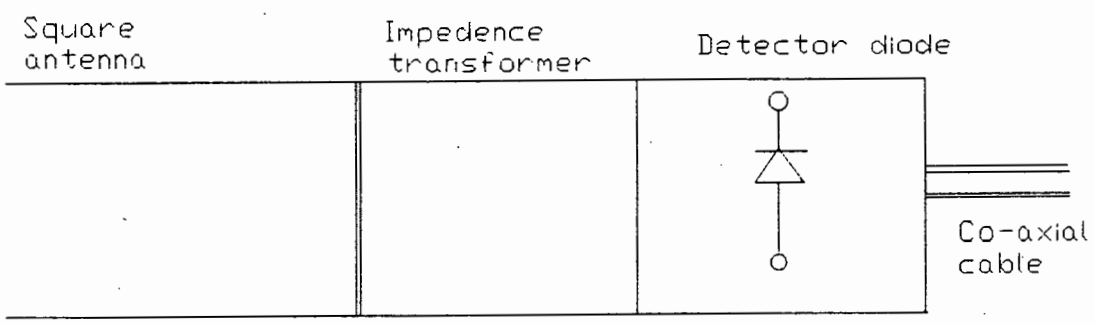

Figure 2.10 Receiver Module Microwave Front-end

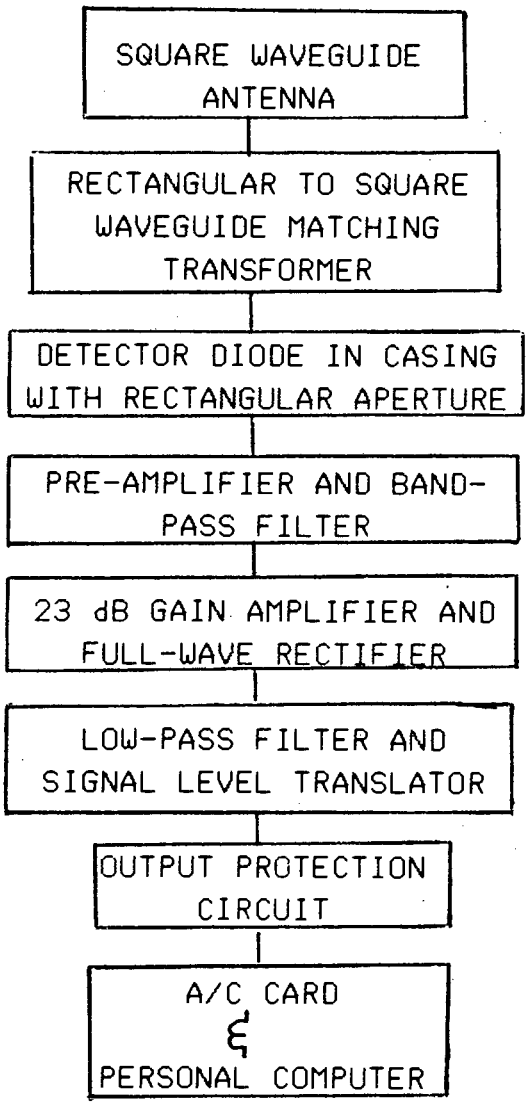

Figure 2.9 Receiver Block diagram

For X-band frequency and using 10.525GHz as centre frequency, the wavelength is given by,

$$\lambda = \frac{c}{f}$$
$$= \frac{3 \times 10^8}{10.525 \times 10^9}$$
$$= 2.85 \times 10^{-2} m$$

The antenna gain can therefore be calculated using equation (1).

$$G = \frac{4\pi \times 5.23 \times 10^{-4}}{(2.85 \times 10^{-2})^2}$$

(where $Ae = 5.23 \times 10^{-4} m^2$)

$$= 8.09$$

Therefore using these parameters, the received power can be calculated given a path length of 2 metres.

The power received by an antenna,

$$P = \frac{P_t G_t G_r \lambda^2}{(4\pi r)^2} \qquad \text{-----(2)}$$

Where P_r = received power; P_t = transmitter power; G_t = transmit antenna gain; G_r = receiver antenna gain and 'r' = path length.

The output power of the Gunn Diode is 10mW, giving the value of P_t in (2) above.

Therefore the received power can be calculated as follows:

$$P_r = \frac{10 \times 8.09 \times 8.09 \times (2.85 \times 10^{-2})^2}{(4\pi \times 2)^2}$$
$$= 8.41 \times 10^{-4} mW$$
$$= 0.841 \mu W$$

This is equal to -30.8dBm. For a given load resistance, the typical performance curves can be used to determine the corresponding output voltage in millivolts. From the performance curves given in Appendix D, the detector diode output at the received power of -30dBm and load resistance of 1.8KΩ is 5.0mV. Measurements of the received signal showed an output voltage of 2.0mV at 1 metre range, and of 0.5mV at 2 metres with the same load resistance.

The output signal of the detector diode is quite small, so that pre-amplification is required before any signal processing can be performed. The LM382 which is used is a low-noise pre-amplifier with a minimum gain of 40dB. This gain was chosen because it proved sufficient to amplify the detector diode output signal without saturating the output of the next stages.

Since the microwave transmitter was modulated, a demodulator of the same frequency is required at the receiver. The receiver modules were designed to operate at any microwave frequency, using the same modulating and demodulating circuits.

Three separate band-pass filters were designed to extract the 1KHz, 5KHz and 10KHz sine-wave fundamental frequencies from the respective square waves. However, as an example, a 1KHz frequency will be used to describe the receiver circuitry.

The circuit diagram of the receiver module is shown in Figure 2.12. Op-amp A1 is a LM 382 low noise pre-amplifier configured to provide a voltage gain of 40dB, as discussed above. This voltage gain is achieved by connecting capacitor C_3 between pin 6 and ground. To improve long-term stability a high quality tantulum capacitor is used.

To ensure a good voltage signal swing, the pre-amplifier is designed to operate from a single power supply so that its output has a large offset. The noise performance of the LM 382 justified its selection. If an amplifier with poor noise performance was used, the output signal of the detector diode would be "buried" in noise and would cause the signal processing module to produce errors. This pre-amplifier is followed by a bandpass filter which also helps to eliminate DC offset.

The active bandpass filter used is a state variable band pass filter. This filter is alternatively called biquadric filter, biquad filter, active resonator or active filter. This biquad filter is much more complex than the equivalent voltage-controlled voltage-source (VCVS) circuits, but it is popular because of its improved stability. It is available as an IC from National but discrete components are used here because the IC was not available at the time of receiver design. Its advantage is that its frequency can be tuned whilst maintaining constant circuit Q. High-pass and low-pass filters are also available.

The three op-amps used are in package LF 347 for thermal tracking. The other advantage of this circuit is that the sensitivity of the centre frequency F_0 and Q to parameter variations is very low. Also high circuit Q's are possible.

The filter is made up of three op-amps, six resistors and two capacitors. The three op-amps are configured as two

integrators (A_3 and A_4) and summing amplifier A_2. The following design procedure was followed:

Design Procedure:

The centre frequency F_0 of 1KHz is used. This centre frequency is given by

$$F_0 = \frac{1}{2\pi}\left(\frac{R_3}{R_4 R_5 R_6 C_5 C_6}\right)^{1/2}$$

and the circuit Q,

$$Q = \left[1 + \frac{R_2}{R_1}\right] \cdot (C_1 R_3 R_5)^{1/2}$$

$$Q = \left[1 + \frac{R_3}{R_4}\right] \cdot (C_2 R_4 R_6)^{1/2}$$

The above equations were derived by Stout and Kaufman [4]. By initially setting $R_3 = R_4$ (fixed resistors) and $C_5 = C_6 = C$ (fixed capacitors), these equations reduce to:

$$F_0 = \frac{1}{2\pi\ (R_5 R_6 C^2)^{1/2}}$$

$$Q = \frac{1}{2}\ (1 + \frac{R_2}{R_1})\ (\frac{R_5}{R_6})^{1/2}$$

For example, R_5 and R_6 may be gauged pots with identical resistance. In this case R_5/R_6 equals unity and the

circuit Q depends only on R_1 and R_2. If the common value of R_5 and R_6 is called R, the equations reduce to

$$F_0 = \frac{1}{2\pi RC}$$

and

$$Q = \frac{1}{2R_1}(R_1 + R_2)$$

The pots R_5 and R_6 are used to set the centre frequency F_0 while R_2 is used for Q adjustment.

With a chosen bandwidth of 200Hz the upper and lower frequency at the half power points is 1100Hz and 900Hz respectively. This bandwidth was chosen because its upper frequency is much less than the centre frequencies of the other two band pass filters. The bandwidth leads to a Q of 5 : $Q = \frac{F_0}{B_w}$ The circuit Q depends on R_2.

The gain of the band-pass filter at resonance depends on R_1 and R_2, thus the gain depends on circuit Q. To keep the gain low, to prevent saturation in the next stages, it was concluded that a Q of 5 is sufficient.

The gain at resonance, $H = R_2/R_1$ and also $R_2 = R_1(2Q - 1)$. From D.F. Stout and M. Kaufman [4], the following design steps were followed.

1. $R_4 = R_3 = \frac{10^8}{F_0}$
   $= 100K\Omega$
2. $C_5 = C_6 = \frac{10^{-7}}{F_0} = 100PF$
3. $R_6 = R_5 = \frac{1}{2\pi F_0 C}$
   $= 1.592M\Omega$

4. $Q = \frac{R_1 + R_2}{2R_1}$

with Q of 5 the above expression becomes

$5 = \frac{R_1 + R_2}{2_1}$

$9R_1 = R_2$

From these results, the gain is 9 which is 19.1dB. To obtain the value of R_2 set $R_1 = R_3$, thus R_1 = 100kΩ and R_2 = 900KΩ.

The component values used were the nearest E-12 resistor values and available capacitors. These values, however, did not change significantly the centre frequency of the band-pass filter. High Circuit Q values can be chosen to eliminate high-frequency square-wave harmonics. The band pass filter was tested and the centre frequency was found to be 995Hz. The difference in centre frequency between the theoretical and measured value is due to the rounding-off error when choosing the nearest manufactured resistor value.

The output of the bandpass filter is a sine-wave of the same frequency as the modulating frequency. This output is fed to the next stage via an AC coupling capacitor C_7. This stage amplifies the sine-wave signal. The LF351 operational amplifier is configured as non-inverting with a gain of 23dB determined by resistors R_{10} and R_{11}. The gain is given by the ratio $(R_{10} + R_{11})/R_{11}$. Resistor R_7 provides a DC path for the AC coupled stage. Resistor R_9 is used to adjust the gain of the amplifier. The output of the amplifier is then fed into a full-wave rectifier which is achieved by using an optional inverter configuration. This is switched using an active clamp. The active clamp is formed by A_6 and D_2 and switches the optional inverter which is formed by A_7 op-amp and resistors R_{12}, R_{13} and R_{14}.

The output of the full wave rectifier is low-pass filtered using an RC passive filter which is made of R_{14} and C_8. This output is then fed to a voltage scaling-circuit made of A_8 and R_a and R_b resistors. The circuit provides voltages of 0 to 5V. But, a protection circuit is required to prevent this voltage range from being exceeded, thus damaging the A/D converter card which is fed from the voltage-scaling circuit. The protection circuit is made of D_3 and D_4.

The voltage is prevented from going beyond 5V by D_4 at the A/D card input, and D_3 prevents damage which might be caused by a negative going output. In the final stage the A/D card is connected to a personal computer to facilitate accurate data capture and fast data processing.

The receiver circuit was constructed on a printed circuit board and the layout of the printed circuit board is shown in Appendix E. The signal scaling circuit was constructed on a vero-board and the receiver module was tested using a laboratory bench power supply operating at +12V/0V/-12V. The last step in the design of the receiver module was the power supply.

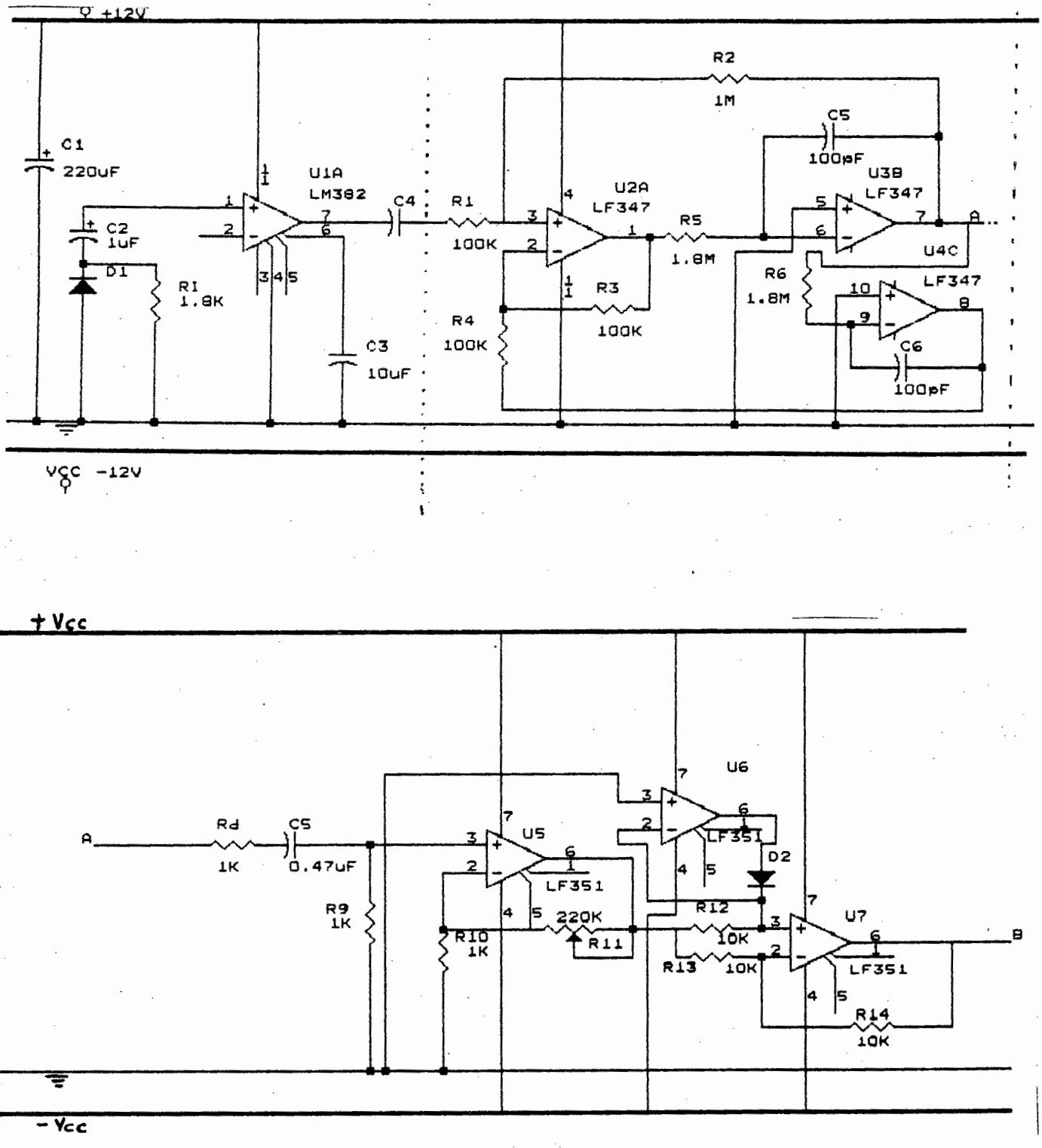

Figure 2.12a Receiver Circuit Diagram

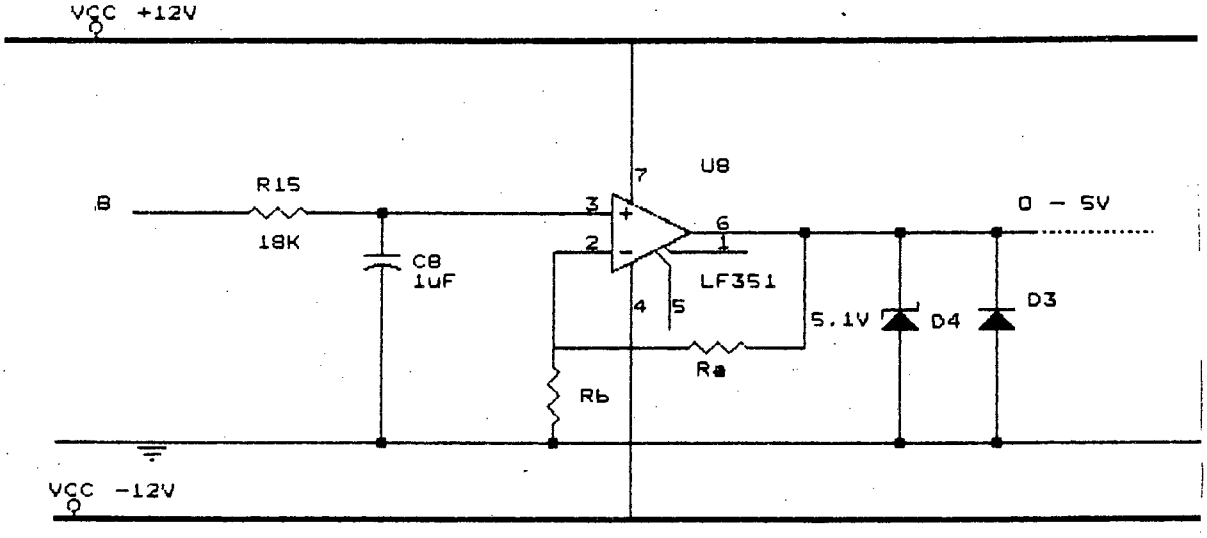

Receiver output circuit

Figure 2.12b

2.4 RECEIVER POWER SUPPLY

The receiver circuitry required +12V/0V/-12V DC voltage power supply. This power supply circuitry is shown in Figure 2.13. The +/- 12V power supply is chosen to suit the power supply requirements of the receiver components and the availability of a suitable mains transformer. The circuit diagram is similar to the one used for the transmitter power supply.

The primary side of the mains step-down transformer is connected to the 220V mains supply by means of a switch and in series with a 1-ampere fuse for protection. The centre-tap of the secondary transformer is connected to ground. The secondary winding is rated at 2A. The output of the secondary winding is full-wave rectified, using a 1A bridge rectifier. The positive output of the rectifier is connected to a 7812, 12V voltage regulator to provide a positive 12V rail. The negative output of the rectifier is connected to a 7912, 12V voltage regulator to provide a negative voltage rail.

The rectifier uses capacitors C_1 and C_2 for smoothing. These are electrolytic connected between ground and +/- 12V rails. The small ceramic capacitors C_3 and C_4 connected in parallel with C_1 and C_2 eliminate high-frequency voltage spikes that may occur.

To ensure smoothing of 12V rails, tantalum capacitors C_5 and C_6 are connected between regulator outputs and ground. The voltage regulators are heat sunk to improve thermal dissipation. The voltage regulators can deliver up to 1 amp if required, without exceeding their rated current. Protection Diodes D_1 and D_2 are provided and they protect the power supply from the output short circuit.

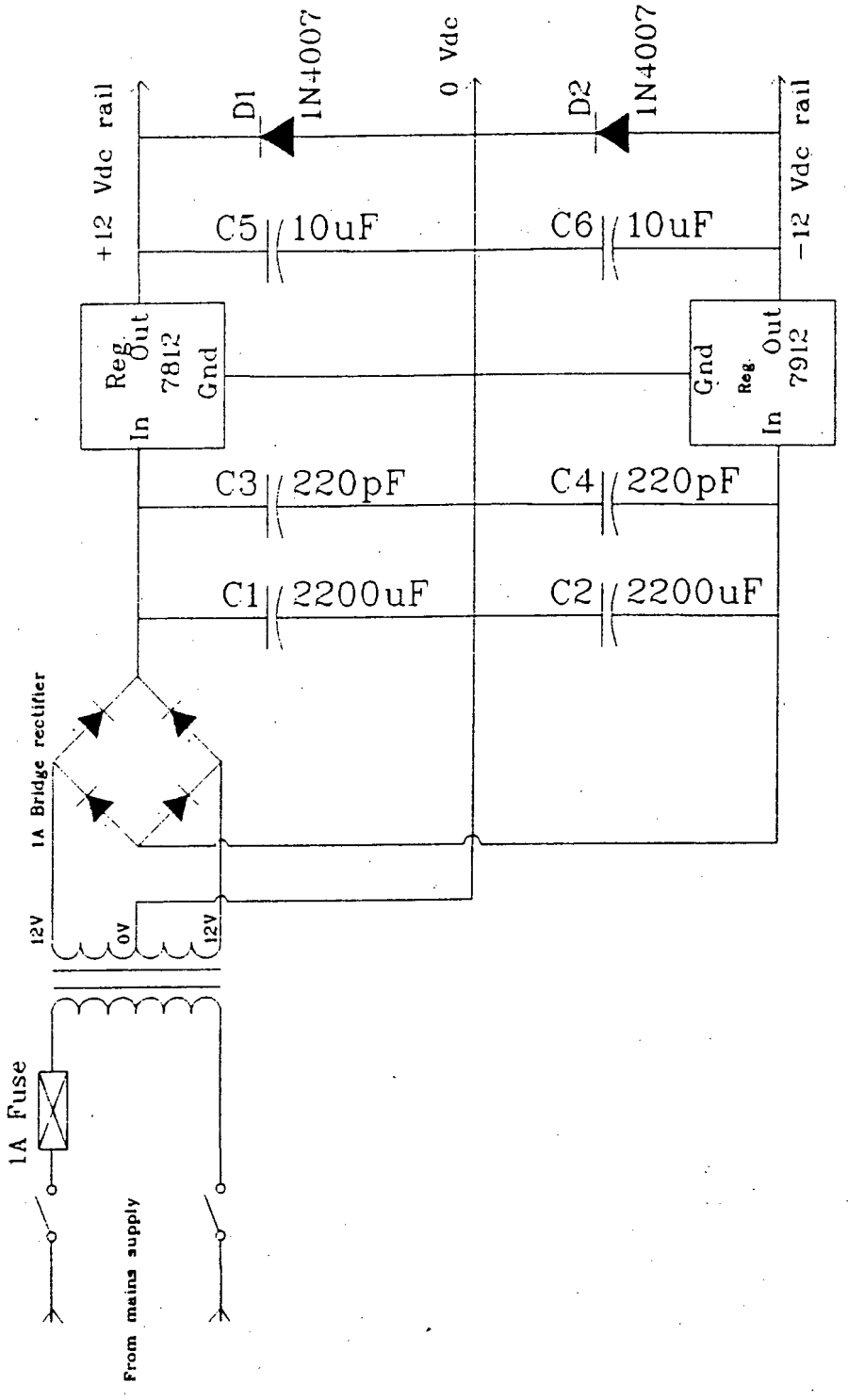

Figure 2.13 Receiver power supply

With the exception of the transformer, the components of the power-supply unit are mounted on a printed circuit board as shown in Appendix F.

2.5 TRANSMITTER AND RECEIVER PERFORMANCE

The transmitter and receiver modules designed above were fabricated and tested. The receiver range performance was tested over 1 metre and 2 metre transmitter and receiver separation. It was found that the detector diode output with 1.8KΩ load resistance is 2mV and 0.4mV at 1 metre and 2 metres respectively.

The theoretical received signal was calculated in section 2.3, and the Gunn Diode oscillator output power of 10mW used as quoted by the manufacturer. This gave the maximum detected signal when the transmitter delivered maximum power. The received power was calculated as 8.4×10^{-4}mW. This was converted to dBm in order to use the given curves from the Microwave Associates' solid state device catalogue and reproduced in Appendix D to obtain the received signal in volts. The actual transmitted power measured was 9mW with the bias voltage of 9V.

$$\text{The received power in dBm} = 10 \log (8.41 \times 10^{-4}\text{mW})$$
$$= -30.8\text{dBm}$$

Graphs shown in Appendix D were used to convert from power to volts. With a load resistance of 1.8KΩ, the received power converts to a signal strength of 5mV. The range performance at 1.8kΩ load resistance was satisfactory. However, as discussed in section 2.3 amplification is necessary before signal-processing is performed. Therefore, the range performance is adequate over a distance of 2 metres and the 0.4mV received signal justifies the choice of the amplifier gains.

2.6 CONCLUSIONS

The transmitter and receiver circuits discussed in this chapter were tested and the performance was satisfactory. The required range performance was achieved.

CHAPTER 3
EFFECTS OF FREQUENCY
3.1 INTRODUCTION

It is important to investigate the effects of various microwave frequencies on the system performance for discriminating between gabbro and kimberlite. After this investigation a choice of a frequency for the ore sorting system is made, based on the system performance at various frequencies.

The variation of attenuation with frequency at microwave, frequencies from 1GHz to 35GHz, with detailed measurements at 1GHz, 3GHz, 10.525GHz, 23GHz and 35GHz was investigated. These frequencies were chosen according to the availability of microwave components and antennas. With the exception of 1GHz and 3GHz, the last frequencies belong to the frequency band X-band, K-band and Ka-band. Because of their common usage, equipment at these frequencies is easily available. For low frequencies such as 1GHz and 3GHz, transistors were used as oscillator building blocks, whereas for frequencies above 4GHz, Gunn Diodes were used as microwave oscillators.

At low frequencies, waveguide antennas have large apertures. They are therefore not utilised, as the rocks to be sorted are too small the receiver antennas cannot be completely obscured by rock samples. Use of high frequencies seems more practical because the antenna aperture size is small, and is thus suitable for the required application. There are certain drawbacks associated with using high frequencies. The surface reflection is the most dominant problem, and it will be discussed later. The optimum frequency at which the attenuation measurement system operates is chosen by comparing the results obtained from all the defined frequencies.

3.2 SYSTEM USING ELECTRICALLY SMALL ANTENNAS AT LOW FREQUENCIES

For low frequencies like 1GHz and 3GHz, electrically (and mechanically) small antennas are required. Two options were considered: resonant patch antennas and dielectrically loaded waveguide antennas. The antenna aperture for these antennas could be reduced by using high dielectric material. Resonant patch antennas were used to investigate the effect that rock samples, passing in close proximity, have on the antenna resonant frequency. A Hewlett Packard network analyser as shown in Figure 3.1 was used to measure resonant frequency of the patch antenna.

Figure 3.1 Resonant Patch Antenna frequency measurement

The rock samples were passed manually in front of the resonant patch antenna with the result that resonant frequency changed. This was caused by the rock coupling to the field as the dielectric body, thus modifying the resonant structure. If this type of antenna is used both as a transmit and a receiver antenna, a shift in resonant frequency will occur and the antenna system will cease to operate.

The wavelength at 1GHz is 30cm and the rocks to be sorted are typically 5cms to 10 centimetres. Consequently the aperture of the waveguide antenna will be large if waveguide antennas are to be used. By loading a waveguide with the substrate material from the R.T. Duroid 6110 (ϵ_r = 10) printed circuit board, the linear dimensions can be reduced by $(10)^{\frac{1}{2}}$ = 3.16 times. This will be too large for a 1GHz waveguide antenna. However, at 3GHz the wavelength is 10cm, and thus the aperture size of the waveguide antenna should be $\lambda/2 < a < \lambda$ which is approximately 7cms. To reduce the aperture size without changing the operating frequency, the waveguide antenna was loaded with this dielectric material which reduced the size to $7/3.16$ = 2.2cms. This was small enough to ensure that the smallest rocks of 5cms would obscure the microwave beam between antennas of this size.

The 3GHz oscillator was designed using a transistor varactor tuned oscillator (VTO). The microstrip mask for this oscillator is shown in Figure G.1 of Appendix G. The advantage of reducing frequency is that the effect of surface reflections (to be discussed later) is less at low frequencies. In designing electrically small antennas, the following design guide lines were considered.

a. In a dielectrically loaded waveguide, for the same cut-off frequency as an air filled waveguide, the cross sectional dimensions and waveguide wavelength are reduced by a factor of the square root of the dielectric constant (ϵ_r) [6]. The material chosen was a low loss R.T. Duroid 6010 with a dielectric constant $\epsilon_r = 10$. This printed circuit-board material was used to load the waveguide, thus reducing the aperture size by $(10)^{\frac{1}{2}}$.

b. The reduced aperture is made up of two sections: the air-filled waveguide and the dielectrically loaded section. To join the two sections, tapering was required to reduce the impedance mismatch between these two sections. The aperture of the dielectrically loaded antenna at 3GHz is approximately equal to the aperture size of a 10.525GHz air-filled square waveguide antenna. This antenna is shown in Figure 3.2. The design of the electrically small S-band antenna and a description of the S-band oscillator is given in Appendix G.

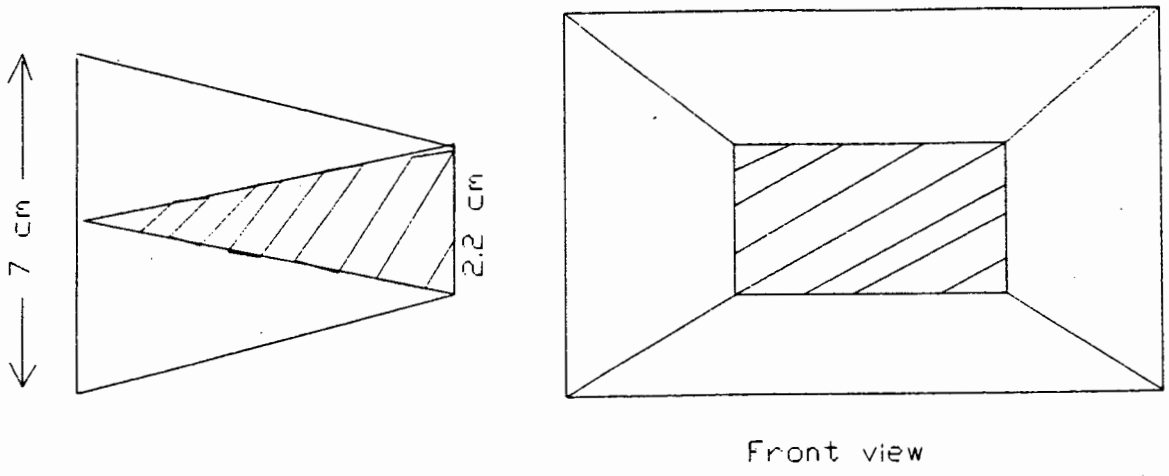

Figure 3.2 Dielectrically Loaded and Tapered Antenna

The 3GHz dielectrically loaded antennas enable lower frequencies to be compared with higher frequencies and still satisfy the requirement that the antenna apertures are fully obscured by a rock passing between them. This antenna is non-resonant and, unlike the resonant patch antennas, its frequency response is not affected by the rocks passing close to the apertures.

3.3 VARIATION OF ATTENUATION WITH FREQUENCY

Investigations were carried out at frequencies of 3GHz, 10,525GHz, 23GHz and 35GHz, to determine whether the optimum signal attenuation varies with frequency. Attenuation measurements, due to rock samples of various sizes, were

performed over a wide range of frequency. The aim of the experiment was to determine if there was any particular microwave frequency that could show a large difference in attenuation between gabbro and kimberlite rocks.

Experiments performed by Mercer [3] using smooth-surfaced, parallel-sided rock samples of different sizes showed that there is an attenuation difference between gabbro and kimberlite. The experiments are repeated here for randomly shaped rocks. The block diagram for the equipment used is shown in Figure 3.3.

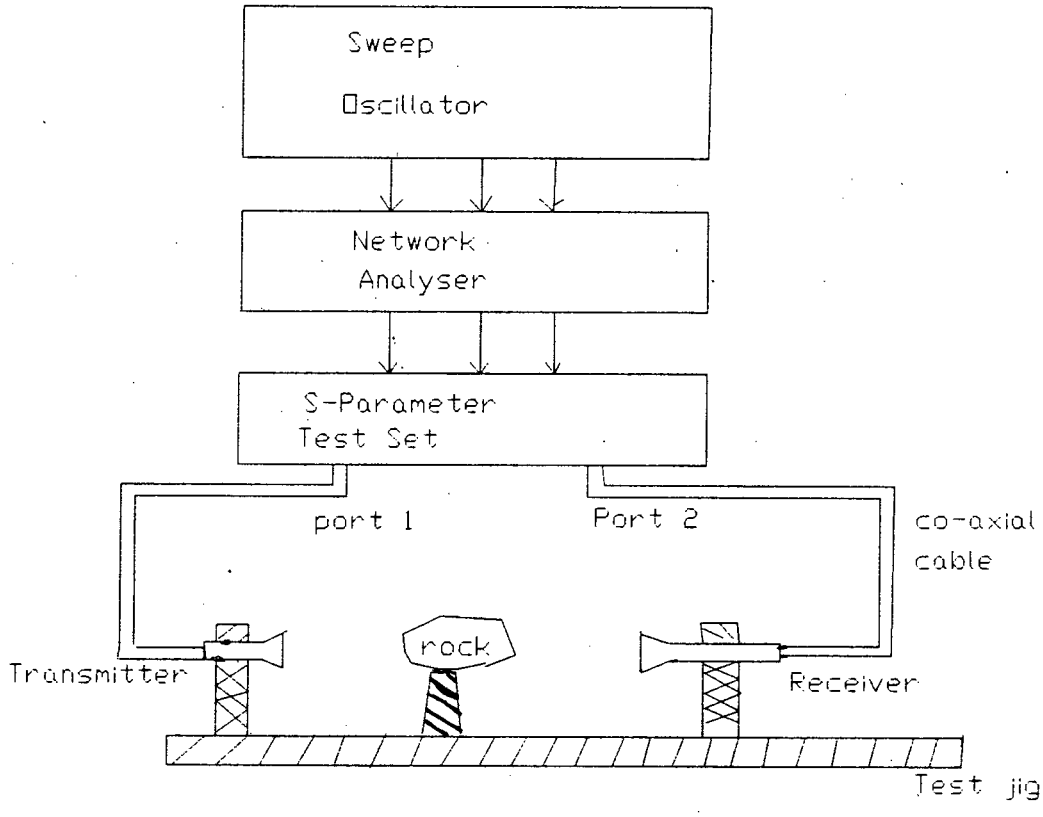

Figure 3.3 Measurement of attenuation variation with frequency

The equipment shown in Figure 3.3 was set to measure S-parameter S_{21} over a frequency range of 3GHz to 16GHz. This measurement of insertion loss is the attenuation caused by rocks of known sizes and irregular shape. The average attenuation per centimeter for smooth-surfaced and parallel-sided rocks, for gabbro and kimberlite at 3GHz, are 0.44 dB/cm and 2.01 dB/cm respectively. Also at 10.525GHz, gabbro and kimberlite gave an average attenuation per centimeter of 0.49 dB/cm and 2.18 dB/cm respectively.

The randomly shaped rocks were also measured and the average attenuation of gabbro and kimberlite was found to increase with frequency. To quote any figures here would be misleading as attenuation was found to be orientation-dependent and shape-dependent. However, from the measurements performed it can be concluded that attenuation increases with frequency.

This result is expected, as the higher frequencies have a greater number of wavelengths present over the same fixed distance, compared to low frequencies, and the attenuation per wavelength is fairly constant. The number of wavelengths attenuated by rock samples is, therefore, greater at high frequencies than at low frequencies. This argument justifies the conclusion drawn from the experiments performed: attentuation increases with frequency.

It would appear that higher frequencies have the dual advantages of a greater attenuation (thus a greater attenuation difference between gabbro and kimberlite) and easily designed small antennas. Meanwhile surface reflections dominate at higher frequencies. Surface reflections are low at 3GHz but the attenuation difference is not high enough. As the operating frequency increases the attenuation difference becomes greater. At the same time the effect of surface reflections increases. Thus,

attenuation becomes more dependent on the rock shape and orientation than the rock type. The mechanism of surface reflections is described below.

3.3.1. SURFACE REFLECTIONS

Measurement of surface reflections proved to be a difficult task. Distinction was made between the reflections from the rock surface and reflections from the bench top where the test jig was placed. Investigations of rock surface reflections were carried out using the configuration shown in Figure 3.4.

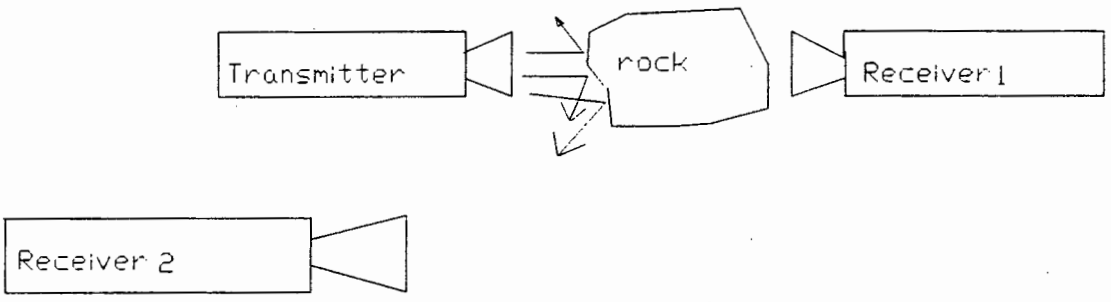

Figure 3.4 Measurement of Reflections

The receiver was placed in a position outside the beamwidth area of the transmitter so that any signal reflected from the rock surface can be detected. The receiver was also placed on top of the transmitter and it was found that the microwave signals are reflected from the rock surface. The magnitude of the reflected signal depends on the angulations present on the randomly shaped rocks. Measurement of surface reflections was further carried out using the configuration in Figure 3.5.

The test jig was placed flat on the laboratory bench top. In theory, when a receiver is moved away from the transmitter, the received power should follow an inverse square power low i.e. $P_r \propto \frac{1}{r2}$

where 'r' is the separation between the transmitter and the receiver.

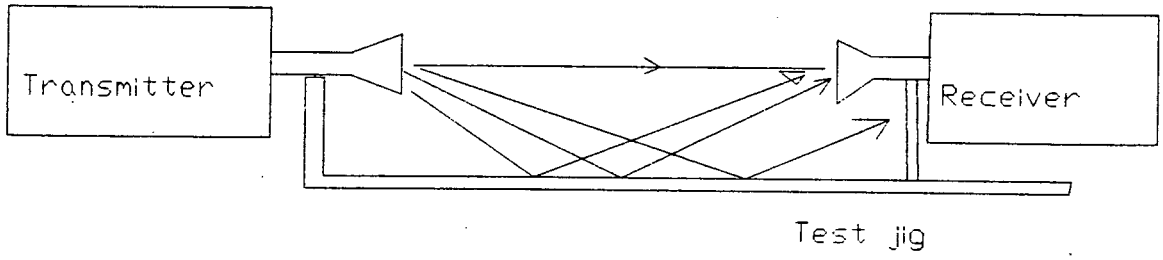

Figure 3.5 Investigation of Surface Reflections using flat test jig.

The transmitter and receiver used for this investigation both operate at defined frequencies. Surface reflections in this case were investigated without rock to obstruct the microwave beams. When the receiver was moved away from the transmitter it was found that the received signal goes through peaks and nulls as shown in Figure 3.6.

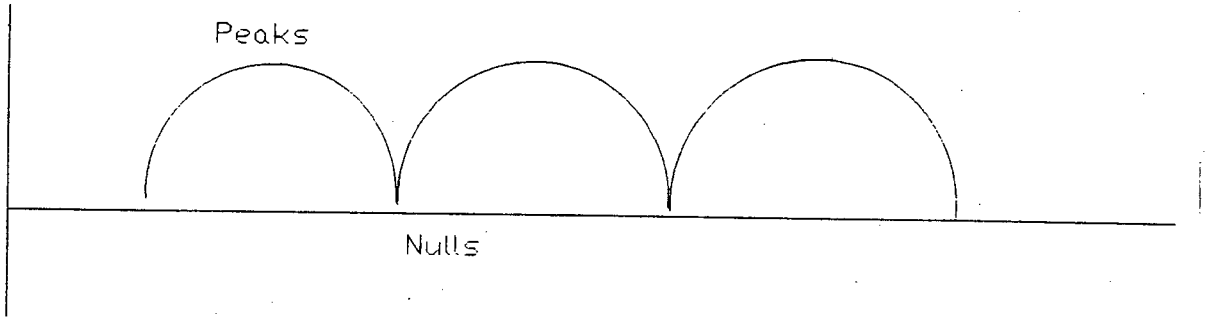

Figure 3.6 Received Signal while moving receiver

The surface reflections cause signal cancellation at certain points and signal addition at other points. To ensure whether these surface reflections do exist an absorbent foam or lossy foam was used to absorb all the microwave signals reaching the horizontal surface of the test-jig. It was then found that with the foam in place, the received power follows the inverse square power law although this is not exact. Results of this investigation are shown graphically in Figure 3.7. The theoretical received power is shown in Figure 3.8.

In measuring the received power at various distances, an HP power meter was used. A method of eliminating the effect of surface reflections was to design a test jig that will compensate for the microwave beam reflected from the surface. This test jig is shown in Figure 3.9a. Results using this test jig show that the reflections are highly reduced because the received power approximates the inverse square power law. These graphical results can be compared with the theoretical curve in Figure 3.8. The "reflection free" test jig was designed for the purpose of performing static tests with minimum effect of surface reflections.

The effect of surface reflections using the frequencies of 3GHz, 10.525GHz, 23GHz and 35GHz, proved to be high at higher frequencies and low at lower frequencies. A comparison of results leads to the conclusion that the optimum frequency, considering antenna size, attentuation and surface reflections is 10.525GHz.

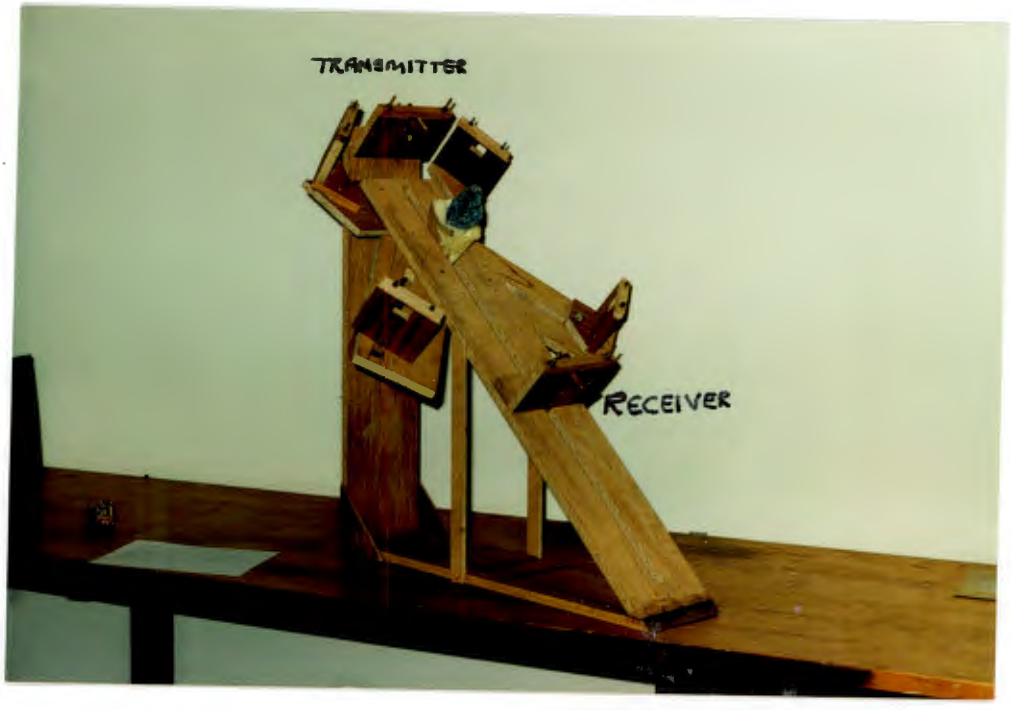

Figure 3.9a "Reflection Free" Test-Jig

The magnitude of the effect of reflections can be seen from graphs in Figures 3.7 to 3.9b.

The static tests were performed using the above test jig which eliminates the effect of signals bouncing from the bench. The transmitter and receiver are at 45° from the bench top, thus preventing the signal reflected from the surface from reaching the receiver.

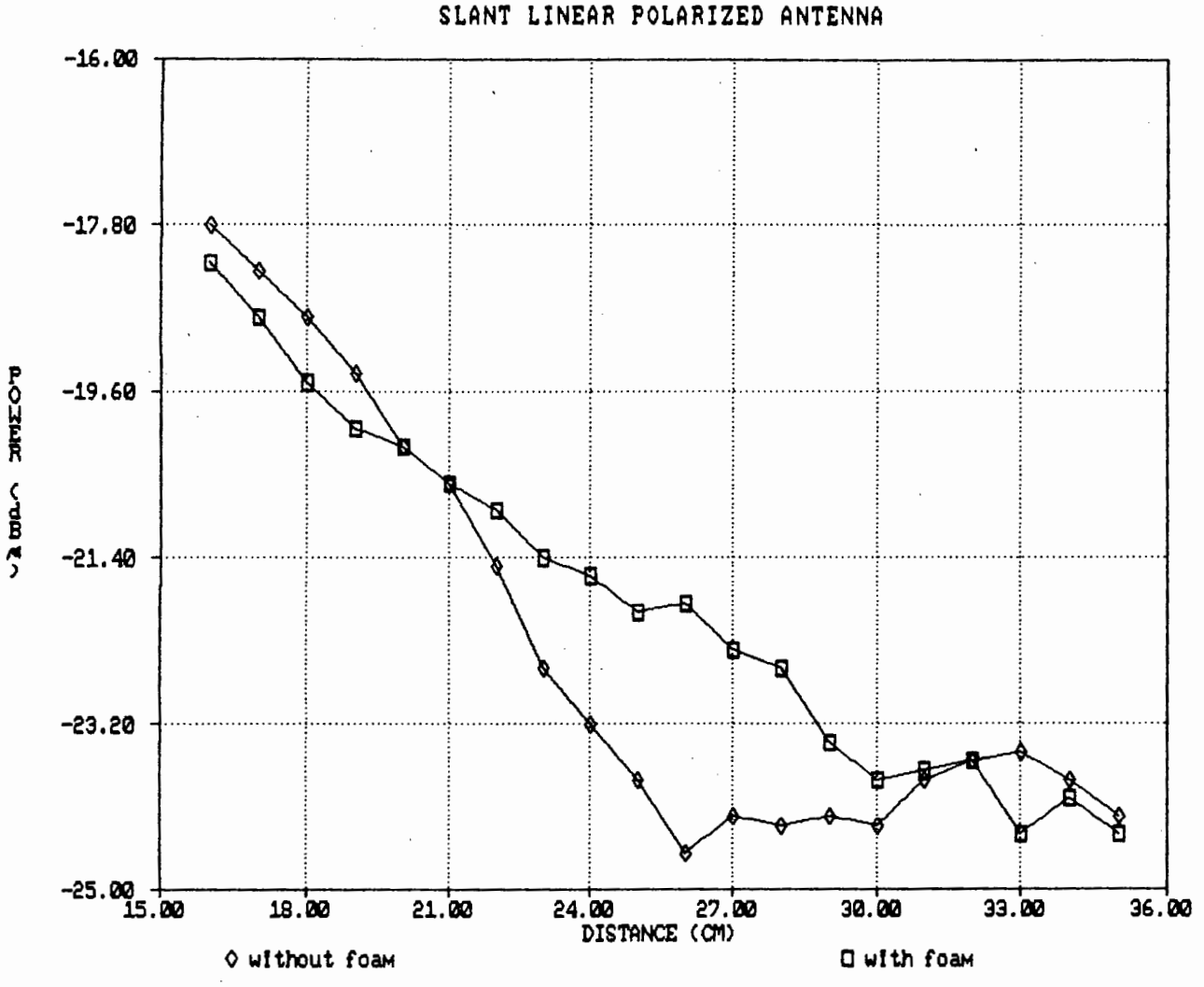

Figure 3.7 Effects of Reflection on Receiver Power

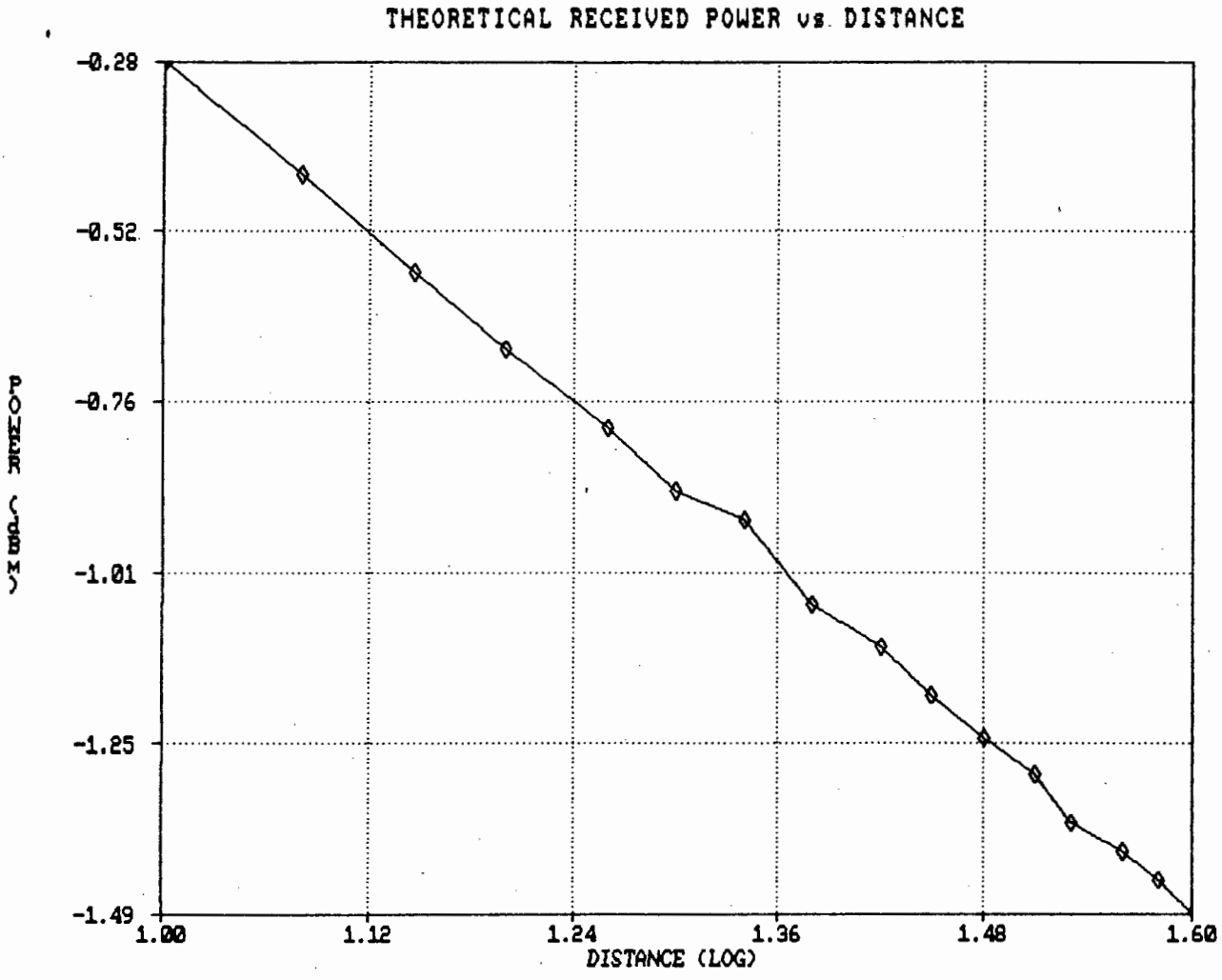

Figure 3.8 Theoretical Curve

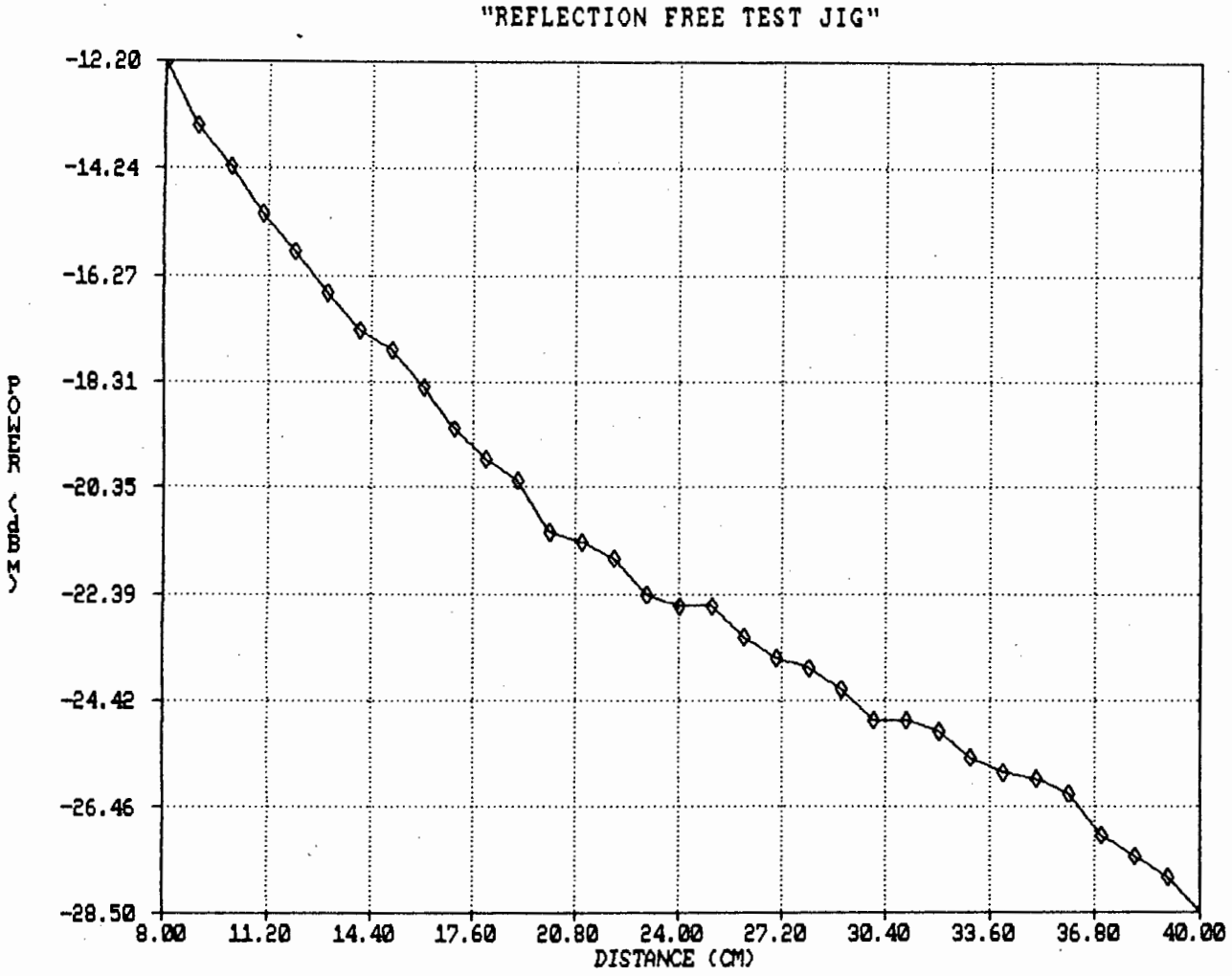

Figure 3.9b Experimental Curve

3.4 STATIC AND DYNAMIC TESTS

3.4.1. INTRODUCTION

Static tests were performed as a preliminary experiment because although the system required must operate in a dynamic mode, static tests are easier and quicker to peform. From the static tests and dynamic tests, conclusions will be drawn about the optimum frequency to use.

The dynamic tests were performed to prove that the system would work when used for the specified application, i.e. sorting gabbro from kimberlite as presented on a conveyor belt. The difference in attenuation for each rock type, when using parallel-sided smooth-surfaced rocks, was found to be higher at 35GHz than at 10.525GHz [3]. While ignoring the disadvantages of using high frequency, Mercer [3] concluded that 35GHz is the optimum frequency to use in differentiating between gabbro and kimberlite. The 35GHz, 10,525GHz, 23GHz and 35GHz frequencies were used for both static and dynamic tests, using randomly shaped rocks.

The transmitter and receiver were arranged as shown in Figure 3.10, for static tests, and in Figure 3.11 for dynamic tests.

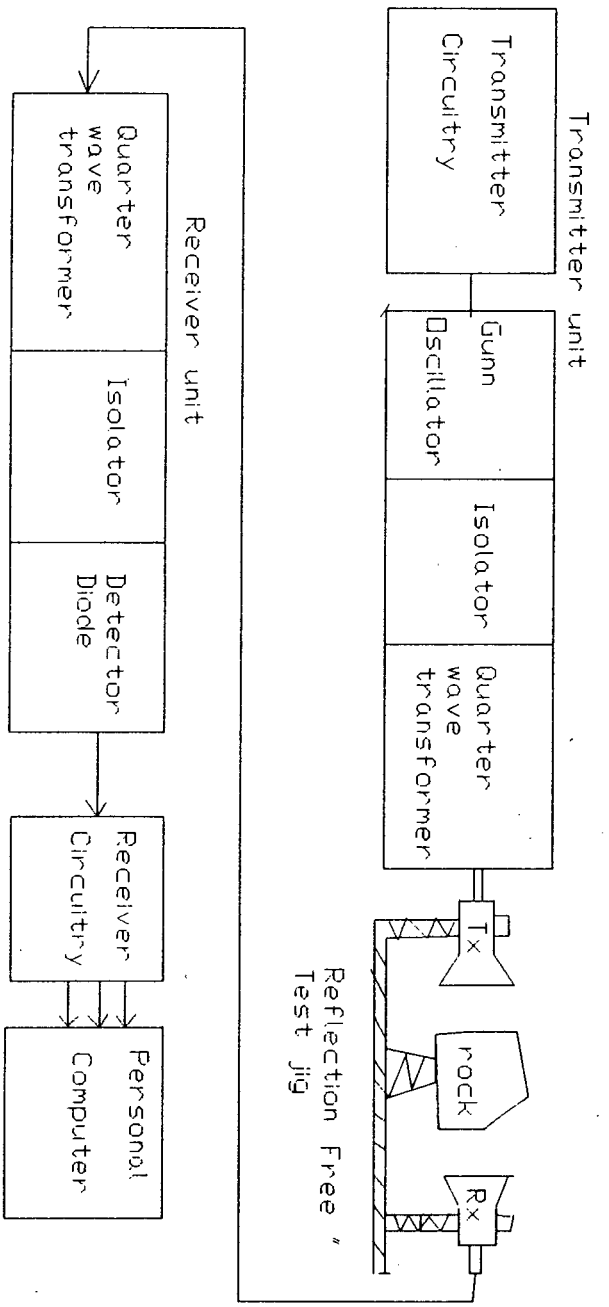

Figure 3.10 System arrangement for static tests

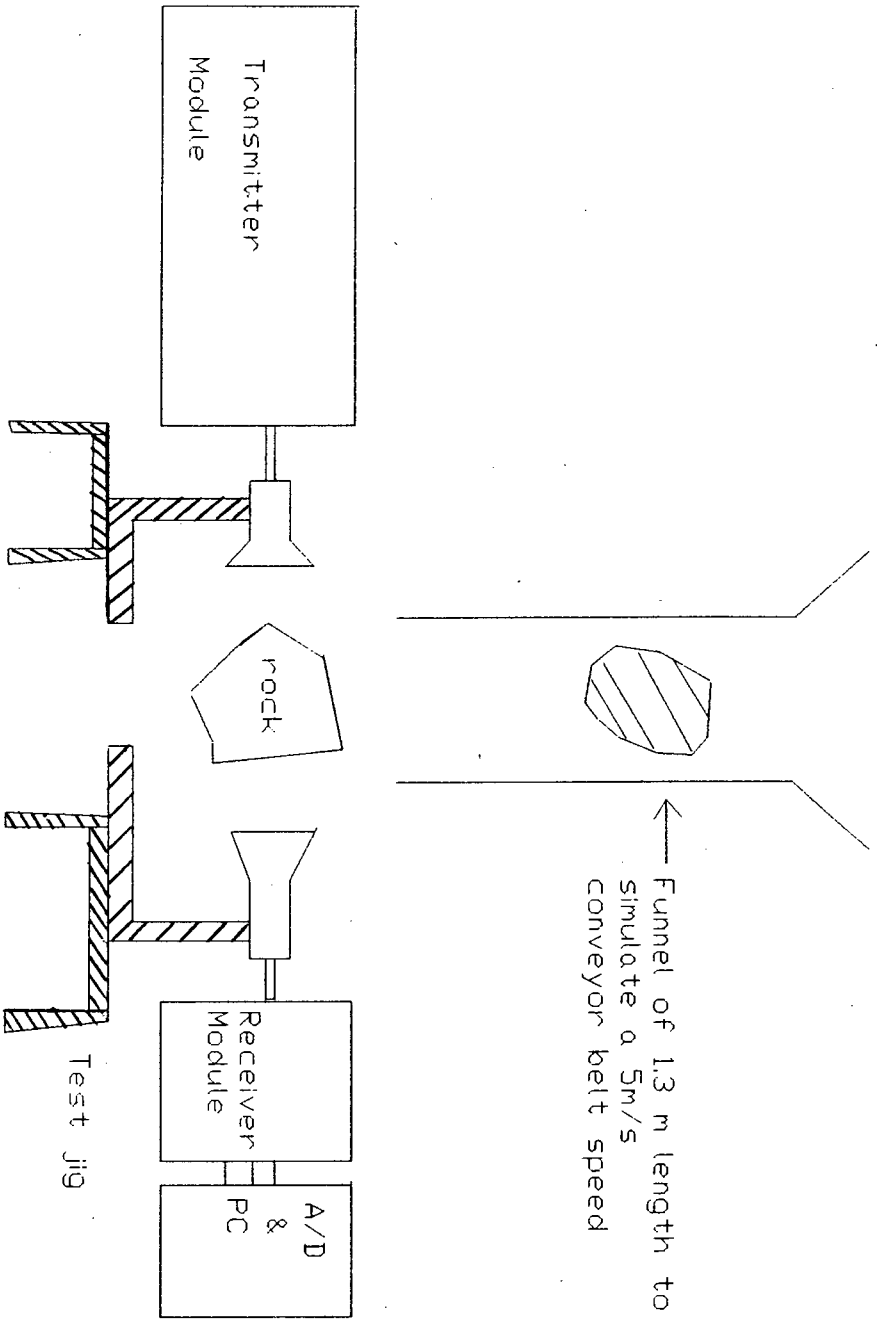

Figure 3.11 System configuration for dynamic tests

3.4.2. STATIC TESTS

Static tests were performed on a rock by rock basis using the system arrangment shown in Figure 3.10. Flat-sided and randomly shaped rocks were used. Known gabbro and kimberlite rock samples were supplied by De Beers for the purpose of these experiments.

The initial part of the experiment was to calibrate the system against a known magnitude of attenuation. This was performed by inserting a rotary vane attenuator in the transmitter front-end as shown in Figure 3.12.

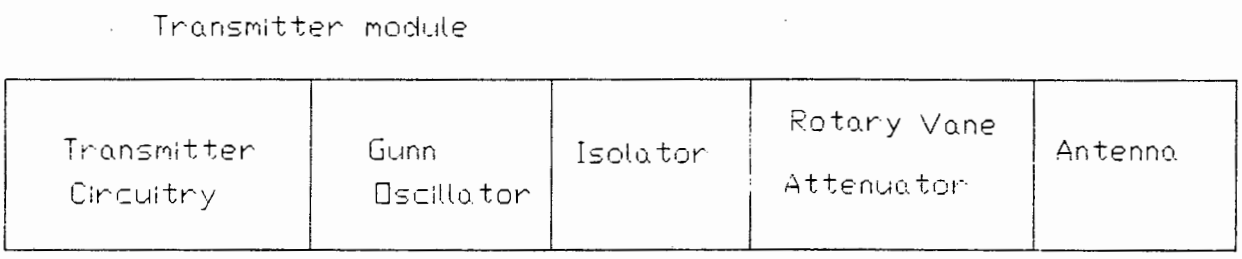

Figure 3.12 Rotary Vane Attenuator in the Microwave Transmitter Front End

The rotary vane attenuator was set to zero and the magnitude of the signal at the receiver was observed on the computer. The attenuator was then adjusted until the received signal was reduced to almost zero. The dc voltage signals captured by the computer, as shown in Figure 3.13 with the rotary vane attentuator, included in the transmitter end, are plotted in Figure 3.14. The dc voltage was plotted as a

function of attenuation. The system configuration including the modified transmitter module is shown in Figure 3.13.

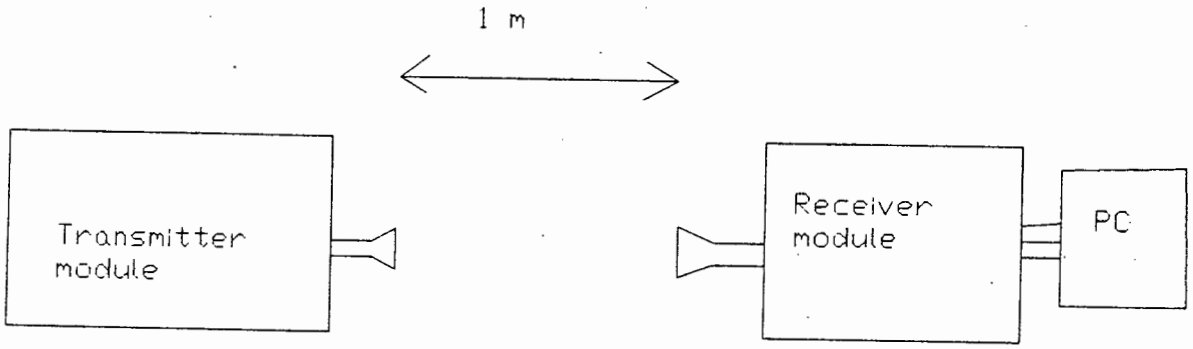

PC = Personal Computer

Figure 3.13 System with Modified Transmitter Module

The system dynamic range is 20dB which is more than adequate for the application.

After performing this experiment, gabbro and kimberlite rock samples were used to measure attentuation of rocks with smooth sides and the following results were obtained at 10.525GHz.

Rock type	Average attenuation in dB/cm
Gabbro	2.5
Kimberlite	7.10

According to Mercer [3] Kimberlite gave 9.3dB/cm and Gabbro gave 2.4 dB/cm average attentuation at 35GHz. The static test results obtained at 3GHz showed a small difference in attenuation between gabbro and kimberlite. Kimberlite gave an attenuation of 9.2dB/cm, whereas gabbro gave an average attentuation of 4dB/cm. The tests performed at 35GHz showed that at this frequency the attentuation difference between gabbro and kimberlite is greater than at any other frequency. When randomly shaped rocks were used, it was found that the shape and orientation of the rock determined the attenuation obtained. The results of static tests cannot be taken as conclusive without considering dynamic tests.

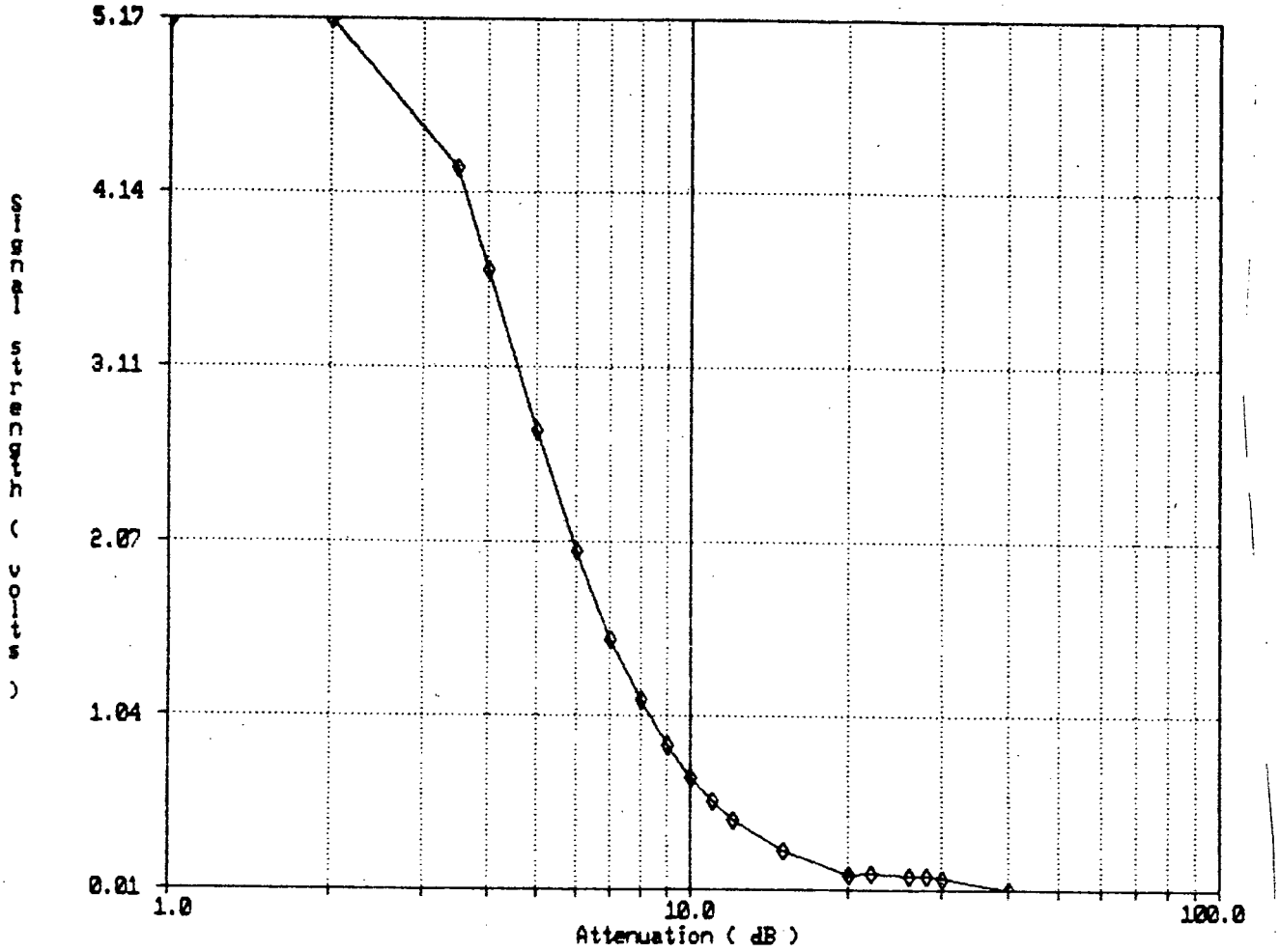

Figure 3.14 Attenuation versus signal strength for 10.525GHz

3.4.3. DYNAMIC TESTS

Dynamic experiments were performed as the system needed to sort rocks has to operate in a dynamic mode. The complete system for performing dynamic tests is shown in Figure 3.11. The dynamic tests system was configured to simulate a conveyor belt with the speed of 5m/s. The conveyor belt is used to move the ore from one place to another and somewhere along the line the ore sorting is required.

The funnel shown in Figure 3.11 was designed by A De Waal [8] to simulate 5m/s rock velocity by dropping the rocks from a chosen height of 1.3m. A test jig was designed to suit this arrangement. The four frequencies i.e. 3GHz, 10,525GHz, 23GHz and 35GHz were used to perform the dynamic tests. The results obtained show a small attenuation difference between gabbro and kimberlite when the 3GHz system was used. A better attentuation difference of 5dB was obtained at 10.525GHz. This frequency was chosen to investigate the throughput of the system. It was found that using a 10.525GHz system and rock size variation of 2 to 1 (from 5cm to 10cms), the percentage of kimberlite detected as 94% correct then 47% was correctly detected as gabbro. From the dynamic tests it was shown that 10.525GHz was the optimum frequency.

Wet rocks were used to investigate the performance of the discriminating system at various frequencies and it was found that at X-band frequencies water does not have attentuation peaks. Thus the effect of moisture on performance was minimal when X-band frequency was used. Also at X-band frequency small rocks can be sorted as well as relatively large rocks. The effect of signal scattering or surface reflections from the rocks is tolerable. The orientation and shape dependence of attenuation still

remains, even at this frequency. The methods of overcoming this problem are discussed in Chapter 4 and Chapter 5.

3.5. SYSTEM CONSIDERATIONS

Systems operating at 10.525GHz, 23GHz and 35GHz use waveguide antennas which are electrically small. When these systems were tested it was found that the dominating factor at high frequencies is surface reflections. However, 10.525GHz was chosen as the optimum frequency. Antennas at this frequency are easy to construct.

The system using 3GHz microwave front-end was no better in performance than 10.525GHz. Electrically small antennas at 3GHz were designed using a dielectrically loaded waveguide. This is an expensive method of making antennas, time-consuming, and is expensive because the dielectric material used should be a low-loss material which is very expensive.

The resonant patch antennas were unsuitable as their resonant frequency shifted when the rock sample passed in front of the antennas. The antennas were detuned and ceased to operate efficiently.

After considering all these systems, it was concluded that the 10.525GHz frequency should be chosen as the systems operating frequency. Using this frequency does not eliminate the effects of surface reflections, so that this problem still remains. The following two chapters deal with methods of minimizing surface reflections.

Comparison was made between the dielectrically loaded X-band antennas and the air-filled square waveguide antennas. The performance of the air-filled antennas was found to be satisfactory. It showed a clear distinction between gabbro and kimberlite with a nominal attenuation difference of 5dB

between gabbro and kimberlite. However, a 100% separation was not possible as additional attentuation occurred due to surface reflections and variations in rock shape, size and orientation.

3.6. CONCLUSIONS

From the findings of this section, it can be concluded that the effects of frequency are important in attentuation measurement. The higher the frequency, the higher the inherent attenuation due to propagation within the rock. However, surface reflections which are rock shape and orientation dependent become worse.

It can therefore be concluded that the 10.525GHz frequency is the most suitable compromise.

CHAPTER 4

EFFECTS OF POLARIZATION

4.1 INTRODUCTION

It was discovered that the attenuation of microwaves caused by rocks depends on the orientation and shape of these rocks as they pass between the transmitter and the receiver. In order to find out the average effect and ensure that the attenuation is independent of orientation, the rock can be rotated. This, however, is difficult to achieve and is thus an impractical process. Therefore, it was decided that, instead of spinning the rocks, microwave signals should be rotated and the same effect would be observed.

This led to the implementation of circular polarization. When linear polarization was used, the orientation dependence of attenuation was observed and in order to solve this problem, circular polarization was employed. Shape and orientation dependence of attenuation caused certain gabbro samples to attenuate the signals as much as kimberlite. This proved that attenuation depends on the shape of a rock. When high frequencies like 35GHz are employed, the signal is scattered by the rock surface because of its irregular shape.

Circular polarization is discussed as a chosen method of solving problems which are encountered when linear polarization of microwave signals is used. The results are presented and comparison is made between use of this technique and the use of linear polarization.

4.2 CIRCULAR POLARIZATION

A circular polarized wave can be regarded as the sum of two orthogonal plane waves in phase quadrature. The method used to convert signal polarization from linear- or plane- to a circular-polarized microwave signal is to load a circular waveguide with a low-loss dielectric material, teflon (PTFE) placed at 45 degrees to the incident wave.

Further, to improve the match between free space and waveguide, the teflon was tapered on both ends as shown in Figure 4.1.

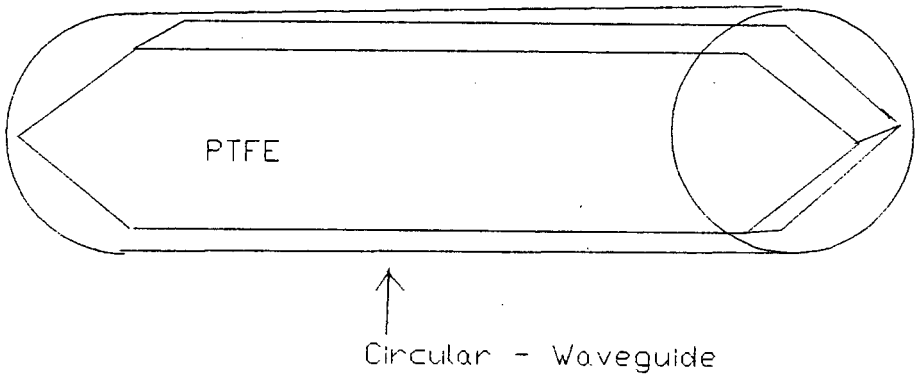

Figure 4.1 Tapered FTPE in Circular Waveguide.

To describe circular polarization, wave directions in a waveguide are considered. The diagrams in Figure 4.2 show the direction of rotation of the electric vector of a circular-polarized wave propagating into the paper. Diagram (a) shows clockwise propagation and (b) shows counter clockwise propagation.

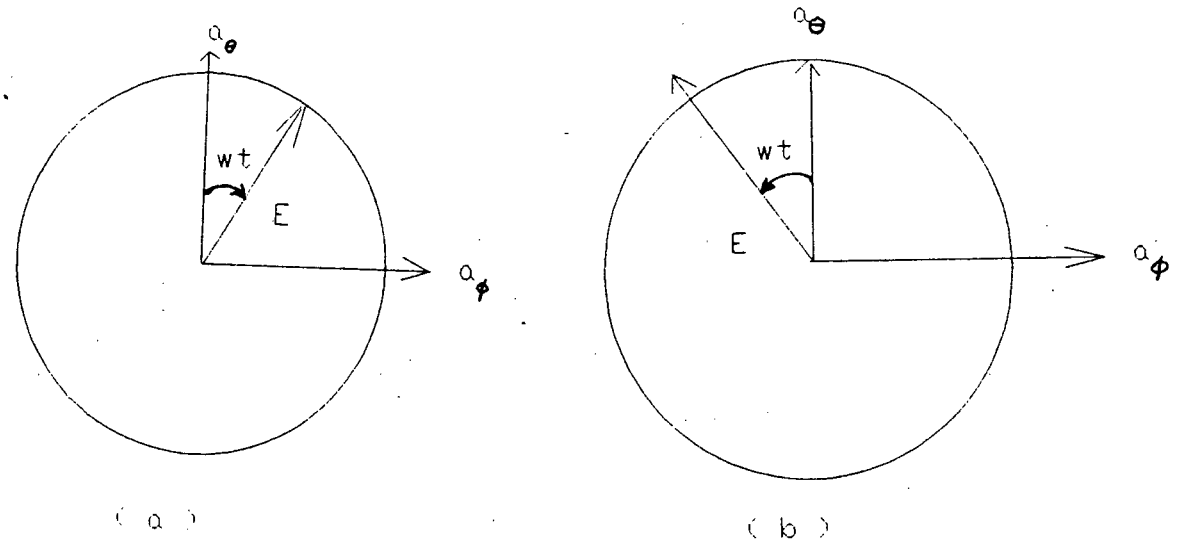

Figure 4.2 Electric vector of circular polarized signal.

The direction of polarization may vary along different radial directions and must be specified with the aid of a co-ordinate system.

The basic polarization transforming element in a circular waveguide is a dielectric slab sometimes called a polarization transducer. The dielectric slab has wedge tapers at each end for impedance matching. The teflon is placed at 45° to the incident field (horizontal). The dielectric slab changes polarization from linear to circular, and is called the polarizer.

For a circular waveguide operating in TE_{11} mode, a polarizer placed at 45° to the incident plane of polarization may be decomposed into two modes:

i. Parallel polarized,
ii. Orthogonal to the polarizer as illustrated in Figure 4.3.

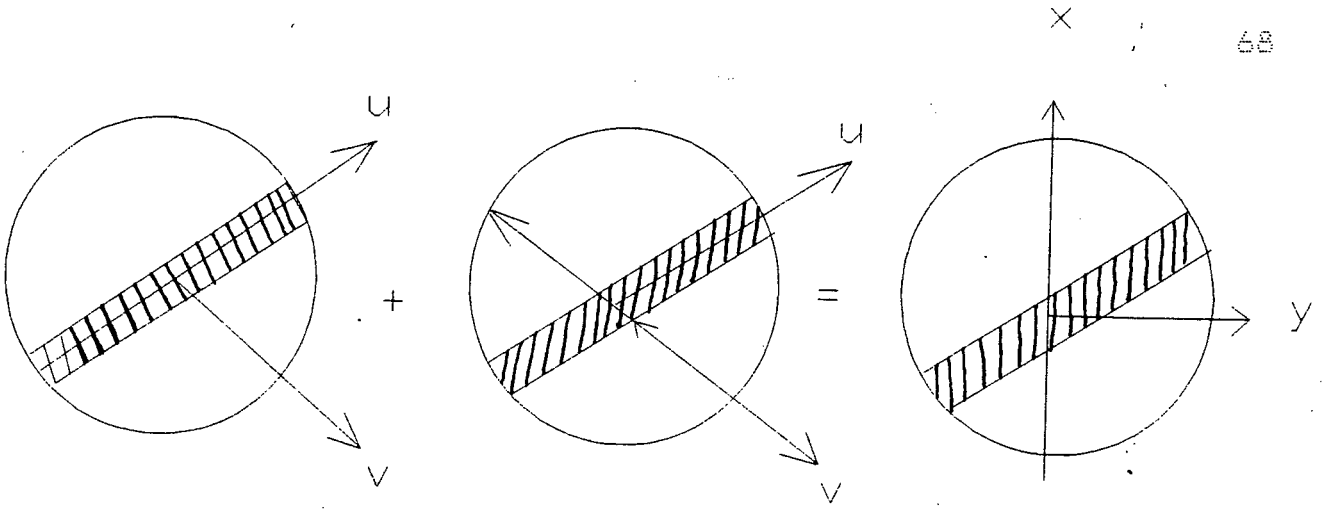

Figure 4.3. Components of incident TE_{11} mode

If the single TE_{11} waveguide mode is incident in such a polarizer, the energy is coupled from the incident TE_{11} mode into the orthogonal TE_{11} mode. The amount of coupling depends on the lengths of the dielectric slab. As predicted by coupled-mode theory [9], there is a sinusoidal dependence of the amplitude of these modes on the length of the dielectric slab. Also, the relative time phase between the two modes remains constant at 90^{o} until the first amplitude null is reached.

The dielectric constant of teflon (PTFE) used for the polarizer is 2.1. The lengths of this teflon was found by experimentation. If the length of the teflon is such that the two modes, i.e. horizontal and vertical, are equal in amplitude, and in phase quadrature, circular polarization will result.

The polarizer was tested using a Hewlett Packard power meter and a sweep oscillator as a source. A quarter-wave impedance transformer was also designed to match the rectangular waveguide output of the Gunn source to the circular waveguide antenna. This antenna is used to propagate the circular polarized microwave signals. The design procedure for the circular to rectangular waveguide

transformer is similar to that of the rectangular-to-square waveguide transformer. The configuration is shown in Figure 4.4 below.

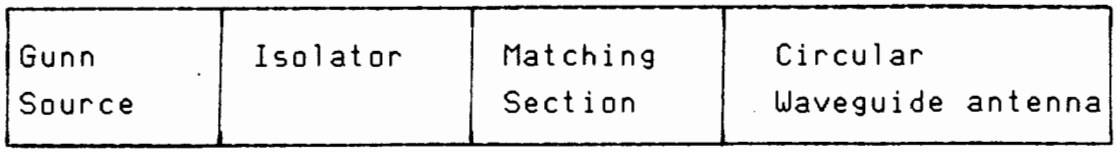

Figure 4.4 Microwave transmitter front-end with matching section

4.2.1. DESIGN OF QUARTER-WAVE IMPEDANCE TRANSFORMER

The following design procedure is carried out, using the formulae derived by Harvey [6]. The design is for an X-band frequency of 10.525GHz.

The cut-off wavelength for a circular waveguide is given by

$$\lambda_c = \frac{\pi D}{2}$$ where D is the diameter of a circular waveguide

This is the cut-off wavelength for TE_{11} fundamental circular waveguide mode. The cut-off frequency is given by:

$$f_c = \frac{X_{np}}{2\pi\, a(\epsilon\, \mu)^{1/2}}$$

where 'a' is the radius of a circular waveguide and X_{np} is a Bessel's constant [10].

Therefore the calculated value of the critical frequency, using the dimensions of the X-band waveguide where 'a' is 12.56mm, is 6.995GHz. This gives a critical wavelength, $\lambda_c = c/f_c$, of 42.9mm.

Also, the waveguide wavelength $\lambda g = \dfrac{\lambda}{(1-(f_c/f)2)^{\frac{1}{2}}}$

Where λ is the wavelength at the operating frequency in free space, λ_g = 28.33mm. This waveguide wavelength is less than the critical wavelength, and the microwaves at 10.525GHz will therefore be propagated through this waveguide without attenuation. After obtaining the dimensions for the circular waveguide, the impedance of the matching section is calculated using $Z_m = (Z_c Z_r)^{\frac{1}{2}}$. [6]. Where Z_c is the impedance of a circular waveguide, Z_r is the impedance of a rectangular waveguide. The impedance of a rectangular waveguide is given by:

$$Z_r = \left[\frac{\mu_0}{\epsilon_0}\right]^{\frac{1}{2}} \times \frac{\lambda_g}{\lambda_0} \times \frac{b}{a} \qquad \text{.....[6]}$$

For X-band 'b' = 10.16mm and 'a'= 22.86mm and λ_g = 38.33mm therefore $Z_r = 224.7\Omega$.

The waveguide impedance for a circular waveguide is

$$Z_g = \frac{W\mu_0}{\beta_g} \qquad \text{..... [10]}$$

where β_g is the mode propagation constant.

$\beta_g = (W^2\mu\epsilon_0 - K^2c)^{\frac{1}{2}}$ where K_c is the wave number given by $K_c = X'np/a$ where 'a' is the radius of the waveguide and $X'np$ is the Bessel constant [10].

Therefore $K_c = 1.841/12.54 \times 10^{-3} = 146.8m^{-1}$. This leads to $\beta_g = 163.875$ rad.metre,

Thus $Zg_c = \frac{W\mu_0}{\beta g}$

$$= \frac{2\pi \times 10.525 \times 10^9 \times 4\pi \times 10^{-7}}{163.875}$$

$$= 505.9\Omega$$

Therefore the impedance of the matching section is given by

$$Z_m = (Z_r Z_c)^{\frac{1}{2}}$$
$$= 224.7 \times 505.9$$
$$= 337.2\Omega$$

The impedance of a rectangular waveguide is proportional to its height. The height is the missing dimension of the matching section because the longer dimension is the same as that of an X-band rectangular waveguide. The height of the matching section is given by:

$$b_m = \frac{Z_r \times b_r}{Z_m}$$

Where 'b_r' is the height of the rectangular waveguide.

Therefore $b_m = \frac{505.9 \times 10.16}{337.2}$

$$= 15.24mm$$

The matching section is illustrated in Figure 4.5.

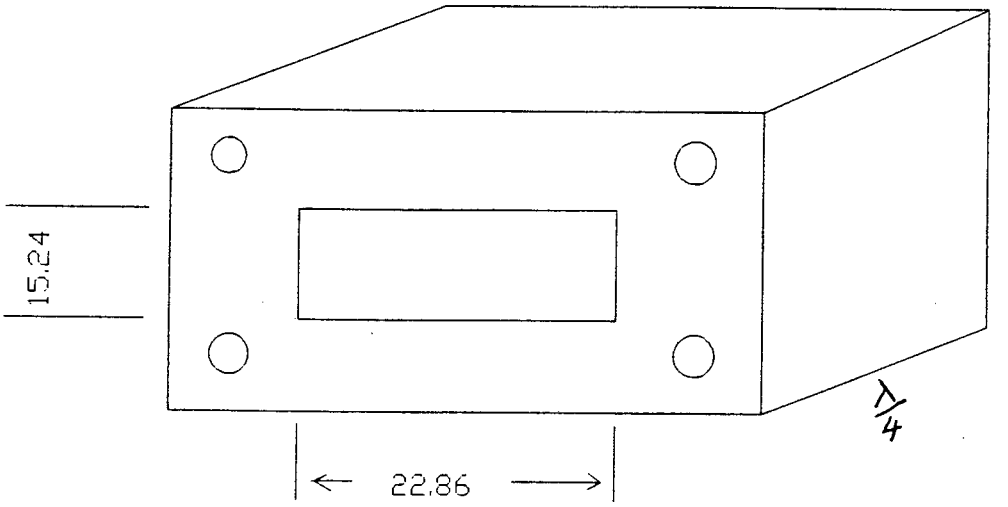

All dimensions in millimeters

Figure 4.5. Quarter wavelength impedance transformer

The quarter-wavelength impedance transformer was used to connect the Gunn source to the circular antenna and polarizer. The circular polarized antenna and rectangular to circular waveguide transformers were designed for both the transmitter and the receiver. On completion of the design, experiments were performed to investigate the performance of the circular polarized antenna and then a comparison was made to the square linear polarized antenna. The experiments are performed using static and dynamic tests.

4.2.2. SYSTEM USING CIRCULAR POLARIZED ANTENNAS

The transmitter and receiver pair described in Chapter 2 were used with microwave front-ends as circular antennas. The system performance was verified before it was used to discriminate between gabbro and kimberlite.

The range performance was investigated as in Chapter 2. It was found that the system performance with circular antennas meets the range requirement of 2 metres. The system was then used to perform tests to investigate if the circular polarization reduces the problems experienced when using linear polarized square antennas.

Configurations used with square antennas when performing dynamic and static tests were used to facilitate comparison of results.

4.3. DISCUSSION OF RESULTS

Static and dynamic tests were performed using circular polarized antennas as transmitter and receiver antennas. Static tests were performed with dry gabbro and kimberlite rocks. Theory predicted that a circular-polarized propagating signal might average the signal scattering effects on attenuation measurements and eliminate the very high attenuation measured with a particular rock orientation. There was some small improvement when dry rocks were used. The system was not noticeably sensitive to orientation measurements performed on static rocks. Thus the circular polarized signals did not eliminate the effects of reflections.

The results of dynamic tests were achieved using the configuration as shown in Figure 4.6. These tests were performed on a conveyor belt travelling at a speed of 5m/s. A personal computer was used to capture and analyse data.

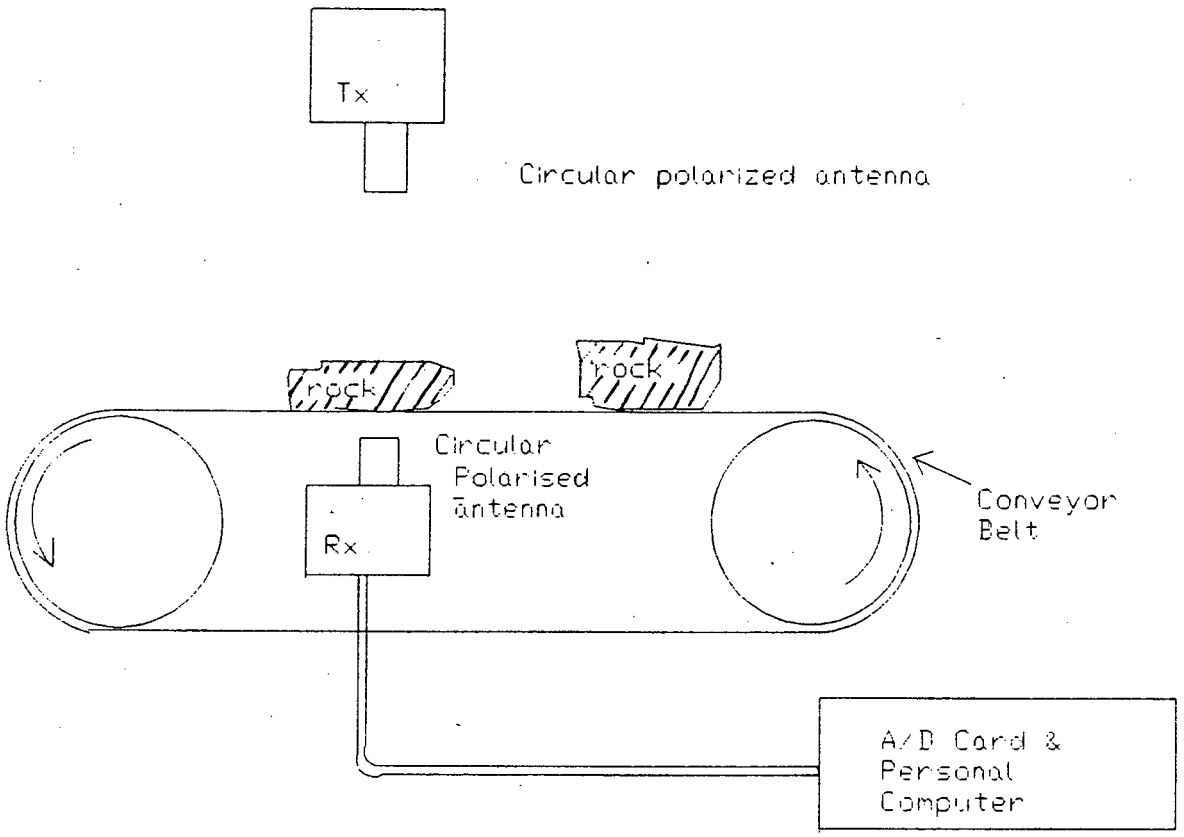

Figure 4.6 Dynamic tests using circular polarized antennas

Tests were performed using both wet and dry rocks because static tests did not produce useful results when only dry rocks were used.

The results of dynamic tests are shown graphically in Figure 4.7 for dry-rock tests and Figure 4.8 for wet-rock tests. All the tests were performed using the 10.525GHz system.

It can be seen from the graph in Figure 4.7 that the circular polarized antennas give a slightly better yield than the linear polarized antennas. However, results from performing wet-rock tests shown in Figure 4.8 show that linear polarized antennas give a marginally better performance. This shows that moisture has some effect on attenuation measurement. Results of wet-rock tests conclude that circular polarization does not reduce the surface reflection problem.

The conclusion to be drawn from the above findings is that circular polarization is not a viable solution to the problems of surface reflections.

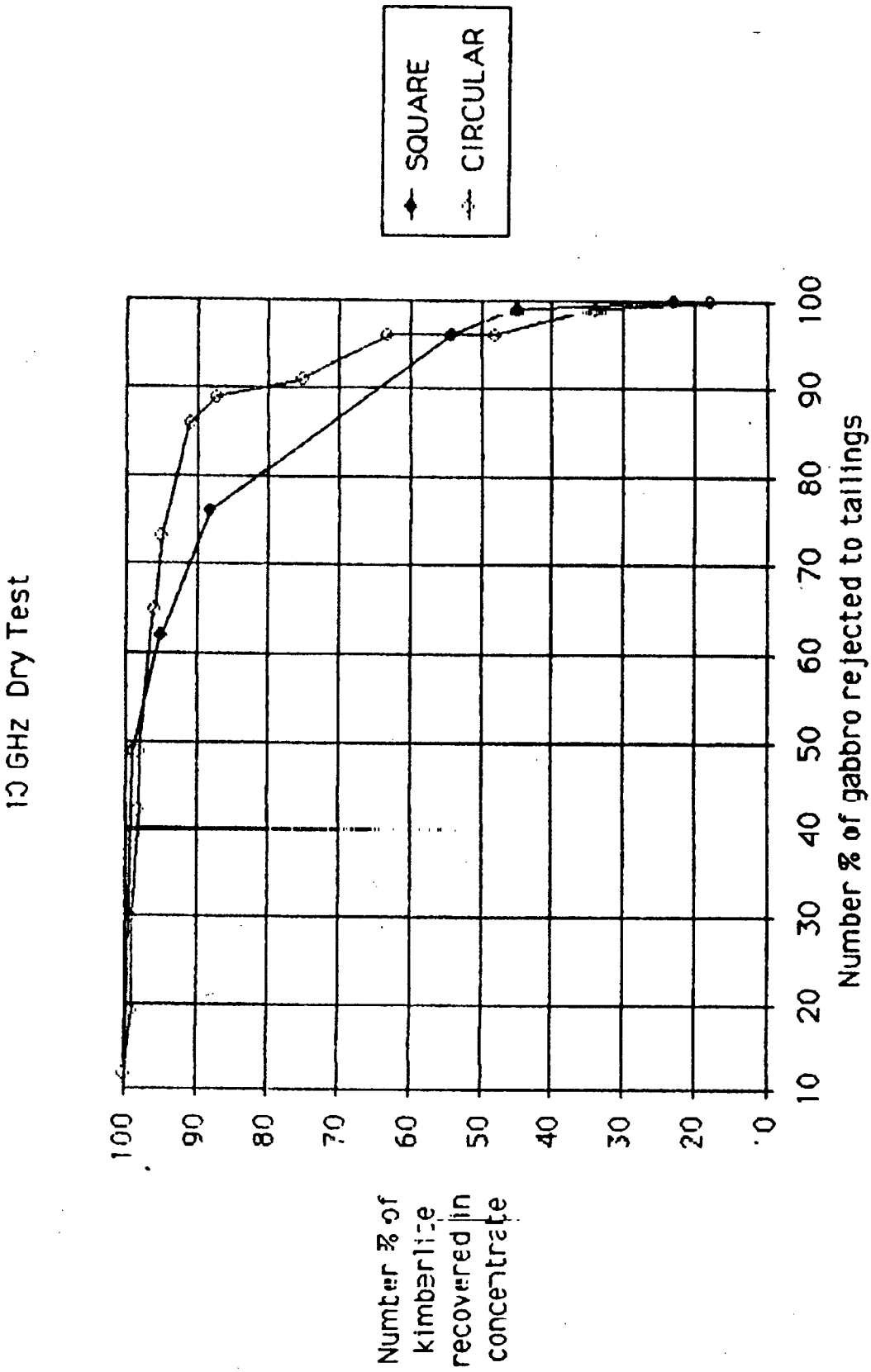

Figure 4.7 10.525GHz Dry Test using Square and Circular antennas.

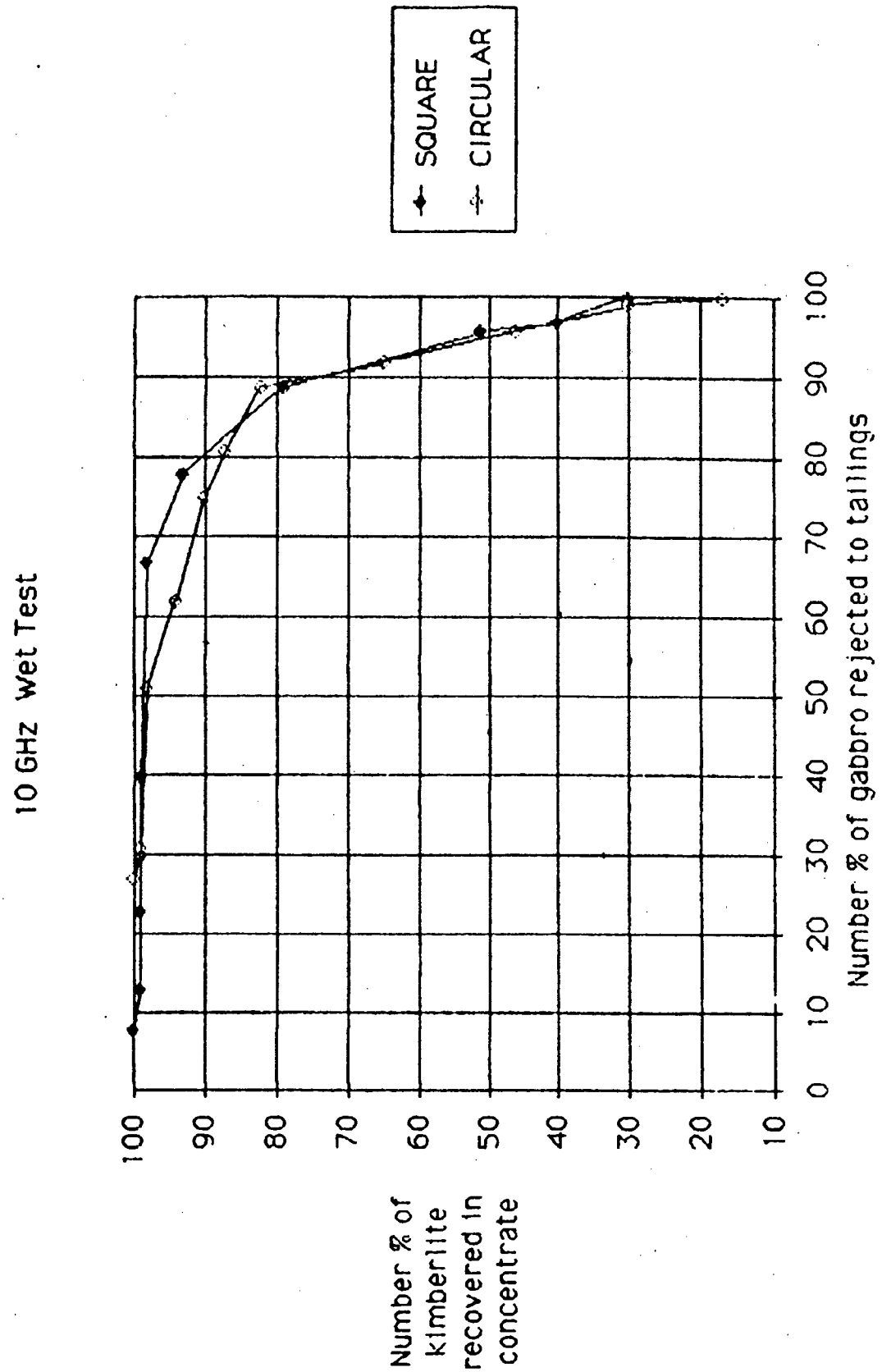

Figure 4.8 10.525GHz Wet Test using Square and Circular antennas.

CHAPTER 5

SPACE DIVERSITY

5.1. INTRODUCTION

This chapter describes techniques for solving the shape and orientation dependence which results in the scattering of microwave signals from the rock surface. Circular polarization provided a small improvement to the system performance. This improvement was not adequate enough to warrant replacing the linear polarized system with a more complex circular polarized system.

Space diversity is discussed in the following section. This technique is aimed at eliminating the effects of reflections during the measurement of attenuation. Various configurations are described and the experimental results of the best configuration are discussed.

5.2. DESCRIPTION OF SPACE DIVERSITY SYSTEM

The name "Space Diversity" is derived from the arrangement of the transmitters and receivers. The System Configuration is shown in Figure 5.1. The transmitter and receiver pair system used initially showed that the effect of reflections is dominant. This system measured attenuation in one plane only. To overcome this problem, circular polarization was employed. This technique used one transmitter and receiver pair and measured attenuation in one plane only. This, however, did not solve all the surface reflection problems.

The space diversity technique gives attenuation measurements from three different planes as selected in this particular application. This system should ensure that surface reflections do not occur simultaneously. There is no technical reason preventing the system from using more than three planes of measurement. Five planes could be used if necessary. However, three transmitter and receiver pairs gave adequate results.

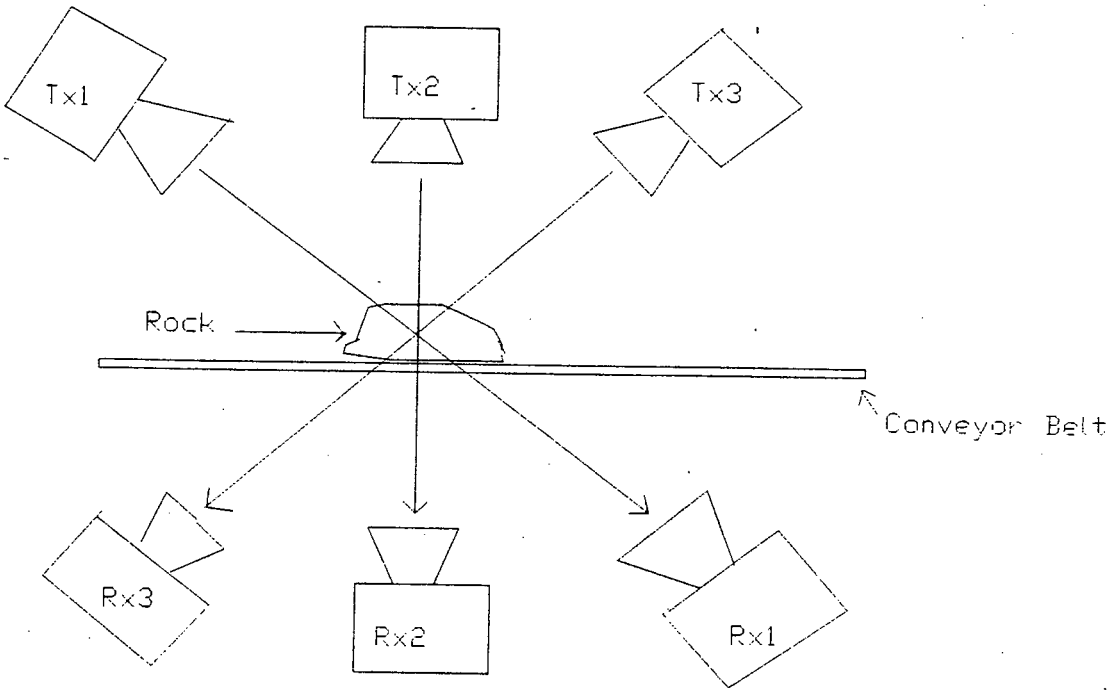

Figure 5.1. Space Diversity System.

Two space diversity techniques were examined. The first uses three transmitters launching separate microwave signals into a single waveguide as shown in Figure 5.2. A single detector is used at the receiver. The transmitters used for the system shown in Figure 5.2 operate at different microwave frequencies.

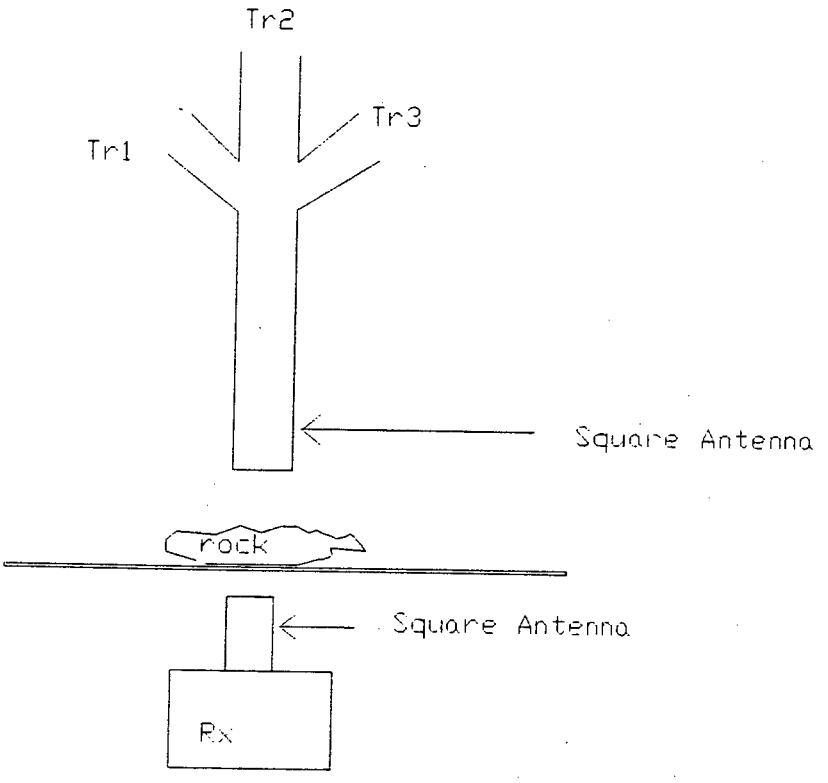

Figure 5.2. Transmitters launching through one waveguide to one wideband detector.

The second technique uses three separate transmitters and receivers as shown in Figure 5.1. Both systems are described below.

5.2.1. THREE TRANSMITTERS LAUNCHING INTO ONE WAVEGUIDE

This system was used to eliminate reflections by transmitting signals from three different planes. Operation of this system is as follows. The system shown in Figure 5.2 transmits signals which are received by a wideband detector. Three transmitters were tuned to operate at 8.5GHz, 10.525GHz and 12.5GHz. This frequency range allows the use of a wideband detector at the receiver. The transmitters were cross-polarized to avoid inter-channel interference.

This system has certain drawbacks which make it non-viable. These are:

(a) The impedance mismatch between the rectangular waveguide outputs of the Gunn oscillators and the square waveguide antenna.

(b) The three signals which are received by a single detector thus creating the problem of one signal dominating the other two and the sensitivity being reduced.

This mechanism is shown in Figure 5.3. below.

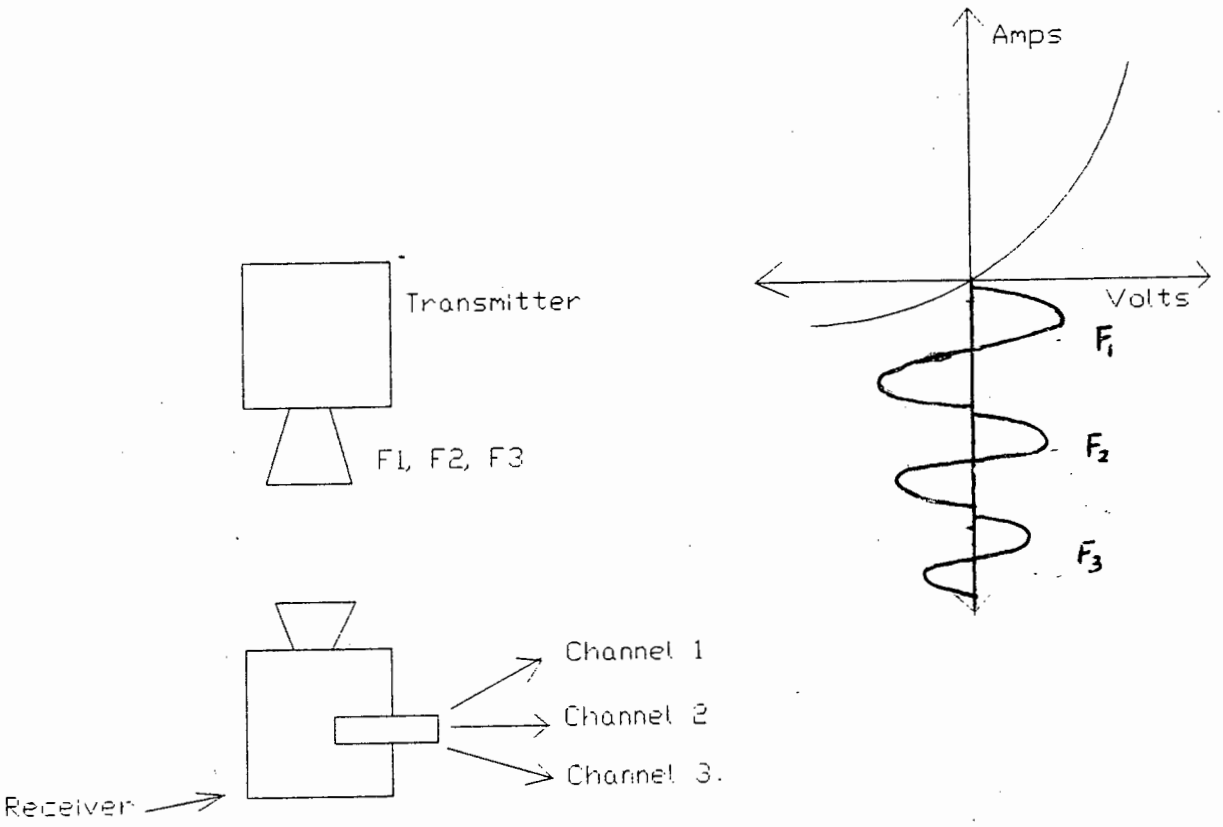

Figure 5.3. Three Channel System with detector diode characteristics.

Frequency F_1 is amplitude modulated with a frequency of 1KHz and is detected by the microwave detector. The signal is received in Channel 1 through a 1KHz bandpass filter. Frequency F_2 and F_3 are modulated with frequencies of 5KHz and 10KHz and are received in Channels 2 and 3 with corresponding bandpass filters. The frequencies were Channel 1 = 8.5GHz, Channel 2, F_2 = 10.525GHz and Channel 3, F_3 = 12.5GHz.

A common detector is used for the three signals. If one signal is much larger than the other two, the output from the detector becomes saturated. A further increase in input amplitude does not result in a corresponding increase in the output. There is thus a signal suppression.

A similar suppression of signals F_2 and F_3 occurs which can result in the sensitivity to these two channels being reduced.

In the system described above a large signal from Channel 1 resulting in detector saturation introduces an apparent attenuation in Channels 2 and 3, thus giving anomolous readings.

Because of these problems, this technique was not developed further and instead, a space diversity technique which uses three separate transmitters and receivers was developed.

5.2.2. SPACE DIVERSITY USING THREE SEPARATE TRANSMITTERS AND RECEIVERS

This system was configured as shown in Figure 5.1. in which attenuation measurements were performed in three different planes. This was done to eliminate the effects of surface reflections which could be less on one plane than the other. However they are dependent on the shape and orientation of rock samples between the transmitters and receivers.

Measurements were performed with the three transmitter and receiver pairs at the same microwave frequency of 10.525GHz and using modulation and demodulation frequency of 1KHz. The three transmitters had the same polarization plane, i.e. all were vertically polarized.

However, interference between the transmitter and receiver pairs did occur. Because of the size of the antenna bandwidth, the signal transmitted by any one of the three transmitters reached the receivers unattenuated by the rock samples passing between them. As a result, the output of the receiver registered no attenuation. This is the cross-talk problem. The solution to it was to cross-polarize the centre transmitters and receiving pair, thus making the signal transmitted to be 90^{0} space displaced from the other two signals. Static tests were performed using this configuration.

The results of the tests were not as good as expected. To eliminate further cross-talk, the modulation frequencies were changed from all being 1KHz to different modulation frequencies for each channel of 1KHz, 5KHz and 10KHz respectively. The system performance improved because there was no interference between the transmitters.

Static tests were performed using the test jig shown in Figure 5.4. The results obtained showed a clear discrimination between kimberlite and gabbro. As a result of the improvement in discrimination shown by the three channel space diversity system during static measurements, a dynamic test jig was constructed. The results of the dynamic measurements are reported in the next section.

Figure 5.4. Static Test using "Reflection Free" test jig.

5.2.3. DYNAMIC TESTS USING SPACE DIVERSITY SYSTEM

When performing dynamic tests using this system, the outputs of the receivers were compared, as in the case of static tests. The receiver output with the largest attenuation value was used to determine the type of rock. Dynamic tests were performed using three microwave transmitters with the same carrier frequency and three modulating frequencies of 1KHz, 5KHz and 10 KHz. The system had cross-talk problems because the antennas were cross polarized and different modulating frequencies were used. The system used for performing dynamic tests is shown in Figure 5.5.

Figure 5.5. Dynamic Test System.

The three transmitters were housed in one box. Each transmitter was shielded to avoid any interference between the circuits.

The receivers were also housed in one box as shown in Figure 5.5. The outputs of the receivers were fed into a computer via an A/D card. The computer was triggered optically to capture data as the rocks were dropped between the transmitters and receivers (through the 1.3m funnel to simulate 5m/s conveyor belt speed).

Measurements were carried out on known kimberlite and gabbro samples. Randomly shaped and parallel-sided, smooth-surfaced rocks were used. The results showed that 49% of the gabbro was correctly identified and 94.5% of the kimberlite was correctly identified. The results of this

experiment show an improvement compared to those using a single transmitter and receiver pair with the effects of reflections being significantly reduced by measuring attenuation in three different planes.

5.3. CONCLUSIONS

Experiments performed using space diversity systems showed that the effect of reflections can be reduced significantly. From the findings of this chapter it can be concluded that surface reflections will always exist in an attenuation measurement system which uses antennas. However, the space diversity system improves the performance from 93% to 95% discrimination on average.

CHAPTER 6

MULTI-CHANNEL OPERATION

6.1. INTRODUCTION

A multi-channel operation is required to improve the mass throughput of the ore-sorting system. (The system initially utilised was a one-channel system which uses one 10.525GHz carrier frequency).

This multi-channel operation is different from the space diversity system in that the mode of operation is the same for each channel. There is one transmitter and an array of receivers in each channel and the attenuation is measured in the same plane. The operation of the ore-sorting system in a multi-channel mode is described and the problems associated with it are discussed. Potential solutions to the problems of multi-channel operation are also discussed.

6.2. INTER-CHANNEL INTERFERENCE

Three channels were used, all using a 10.525GHz carrier frequency and a 1KHz modulation frequency. The modulated signal is demodulated at the receiver by a bandpass filter with a centre frequency of 1KHz. The three channel system is shown in Figure 6.1.

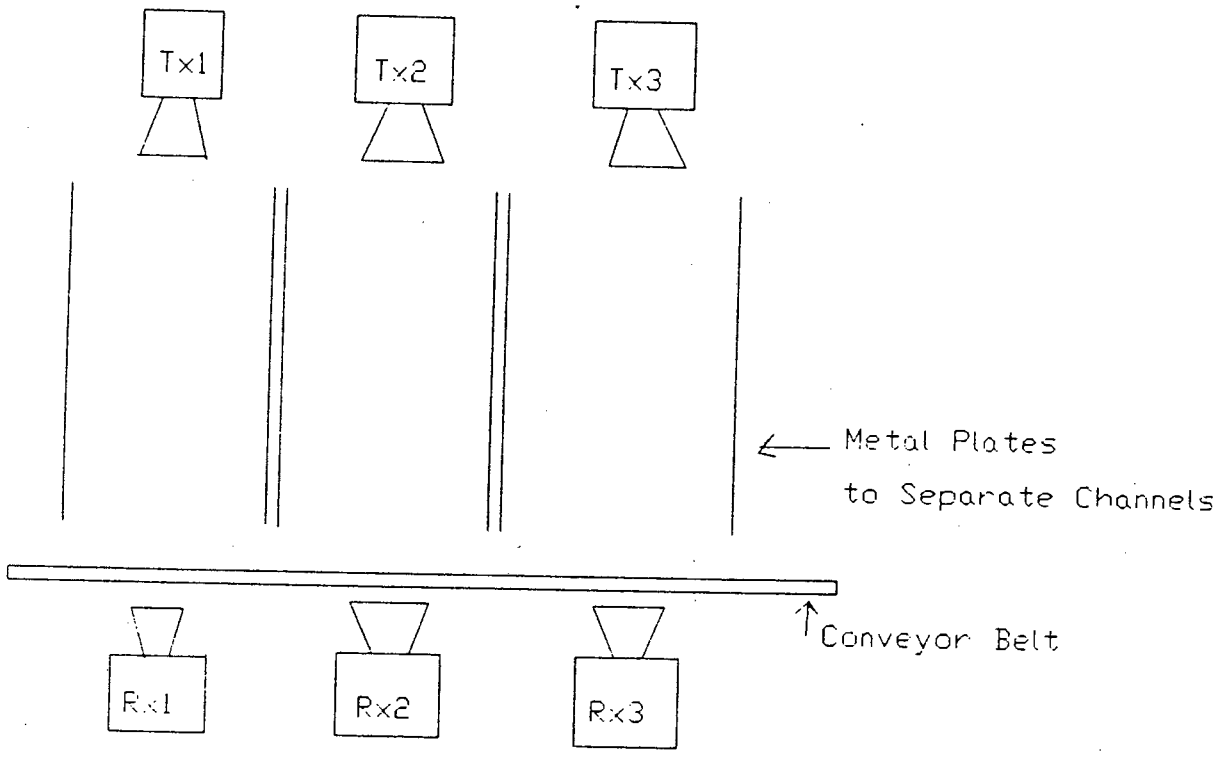

Figure 6.1. Multi-Channel system.

The conveyor belt carrying the rock samples runs between the transmitters and receivers. Figure 6.1 shows the front view of the multi-channel system. The three channels are placed close to each other. This is dictated by the width of the conveyor belt. There is consequently interference between the channels.

This inter-channel interference posed a problem in the measurement of attenuation. Inter-channel interference is

caused by the size of the antenna beam-width. The three transmitter antennas also had the same plane of polarization, and these antennas led to the received signals not being attenuated by the rock samples. For example, when the rock obscures transmitter TR1, the signal from transmitter TR2 is not obscured by that rock sample. This results in false attenuation measurement.

The channels are separated by metal plates. This confines the signal from the transmitter antenna until it reaches the conveyor belt. However, these metal plates do not eliminate inter-channel interference. Instead they create more problems, such as the multi-path effect which will be discussed in the next section.

The multi-channel operation is configured in the following way: for each transmitter there is a corresponding array of receivers. This ensures that the attenuation due solely to rock samples is measured accurately. This can be achieved by taking the output of the receivers, which correspond to one transmitter, and comparing the signal strengths. The receiver with the highest attenuated signal is taken as the attenuation measure. As mentioned, these channels interfere with each other and give anomalous results.

The problem of inter-channel interference was solved by cross-polarizing each transmitter with the corresponding receivers. The transmitters and the corresponding receivers were positioned to be 90^{0} apart electrically. This technique eliminated the interference between the three channels. A further problem is associated with multi-channel operation; the inaccuracy in signal detection, which causes an anomalous attenuation measurement. This is the multi-path problem.

6.3. MULTI-PATH EFFECT

In every line-of-sight communication, the signal transmitted from a source will always take more than one path to reach the receiver. In most cases, this is governed by the beamwidth of the relevant antennas and the distance between the transmitter and receiver. This multi-path effect is shown in Figure 6.2.

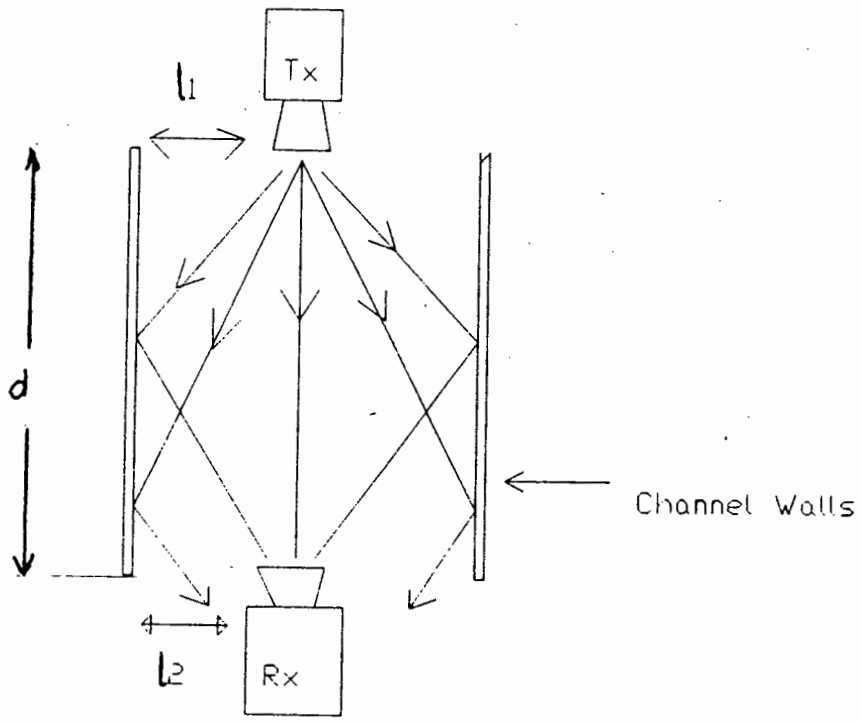

d = distance between the transmitter and the receiver
$'l'_1$,$'l'_2$ = distance between channel wall and the transmitter and receiver respectively.

Figure 6.2. Multi-path effect.

The distance between the transmitter and receiver contributes much to the existence of multi-paths. This multi-path effect was experienced after the separation between transmitter and receiver had been determined. One way of reducing the multi-path effect would be to alter the existing sorter. This however, could be expensive and time-consuming. The alternative was to confine the transmitted signal to the position where the multi-paths would not affect the received signal. Thus, the signal should be confined to a distance where the reflected signals would not affect the direct signal.

The received signal is the combination of the reflected signals and the direct signal. These signals are different in phase because of the path difference which is as follows:

$$\Delta d = \frac{2 l_1 l_2}{d} \qquad [6]$$

where 'l'_1 and 'l'_2 are the distances of the transmitter and receiver from the channel walls and 'd' is the distance between the transmitter and receiver [6].

According to Harvey [6] the phase difference between the reflected signals and the direct signals is given by:

$$\emptyset = \frac{4\pi l_1 l_2}{\lambda d} \qquad .....$$

where λ is the free space wavelength of the transmitted signal.

The ϵ-field at the receiver antenna from a direct signal is given by $\epsilon \sin \omega t$ and from the reflected path is given by $\rho\epsilon \sin(\omega t - \emptyset)$. Where $\emptyset$ is the phase difference and ρ is the reflection coefficient and ϵ is the signal strength. The

resultant field is therefore shown in the following equations:

$$E_r = 2\sin\frac{\phi}{2}$$ where ϕ is the phase difference.

The nulls occur when $\frac{\phi}{2} = n\pi$, when n is

an integer or when $d = \frac{2l_1l_2}{\lambda n}$

This equation shows that small values of 'n' correspond to long distances between transmitter and receiver. It is due to these nulls that the multi-path effect poses a problem to the system performance.

Peaks occur when $\frac{\phi}{2} = \frac{(2n+1)}{2}\pi$

or when $d = \frac{4l_1l_2}{(2n+1)\lambda}$

These peaks result from the addition of the reflected and the direct signal at the receiver, whereas nulls occur when the reflected and direct signals cancel at the receiver antenna. The problem of the multi-path effect was solved by choosing the separation between transmitter and receiver to correspond to a signal peak and not a signal null.

When using the multi- channel operation for ore sorting, it was necessary to eliminate the multi-path effect from all three channels. This was done by choosing the correct distance between the transmitters and the receivers. To eliminate the mechanism of multi path reflections Horn

antennas were used on the transmitters. Horn antennas of 1.2 metres length were designed and are shown in Figure 6.3.

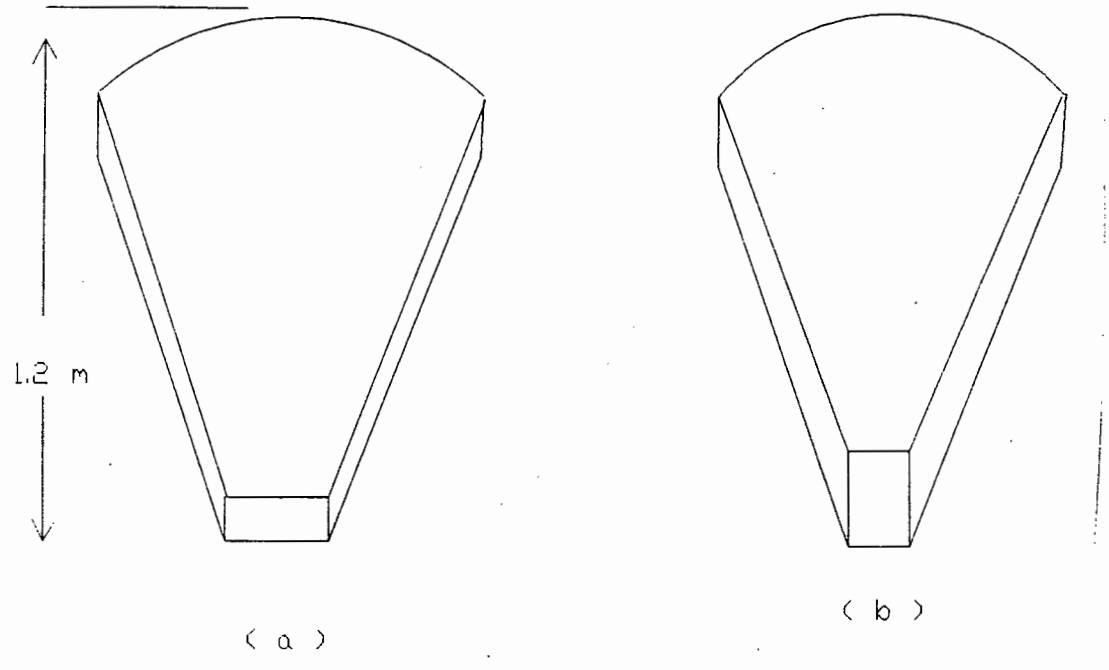

Figure 6.3. Horn antennas for multi-path effect reduction.

Three antennas of different shapes were designed, two of which are shown in Figure 6.3(a) and the other in Figure 6.3(b). These shapes were designed to facilitate the cross- polarization of the antennas in the three channels to eliminates cross-talk. The curved ends ensure constant phase across the aperture and an improved match to free space.

In this case, wide-transmitter antennas, and small-receiver antennas were used. Experiments were performed using the long-horn and small-square antennas, all operating at 10.525GHz.

The Horn antennas were tested initially using a network analyser measuring S_{11} which measured the reflected power. The horn antennas were tapered to improve the signal impedance match.

During the antenna test procedure it was found that a matching was required. The matching section was designed for a 10.525GHz operating frequency. The return loss measured including the matching was 40dB.

The matching section is shown in Figure 6.4. After testing the antennas individually, dynamic tests were performed using a 10.525GHz transmitter and receiver system. The system used a small-square antenna as a receiver antenna and a large horn antenna as a transmitter antenna.

Rocks were dropped under gravity down a funnel to simulate a 5m/s conveyor belt speed. The system showed that using the small and large antenna pair does not impede the signal strength and the performance is the same as when two square antennas were used.

When a large and a small antenna pair is used, it is important that the small antenna be completely obscured by the rock sample. After testing the antenna performance, the system was tested to see if it would eliminate the multi-path effect in a multi-channel operation. It was found that with the use of long horn antennas, the multi-path effect is completely eliminated.

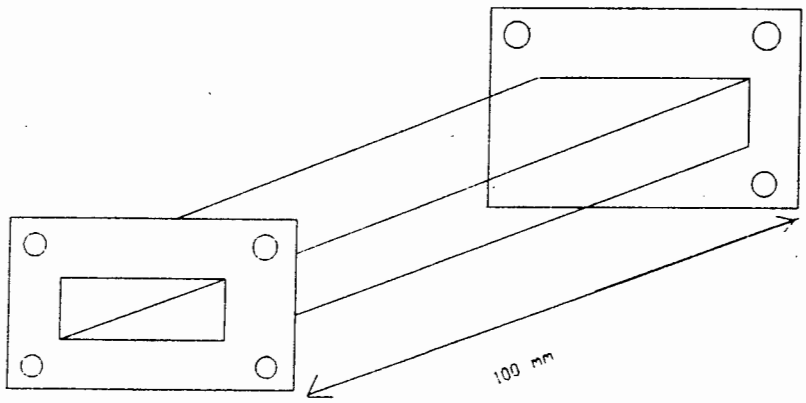

Figure 6.4. Matching posts for horn antennae.

6.4. CONCLUSIONS

In view of the findings of this chapter, the problems associated with multi-channel operation, such as inter-channel interference and the multi-path effect, were solved.

CHAPTER 7

CONCLUSIONS AND FUTURE RESEARCH

In this thesis, the Microwave attenuation discrimination method used previously for rock differentiation was re-evaluated and the problems associated with it were discussed.

The major problems identified were reflections from the rock surface, rock orientation and shape dependence of measured attenuation.

In view of the findings of this thesis, the following conclusions can be drawn:

(1) When microwave attenuation is used for rock discrimination the effects of frequency on the attenuation measurement must first be examined. Considerations of cost, performance and component availability resulted in the most suitable microwave frequency being 10.525GHz

(2) From the findings of the effects of frequency it can be concluded that attenuation increases with frequency.

(3) Techniques used to reduce the effect of surface reflections proved that, when using the antenna system, surface reflections cannot be eliminated completely. They can, however, be reduced to a level where the rock discrimination system can be used. Circular polarization is not a solution to the problem of surface reflections caused by rock shape dependence of attentuation.

(4) The Space diversity technique does not eliminate the effect of surface reflections but it reduces them appreciably.

(5) The problems associated with the implementation of space diversity, namely cross-talk and multi-path effects were solved. However, the effects of surface reflections still need to be eliminated completely, leaving scope for future research.

(6) The multi-path effect in the multi-channel system was completely eliminated by the use of long horn antennas on the transmitter end.

LIST OF REFERENCES

1. CORNELIUS, S., HURLBUT, J.R, (Harvard University) & CORNELIS KLEIN (Indiana University); Manual of Mineralogy: John Wiley & Sons, New York, pp.145-154, p.360, 1977.

2. BERRY, L.G. and MASON, B., Mineralogy: Concepts, descriptions and determinations: San Francisco, Freeman, pp.296-298, 1959.

3. MERCER, S., Rock Differentiation using Microwave irradiation: M.Sc. Thesis, Department of Electrical and Electronic Engineering, University of Cape Town, 1987.

4. STOUT, D.F., Kaufman, M., Handbook of Operational Amplifier Circuit Design: New York, McGraw-Hill, 12.7 - 12.12, 1976.

5. HOROWITZ, P., HILL, W., The Art of Electronics, Cambridge University Press, p. 164, 1980.

6. HARVEY, A.F., Microwave Engineering. Bristol: The Stonebridge Press, p. 27, pp. 630-631, 1963.

7. SUCKER, M., and FOX, J., Handbook of Microwave Measurements: Third Edition, (Volume 2): New York, Polytechnic Press, pp. 339 - 346, 1963.

8. DE WAAL, A., Rock differentiation using the properties of resonant waveguide cavities at 500MHz; Unpublished Final Year Thesis in Department of Electrical Engineering, UCT., p.7.3, 1987.

9. KRAUS, D.J., Electromagnetics, International Student Edition, Third Edition: McGraw-Hill Book Company, New York, pp. 495-509, 1984.

10. LIAO, S.Y., Microwave Devices and Circuits, Prentice-Hall, pp. 95-126, 1980.

BIBLIOGRAPHY

1. DENNEN, W.H., Principles of minerology, The Ronald Press Company, New York; 1960.

2. STRENS, G.R.J., The Physics and Chemistry of Minerals and Rocks, John Wiley & Sons, London, pp. 93-137, 1976.

3. SHURMER, H.V., Microwave Semiconductor devices, Pitman Publishing, 1971.

4. WARNER, F.L., Microwave attenuation measurement, Peter Pergrinus Ltd., 1977.

APPENDIX A **Printed Circuit Board foil patterns.**

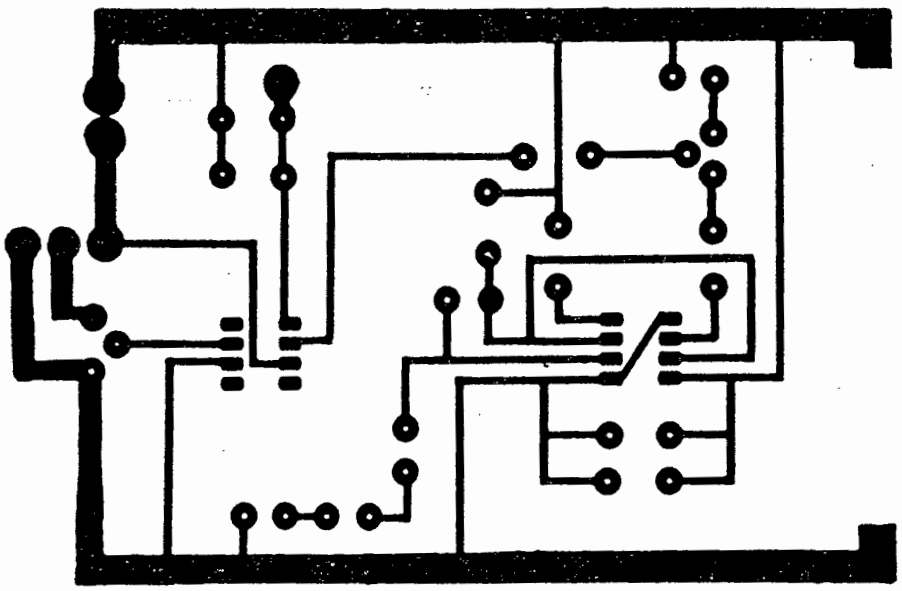

Transmitter printed circuit board foil pattern.

APPENDIX A

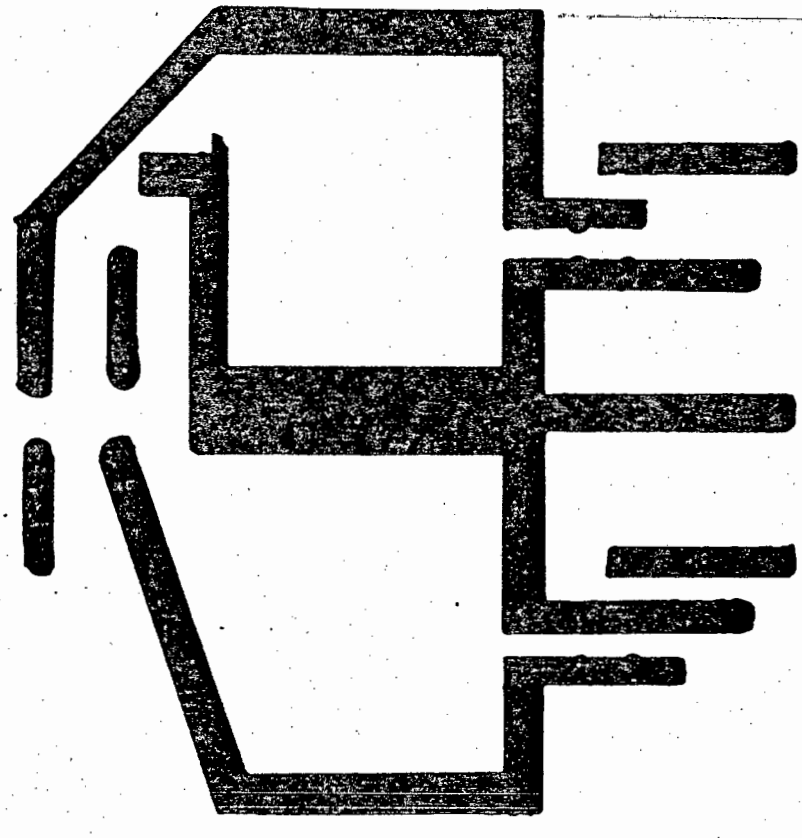

Transmitter power supply printed circuit board foil pattern.

APPENDIX B: Design criteria for square waveguide antennae and rectangular to square waveguide transformers

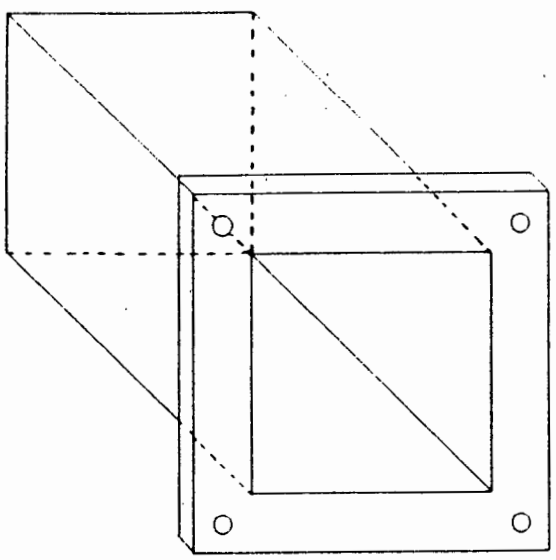

All dimensions in mm.

	A	B	C	D	X	L	Hole diameter
X band	16.3	15.5	41.3	20.6	22.9	50.8	4.3
J band	12.1	12.6	33.3	16.7	15.8	50.8	4.7
K band	8.1	8.5	22.2	11.1	10.7	50.8	2.9
Q band	6.4	6.7	19.1	9.5	7.1	50.8	3.0

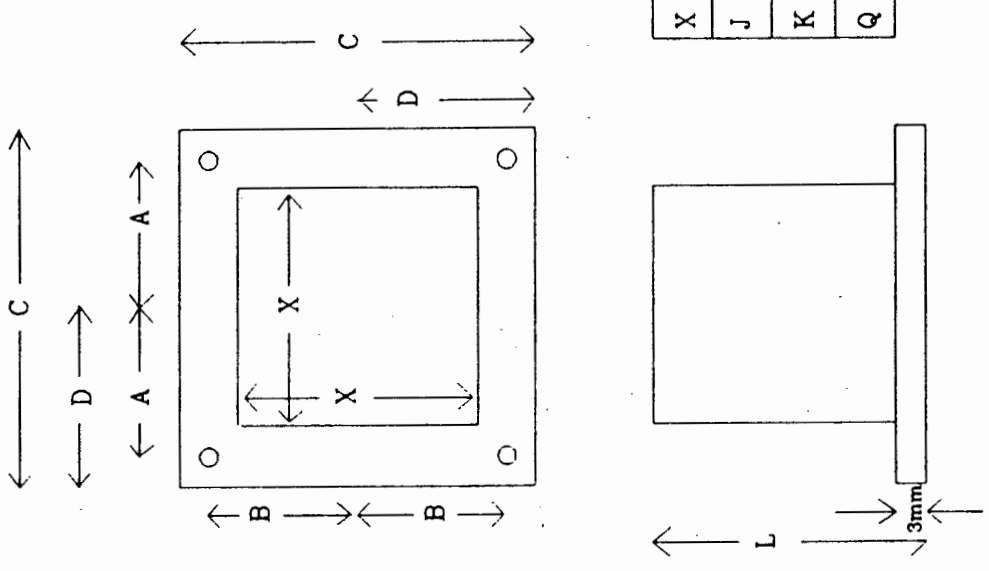

Square waveguide antennae.

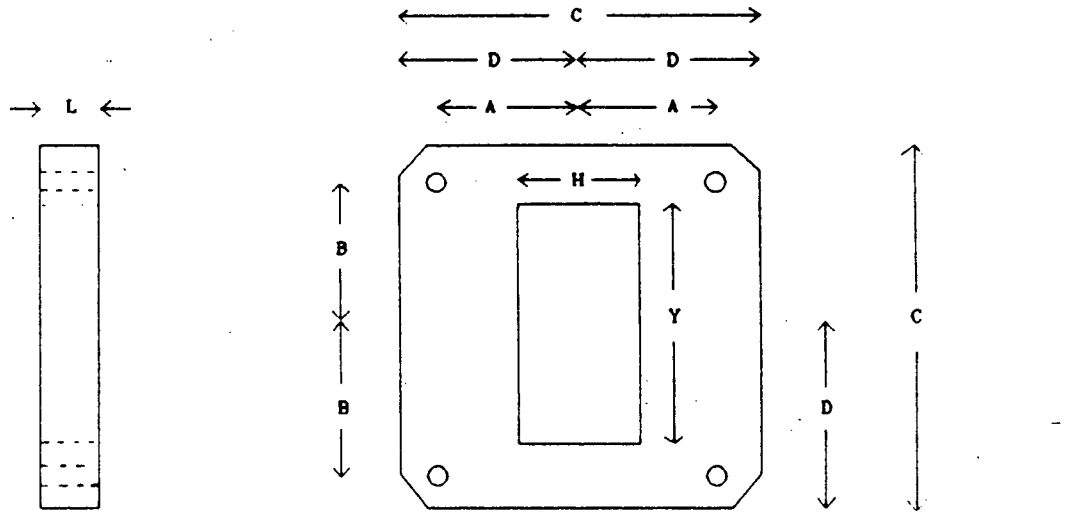

	A	B	C	D	L	H	Y	Hole diameter
X band	16.3	15.5	41.3	20.6	9.9	15.2	22.9	4.3
J band	12.1	12.6	33.3	16.7	6.3	11.2	15.8	3.7
Q band	6.4	6.7	19.1	9.5	2.7	5.0	7.1	3.0

All dimensions in mm.

Rectangular to square waveguide transformers

APPENDIX C

DESIGN OF SQUARE ANTENNAS AND RECTANGULAR TO SQUARE WAVEGUIDE TRANSFORMER

The antennas and rectangular-to-square waveguide transformer had to be designed to cover the required frequency range i.e. X-band, J-band and K-band frequencies. Decision to use square waveguide antennas made it necessary to design rectangular to square waveguide transformers as the Gunn oscillators and detector diodes are housed in a metal casing with a rectangular aperture.

If we consider the design of the X-band rectangular to square waveguide transformers, the following procedure can be followed:

for rectangular waveguide $\lambda_g = \dfrac{\lambda}{(1-\left(\dfrac{\lambda}{2a}\right)^2)^{\frac{1}{2}}}$ ..(1)

Where 'a' is the width of a waveguide and is the free space wavelength at an X-band frequency of F = 10GHz, which is the approximate centre frequency of X-band.

$\lambda = \frac{C}{f}$ where C is the speed of light = $3 \times 10^8 mS^{-1}$

$= 3cm$

for X-band waveguide, 'a' = 2.286cm.
This leads to a waveguide wavelength λ_g = 3.976cm.

A $\lambda_g/4$ long rectangular to square waveguide transformer is shown in Figure C.1.

A matching transformer of $\lambda/4$ length matches the impedance of a rectangular waveguide to that of a square waveguide antenna.

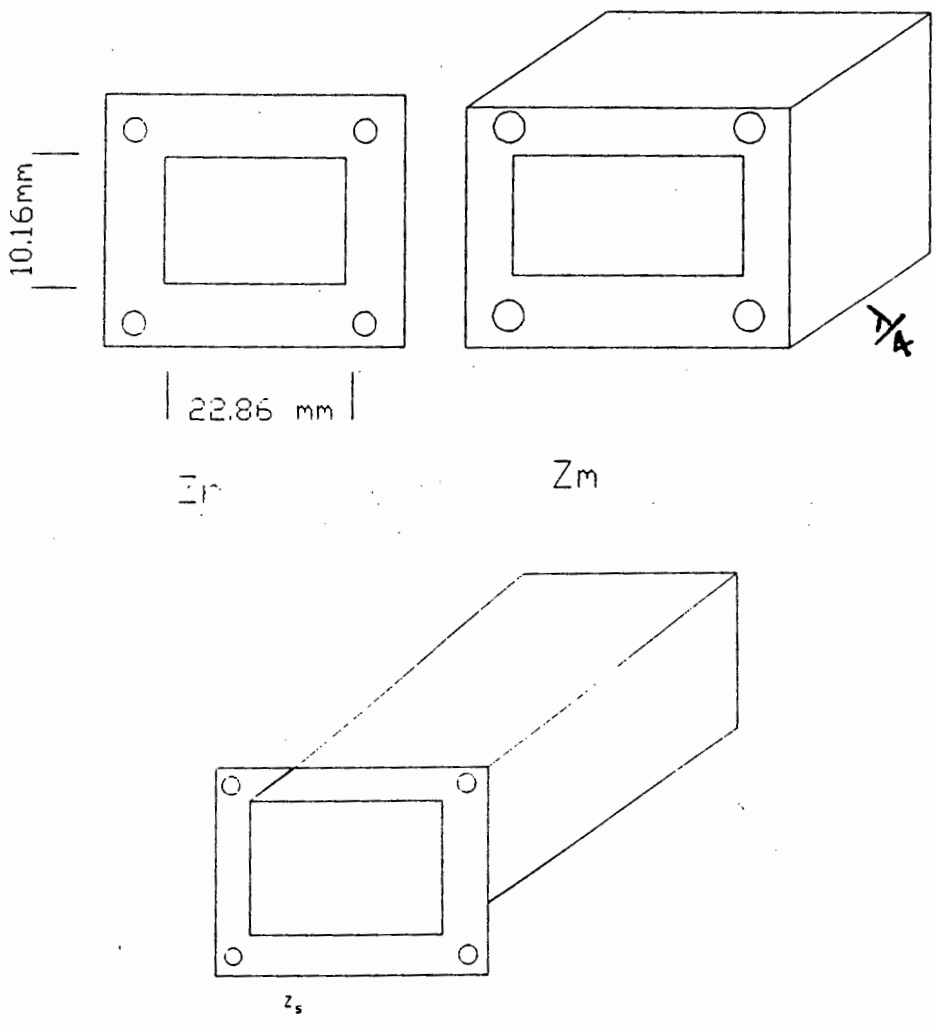

Figure C.1 Quarter-wave matching transformer and square antenna.

$Z_m = (Z_r Z_s)^{½}$ for quarter wavelength matching section.

The impedance of a rectangular waveguide is proportional to its height. According to Harvey [6] this impedance is given by the following expression:

$$Z_r = \left[\frac{\mu}{\epsilon_0}\right]^{½} * \frac{\lambda_g}{\lambda} * \frac{b}{a} \quad \ldots (2)$$

Where 'a' is the longest dimension and 'b' is the shortest dimension of the rectangular waveguide.

For X-band waveguide the cut off frequency is 6.7GHz and the waveguide wavelength is given by:

$$\lambda_g = \lambda/(1-(\lambda/2a)^2)^{½}, \quad \text{where 'a' = 2.286cm}$$

$$\lambda_g = 3.976\text{cm}$$

$\mu_0 = 4\pi \times 10^{-7}$ and $\epsilon_0 = 8.85 \times 10^{-12}$

The impedance of the rectangular waveguide given by equation (2) is 233.6Ω and is calculated below.

Waveguide which is given by:

$$Z_r = \left[\frac{\mu_0}{\epsilon_0}\right]^{½} * \frac{\lambda_g}{\lambda} \times \frac{b}{a}$$

$$= \frac{(4\pi \times 10^{-7})^{½}}{8.85 \times 10^{-12}} \times \frac{3.976}{2.85} \times \frac{1.016}{2.286}$$

$$= 233.6\Omega$$

If $'b'_1$ is the height of a rectangular waveguide and $'b'_2$ is the height of a square antenna. then the matching section is given by:

$$b_m = (b_1 b_2)^{½}$$

For X-band, $b_1 = 10.16\text{mm}$ and $b_2 = 22.86\text{mm}$,
therefore $b_m = 15.24\text{mm}$

This design procedure was used to design the rectangular to square waveguide transformers detailed in Figure C.2. L is the length of the transformer given by, $L = \lambda g/4$.

All dimensions in cm

	L	a	b	h
X-band	0.994	2.286	1.016	1.52
J-band	0.632	1.579	0.789	1.12
K-band	0.432	1.067	0.432	0.68

Figure C.2 Dimensions of rectangular to square waveguide transformer.

TYPICAL PERFORMANCE FOR MA-40200 SERIES

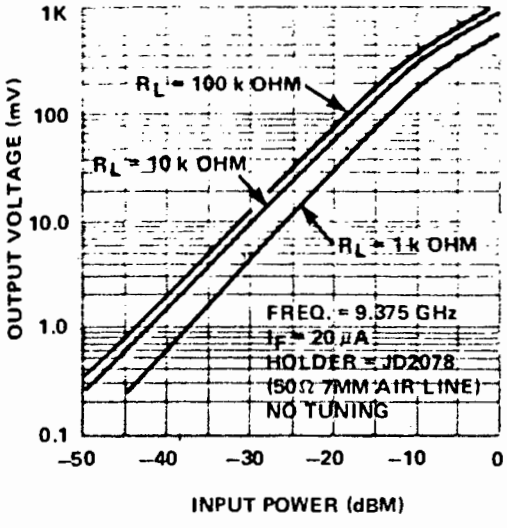

TRANSFER CHARACTERISTICS (I_F = +20 μA)

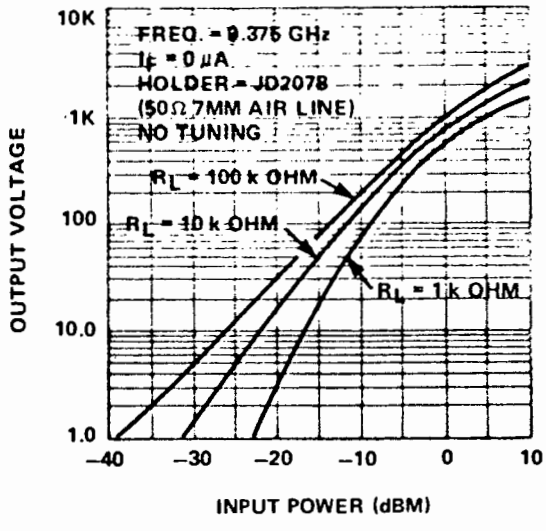

TRANSFER CHARACTERISTICS (I_F = 0 μA)

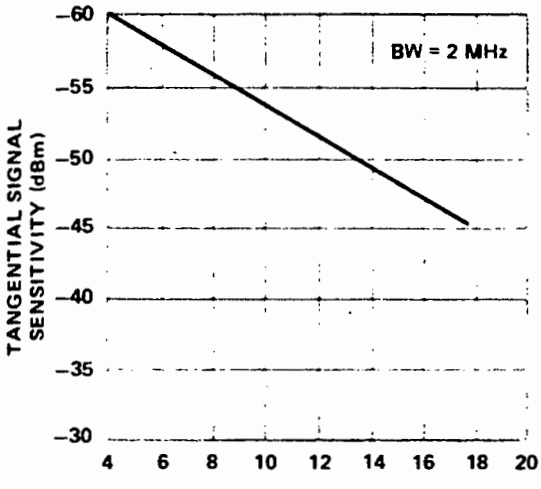

T_{SS} VS FREQUENCY

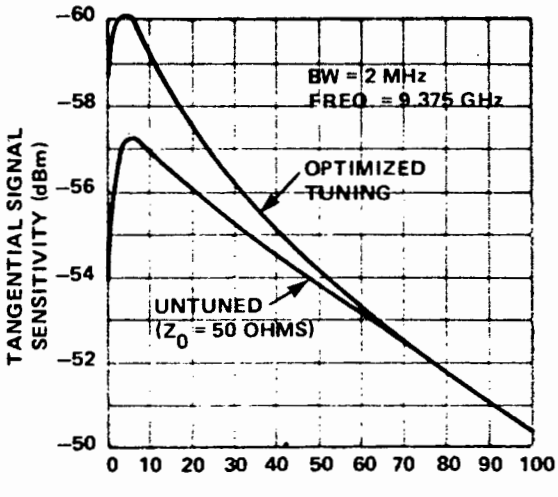

T_{SS} VS DC BIAS LEVEL

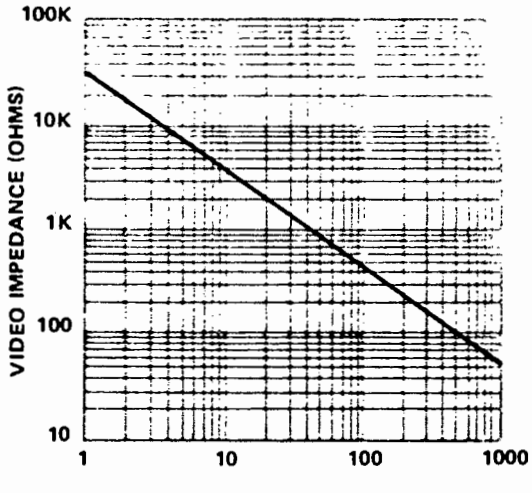

VIDEO IMPEDANCE VS dc BIAS

APPENDIX E RECEIVER PRINTED CIRCUIT BOARD LAYOUT

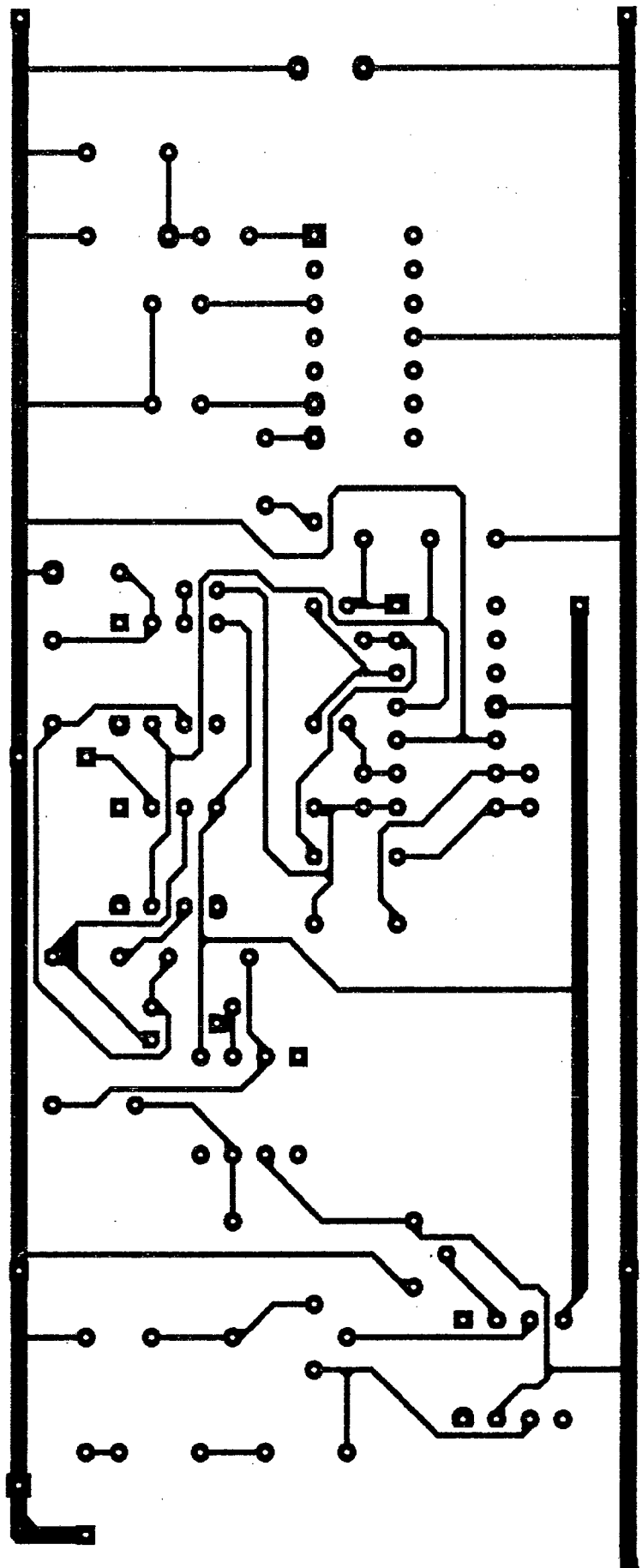

APPENDIX F

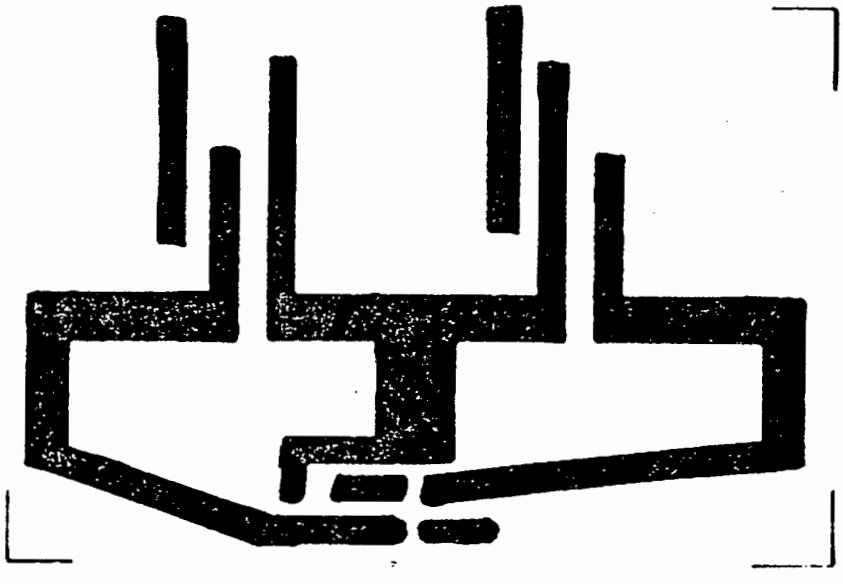

Receiver power supply printed circuit board foil pattern.

APPENDIX G

S - BAND SYSTEM

An operating frequency of 3GHz was used with dielectrically loaded antennas which have approximately the same aperture size as the 10.525GHz air-filled square antennas.

G.1. S-BAND OSCILLATOR

The S-band oscillator used is an Aventek VTO 8240 voltage controlled oscillator (VCO). Specifications of this VCO are given in Appendix H.

The tuning voltage for the 3GHz was 8.2V and was supplied by an LM317 variable voltage regulator. The oscillator requires a 50Ω output line and R.T. Duroid 5880 0.5 ounce microstrip board with a dielectric constant of 2.2 was used. This had a line width of 0.76mm and wavelength of 72.79mm.

A decoupling capacitor (100pf) was placed half a wavelength away from the output of the oscillator. A computer-aided printed circuit board package was used to make the mask for the microstrip, as shown in Figure G.1.

The oscillator was connected to the co-axial to waveguide transformer by an SMA connector and an impedance matching section.

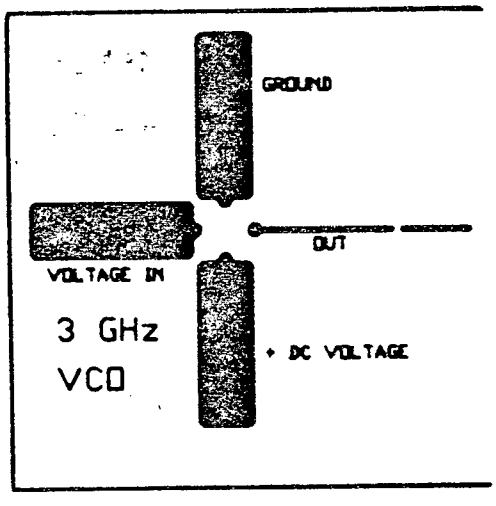

Figure G.1 Microstrip Mask for VCO

G.2. DESIGN OF ELECTRICALLY SMALL S-BAND ANTENNAS

Electrically small antennas were designed to operate at 3GHz. The dimensions of the S-band rectangular waveguide are 72.14mm by 34.04mm.

The free space wavelength at 3GHz operating frequency is

$\lambda_a = c/f = 3\times10^8/3\times10^9 = 10\text{cms}.$

From this and the dimensions of the S-band rectangular waveguide, the dimensions of the antenna can be calculated.

(a) Air filled waveguide wavelength:

$$\lambda_g = \frac{\lambda_0}{\left\{1 - \left\{\frac{\lambda_0}{2a}\right\}^2\right\}^{\frac{1}{2}}} \qquad \ldots\ldots(1)$$

where λ_0 is the free space wavelength.
λ_g is the waveguide wavelength - air filled
λ_g = 13.87cm

(b) Dielectric filled waveguide:

$$\lambda_g = \frac{\lambda_0}{(1 - (\lambda_0/2a)^2)^{\frac{1}{2}}} \qquad \ldots\ldots(2)$$

Where λ_0 = wavelength is dielectric.
λ_g = wavelength dielectrically filled waveguide.

at 3GHz λ_0 = 10cm.

$$\lambda_0 = 10/\quad(10)^{\frac{1}{2}}$$
$$= 3.16\text{cm}$$

from (2)

$$\lambda_g = \frac{3.16}{\left[1 - \left(\frac{3.16}{2 \times 2.714}\right)^2\right]^{\frac{1}{2}}}$$

λ_g = 3.24cm

The critical or cut-off wavelength

$$\lambda_c = 2a$$
$$= 2 \times 7.214$$
$$= 14.428\text{cm}$$

and the cut-off frequency $f_c = \frac{c'}{c}$

$$= \frac{3 \times 10^{10}}{\frac{(10)^{\frac{1}{2}}}{14.428}}$$

$$= 657.5\text{MHz}$$

To improve the impedance match a taper is designed to connect the S-band dimensions of an antenna to the reduced aperture. This is achieved by dielectrically loading the S-band antenna. The average wavelength is:

$$\text{ave}\,\lambda_0 = (\lambda_g + \lambda_g)/2$$
$$= (3.24 + 13.87)\text{cm}/2$$
$$= 8.55\text{cm}.$$

Therefore the length of the taper is $\text{ave}\lambda/2 = 4.28\text{cm}$

Dimensions of the rectangular aperture are 'a' = $72.14/(10)^{\frac{1}{2}}$ = 22.81mm and 'b' = 10.76mm. For the square aperture, dimensions are 'a' x 'a'. This completes the design of dielectrically loaded antenna.

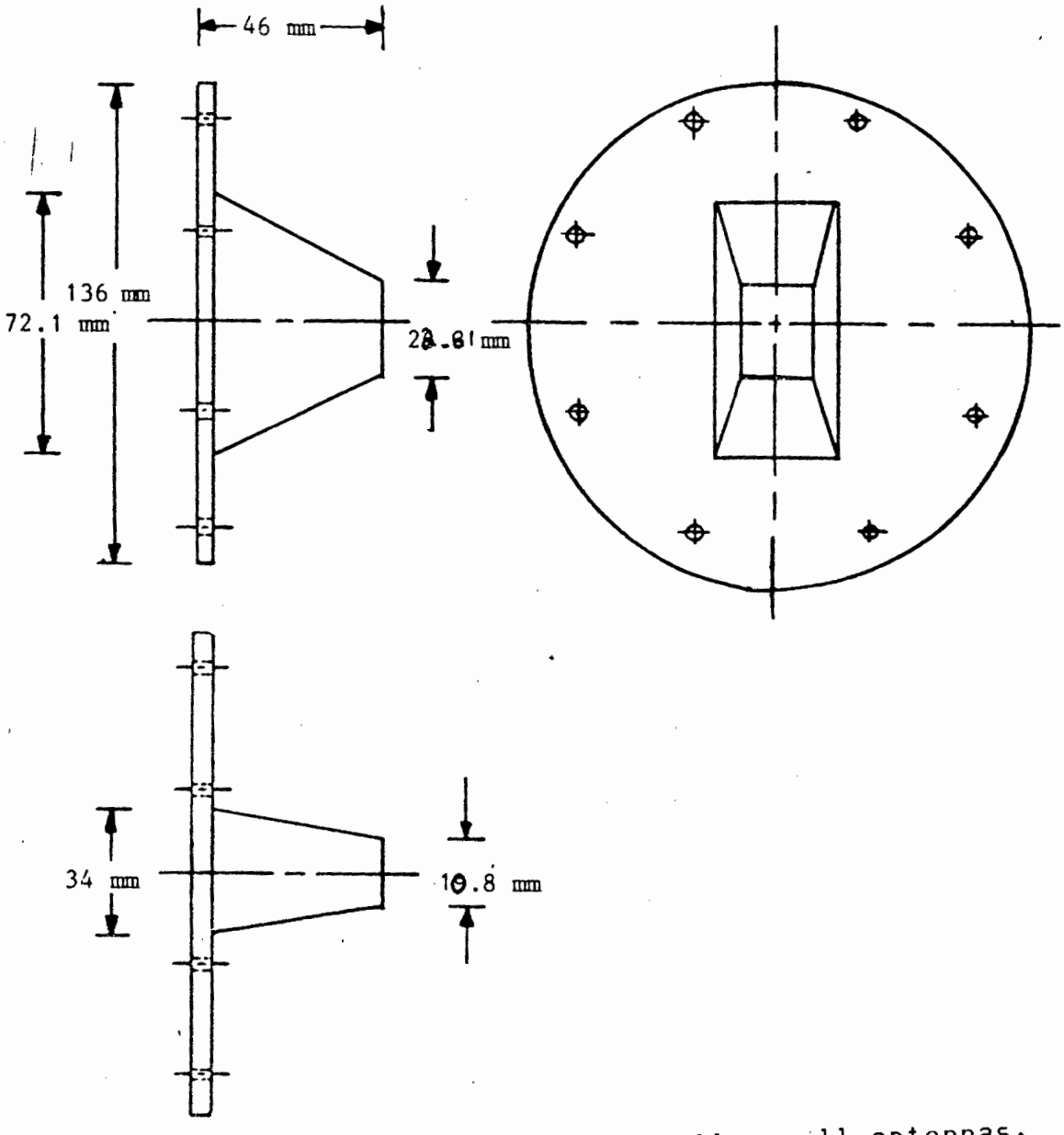

Figure G.3. S-Band electrically small antennas.

FIGURE G.4

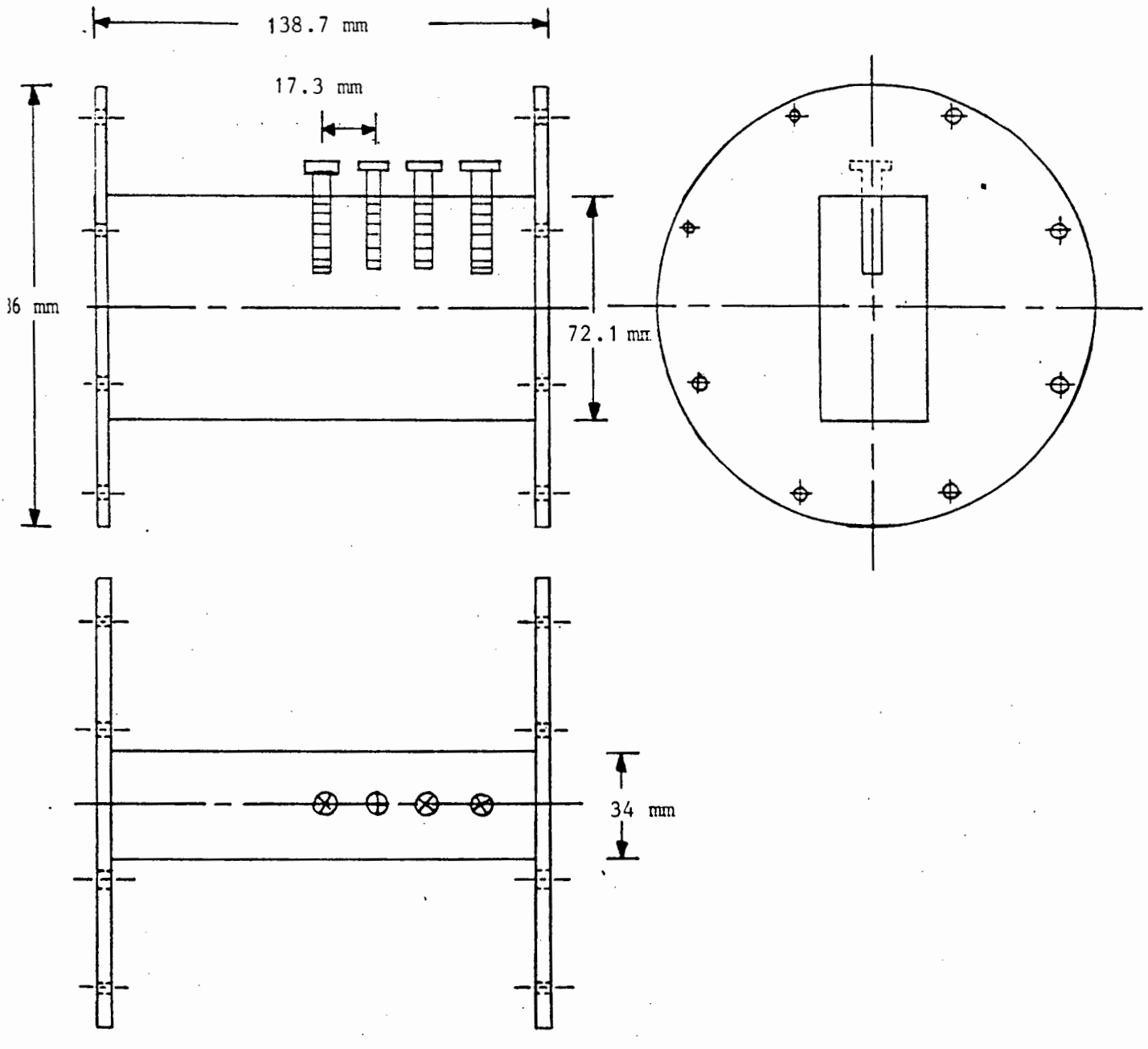

APPENDIX H SPECIFICATIONS OF AVENTEK VTO 8240 VCO

LIMITED FREQUENCY RANGE VARACTOR-TUNED OSCILLATORS

COMMERCIAL VARACTOR TUNED OSCILLATORS

Avantek VTO-8000 Series oscillators use a silicon transistor chip as a negative resistance oscillator. The oscillation frequency is determined by a varactor diode acting as a voltage-variable capacitor in a thin-film microstripline resonator. This provides extremely fast tuning speed, limited primarily by the internal impedance of the user-supplied voltage driver.

A typical oscillator can be swept across its frequency band in less than one microsecond.

The VTO-8000 Series varactor-tuned oscillators are packaged in TO-8 transistor cans for simple installation in a conventional 50-Ohm microstripline PC board. They are ideal for the most compact, lightweight commercial and military equipment designs.

VTO-8000 SERIES

Guaranteed Specifications at 25° C Case Temperature (0 to 65° C Operating Temperature)

PCB

Model	Frequency Range (GHz)	Power Output into 50 Ohms, Min. (dBm)	Power Output Variation Maximum (dB)	Tuning Voltage Limits (at each end of specified freq. range) +VDC @ Low Freq.	+VDC @ High Freq.	Input Power (±1% Reg.) Voltage (VDC)	Current (mA) Maximum	All Harmonics Typical (dBc)	Case Type
VTO-8030	0.3-0.45	+10	±1.5	5±4	50±10	+15	50	-15	TO-8V
VTO-8040	0.4-0.6	+13	±1.5	3±1	40±6	+15	50	-15	TO-8V
VTO-8060	0.6-1.0	+13	±1.5	3±1	40±6	+15	50	-15	TO-8V
VTO-8080	0.8-1.4	+13	±1.5	2±1.5	35±10	+15	50	-15	TO-8V
VTO-8090	0.9-1.6	+13	±1.5	2±1	48+8; -10	+15	50	-15	TO-8V
VTO-8100	1.0-1.4	+10	±1.5	8±1	48±8	+15	50	-15	TO-8V
VTO-8150	1.5-2.5	+10	±1.5	2.5±1	47±6	+15	50	-15	TO-8V
VTO-8200	2.0-3.0	+10	±1.5	2+2, -1	30±6	+15	50	-15	TO-8V
VTO-8240	2.4-3.7	+10	±1.5	2+2; -1	30±6	+15	50	-15	TO-8V
VTO-8300	3.0-3.5	+10	±1.5	3.5 min.	11 max.	+15	50	-15	TO-8V
VTO-8350	3.5-4.5	+10	±1.5	6 min.	35 max.	+15	50	-20	TO-8V
VTO-8360	3.6-4.3	+10	±1.5	8±2	34±4	+15	50	-25	TO-8V
VTO-8400	4.0-4.5	+10	±1.5	2 min.	14 max.	+15	50	-25	TO-8V
VTO-8420	4.2-5.0	+10	±1.5	7.5±2.5	25+2.5; -4	+15	50	-25	TO-8V
VTO-8430	4.3-5.8	+10	±1.5	5.5±2	24+3	+15	50	-25	TO-8V
VTO-8490	4.9-5.9	+10	±1.5	6.5±2	24+3; -4	+15	50	-25	TO-8V
VTO-8520	5.2-6.1	+10	±1.5	6.5±2	24±3	+15	50	-25	TO-8V
VTO-8540	5.4-5.8	+10	±1.5	8 min.	26 max.	+15	50	-15	TO-8V
VTO-8560	5.8-6.8	+7	±1.5	5±2.5	24+3; -6	+15	50	-25	TO-8V
VTO-8650	6.5-6.8	+10	±1.5	2±1	20±5	+15	100	-20	TO-8V
VTO-8790	7.9-10.1	+10	±2	3±2	26±4	+15	150	-10	TO-8V
VTO-8810	8.1-9.1	+10	±2	2 min.	16 max.	+15	100	-15	TO-8V
VTO-8850	8.5-8.8	+10	±1.5	5±2	13±6	+15	100	-25	TO-8V
VTO-9050	9.5-10.5	+10	±1.5	4±1	10 max.	+15	100	-20	TO-8V
VTO-91000	10.0-10.25	+10	±1.5	0 min.	15 max.	±15	100	-15	TO-8V